Avalanche release areas and their influence on uncertainty in avalanche hazard mapping

Dissertation
zur
Erlangung der naturwissenschaftlichen Doktorwürde
(Dr. sc. nat.)
vorgelegt der
Mathematisch-naturwissenschaftlichen Fakultät
der
Universität Zürich
von

Margherita Maggioni
aus Italien

Promotionskomitee
Prof. Dr. Robert Weibel (Vorsitz)
Dr. Urs Gruber
Dr. Ross Purves
Dr. Christian Hennig

Zürich 2004

Acknowledgements

This PhD Thesis is the result of the collaboration of many people, who I would like to thank sincerely.

First of all, many thanks to Dr. Urs Gruber and Dr. Ross Purves: without them my thesis would have never been possible... *'Thank you for your constructive discussions, for the hours of sitting in front of the computer and for your encouraging words especially in the last months of my thesis!'*

I would like to thank Prof. Robert Weibel, who supervised my thesis contributing with important remarks, Dr. Christian Hennig, who, though from far away, supported me greatly and punctually concerning statistics, and Dr. Richard Aspinall, who made constructive criticism that have been helpful to improve the final version of the thesis.

Many thanks also to Bruno Tona and Joachim Heierli for their statistic help, to Andi Stoffel for his support with GIS (and also for his friendship), to Martin Stoffel for his help in programming, to Rebecca Hiller for her great work in organizing the SLF digitized avalanche database and to many persons at the SLF and at the University of Zurich for their patience in answering my questions.

Thanks to all the members of the European project CADZIE, especially to Dr. Massimiliano Barbolini who gave me the starting point for my thesis. Thanks to all the members of the avalanche dynamics team at the SLF, who have been very important to improve my knowledge in avalanche science and to create a really nice working atmosphere.

Finally, I deeply thank all the nice friends I've met in Davos, in particular Anja, Betty, Ariane, Katharina, Felix, Andi, Monique, Dani, Marc-Andrè, Norbert and Alejandro. I had very good time with them and they stood me with patience during the last months of my thesis... *'grazie!'* And of course I cannot forget to thank my family and Marcolino, who believed in me giving me my time to do this research... *'presto torno in Italia!'* ;o)

A part of this work was in the frame of the European project 'Catastrophic Avalanches: Defence structures and Zoning in Europe' (EU-No: EVG1-CT-99-00009); funding for this research was provided by the European Union via the Swiss Foundation for Education and Science (OFES-No: 99.0381).

Contents

Abstract

Avalanche hazard maps are very useful for use in planning land use in mountanous areas. In the avalanche hazard mapping procedure used in Switzerland a very important first step is to determine the potential release areas of avalanches that may endanger villages or human activities in general. The most useful sources of information are historical avalanche events but, for areas where no historical data are available, the expert must estimate the avalanche danger by considering other methods. Simulations using models of avalanche dynamics are one possibility, but, common to all numerical modelling, data which include uncertainties are used as inputs, with the resulting uncertainties therefore impacting on the output of the simulations.

This thesis addressed this problem paying particular attention to the definition of avalanche release areas. The aim was to create a procedure which can produce avalanche hazard maps which quantify uncertainty. A method to define potential avalanche release areas, based on topographical parameters such as *slope angle*, *curvature* and *aspect*, in combination with forest cover, was developed in a Geographical Information System. A detailed analysis of other topographical characteristics, such as *mean and maximum slope angle*, *slope angle variability*, *mean aspect*, *distance to the next ridge*, *plan and profile curvature* and *shape* of the potential release areas was carried out to identify possible relationships between topography and avalanche activity (e.g. frequency and size of avalanches from a potential release area). The aim was to explore possible statistical relationships between avalanche activity and topographical characteristics. A range of techniques, such as linear regression model, Classification and Regression Trees and cluster analysis, were applied but significant statistical relationships were not identified.

Nonetheless, an empirical method to determine avalanche activity for avalanche paths with no historical data, relying on the release area information of topographically similar potential release areas was developed. Moreover, a proposal to determine the extent of the release area for avalanches with specific return periods through the use of Gumbel statistics applied on historical data was developed.

With these input data, in terms of distributions, Monte Carlo techniques were applied to generate avalanche hazard maps containing quantifications of the uncertainties present in the hazard limit delineation. Three case studies show that the procedure developed in this work is able to create realistic avalanche hazard maps which derive limits for zones with similar properties to existing avalanche hazard maps generated by more traditional techniques.

Zusammenfassung

In der Landnutzungsplanung von Gebirgsgemeinden ist die Erstellung von Lawinengefahrenkarten obligatorisch. Sie dienen dazu, lawinengefährdete Gebiete zu identifizieren und entsprechend in der Landnutzungsplanung zu berücksichtigen. Die Erstellung einer Lawinengefahrenkarte basiert in der Schweiz auf mehreren Teilschritten. Neben der Analyse des Lawinenkatasters und einer genauen Geländeanalyse vor Ort spielen auch numerische Simulationsmodelle eine wichtige Rolle. Die Eingabeparameter für diese numerischen Modelle weisen dabei teilweise beträchtliche Unsicherheiten auf. Diese Unsicherheiten können die Ergebnisse der Simulationsrechnungen unter Umständen stark beeinflussen. Das Ziel dieser Arbeit war es, die Unsicherheiten bei der Bestimmung der massgebenden Anrissfläche in Abhängigkeit der Wiederkehrdauer eines Lawinenanrisses zu untersuchen. In einem ersten Schritt wurde mittels eines Geographischen Informationssystems (GIS) eine Methode erarbeitet, die es erlaubt, aufgrund der topographischen Merkmale *Hangneigung*, *grossräumige Rippen- und Muldenstrukturen* und *Exposition* einerseits und der Bewaldung andererseits, potentielle Anrissgebiete zu identifizieren. Anschliessend wurden diese potentiellen Anrissgebiete hinsichtlich der topographischen Parameter *mittlere Hangneigung*, *maximale Hangneigung*, *Hangneigungsvariabilität*, *mittlere Exposition*, *Kammnähe*, *kleinräumige Geländekrümmungen* in Fallrichtung und parallel zum Hang sowie der *Form* des potentiellen Lawinenanrissgebietes analysiert. Parallel dazu wurden die potentiellen Anrissgebiete auch hinsichtlich der Grösse und Häufigkeit der Lawinenereignisse analysiert. Das Ziel dieser beiden Anrissgebiets-Analysen war es, eine statistische Beziehung zwischen den topographischen Variablen und den Lawinenereignissen zu finden. Obwohl mehrere statistische Methoden getestet wurden, konnte kein eindeutiger und signifikanter Zusammenhang zwischen der Topographie und der Lawinenaktivität festgestellt werden. Um trotzdem die Anrissgrösse und -häufigkeit in Lawinenzügen ohne detaillierte historische Katasterdaten abschätzen zu können, wurde eine Methode entwickelt, die auf der empirische Lawinenaktivität von topographisch ähnlichen Anrissgebieten beruht. Zusätzlich wurde auch ein Weg aufgezeigt, der es erlaubt, die Grösse eines Anrissgebietes für spezifische Wiederkehrperioden mittels Gumbel-Extremwertstatistik zu bestimmen. Die so gewonnen Anrissgebietsgrössen und ihre Verteilung wurden anschliessend für Monte-Carlo Simulationen verwendet. Die Ergebnisse dieser Simulationen ermöglichten – im Gegensatz zum bisher in der Schweiz verwendeten Vorgehen – die in den Eingabeparametern vorhandenen Unsicherheiten mit in die Lawinengefahrenkartierung einzubeziehen. In drei Beispielen konnte gezeigt werden, dass es mit dem in dieser Arbeit entwickelten Vorgehen möglich ist, realistische Lawinengefahrenkarten zu erzeugen.

Chapter 1

Introduction

1.1 Motivation and goal of this study

Avalanches are a natural hazard that hasve considerable influence on human activities in mountain regions. In the past, not much knowledge existed about this phenomenon and people simply tried to avoid building villages in dangerous places. Today, better knowledge exists, but the problem remains because demographic changes and expansion through tourism have led to many people living or spending free time in mountain areas. In Switzerland, a country with about two thirds of its land area covered by mountains, the problem of living with this natural hazard is well known and must be addressed. Before the avalanche winter of 1951, only memories of past avalanche events and terrain inspection helped people to recognize avalanche terrain, but after that winter such knowledge was considered insufficient to predict possible future avalanche events and related damages. In course of time, much effort has been made to deal with this problem. In 1984 the "Swiss Guidelines for avalanche zoning" were issued, in order to have a reference to delineate homogeneously different levels of avalanche danger and the consequent land use planning [BBF & SLF, 1984].

The procedure of avalanche hazard mapping includes several steps that are affected by uncertainties which, consequently, influence the quality of the final avalanche hazard maps. Some of these uncertainties became clear after the catastrophic winter of 1998/99, when all over the Northern side of the Alps many avalanches occurred and caused damages and loss of life. In Switzerland, most of these avalanches remained within the boundaries given by the available hazard maps, but approximately 40 from about 1200 large avalanches surpassed these limits [Gruber & Margreth, 2001].

In the Swiss avalanche hazard mapping procedure a very important first step is to determine potential release areas for avalanches that may endanger villages or human activities in general. The most useful source of information are historical avalanche events, because they provide data about the extent of the release area, as well as the runout distance, the fracture depth or the avalanche type. But, for areas where no historical data are available, the expert cannot make use of these data and must estimate the avalanche danger by

considering other methods. Simulations using models of avalanche dynamics are one possibility, as they are able to create hazard scenarios after proper inputs have been defined. The goal of this research is to develop a procedure which aims to help the expert to define model inputs for avalanche dynamics models in areas where no historical data are available. These models can then be used to assess the avalanche hazard for paths with no historical data.

The four main goals of this work are:

1. to define potential avalanche release areas on the basis of topographical characteristics;

2. to find a possible relationship between topography and avalanche activity, defined as release area extent and frequency;

3. to determine the extent of the release area for avalanches with specific return periods in areas where no historical data are available;

4. to determine the uncertainties present in the avalanche hazard mapping procedure by a Monte Carlo technique.

In this work, Geographical Information Systems (GIS) and Digital Elevation Models are combined to create an automatic procedure for the definition of potential avalanche release areas on the basis of rules related to topographical characteristics.

Lack of data about past avalanches, and therefore about release conditions, is the main reason for trying to find a statistical relationship between topographical features and avalanche activity. Whilst being aware of the fact that the release of an avalanche is a combination of many factors, the attention is here focused only on topographical factors, because the underlying hypothesis is that, in regions with the same meteorological conditions, the topography is the primary factor influencing avalanche formation. The idea is to analyze potential avalanche release areas, in terms of detailed topographical features, and the related avalanche activity, in terms of release frequencies and extents of past avalanche events, and to try classify avalanche activity with respect to topographical features. The goal is to create a database where potential release areas with similar topographical features are related to the same type of avalanche activity.

With the help of this database, avalanche activity for avalanche paths where no data of past avalanches are available might be estimated using the following procedure:

- definition of the potential release area (PRA) applying the automatic procedure developed in the GIS,

- characterization of the PRA on the basis of detailed topographical features,

- searching within the database for the most similar PRAs in terms of topographical characteristics, in order to use the related avalanche activity to determine the avalanche activity of the undocumented PRA.

Finally, Monte Carlo simulation can be applied for this avalanche path to produce an avalanche hazard scenario which includes uncertainties. The input for the release area to the Monte Carlo simulation would be the distribution representing the avalanche activity, derived by the proposed procedure.

In summary, this thesis aims to investigate the following principal research questions:

1. How can potential avalanche release areas be defined?
2. Is there a statistical relationship between the topographical characteristics of these release areas and avalanche activity?
3. How can the extent of the release area for avalanches with specific return periods be determined?
4. How can the uncertainties present in the avalanche hazard mapping procedures be quantified?

1.2 Structure of the Thesis

Following this introduction, the thesis is structured in seven chapters:

- Chapter 2 introduces the reader into avalanche problems, such as avalanche classification, avalanche formation, avalanche dynamics and avalanche hazard maps. In addition, it gives an overview of Geographical Information Systems and Digital Elevation Models, mostly with respect to their usefulness in the geomorphological characterization of the terrain.
- Chapter 3 contains a description of the study area and of the avalanche database.
- Chapter 4 presents an automatic procedure to define and characterize potential avalanche release areas and to derive related avalanche activity (or release area distribution) from past avalanche events.
- Chapter 5 explains the different methods used in order to investigate the statistical relationship between topographical parameters and avalanche activity.
- Chapter 6 proposes the Monte Carlo approach to the avalanche hazard mapping procedure, in order to quantify existing uncertainties. It also utilizes the method to derive the extent of the release area for avalanches with specific return periods.
- Chapter 7 proposes a procedure to define avalanche hazard in areas where no or limited historical data are available. It describes the application of the procedure, from the definition of PRAs to the Monte Carlo simulation, for some real case studies.
- Finally, Chapter 8 reviews the thesis results with respect to the research questions and proposes possible avenues for future research.

Chapter 2

Theoretical background

2.1 Classification of snow avalanches

A snow avalanche is a mass of snow moving down a slope which can be so small as to be harmless to people or large enough to destroy entire forests and villages. There are different types of snow avalanches according to the many features that characterize them, such as for example dimensions, the manner of triggering and the form of movement.

The topic of avalanche classification was and is still under discussion and development. An overview of the history of snow avalanche classifications is given in McClung & Schaerer [1993] and Barbolini [1999]. Currently, the most commonly used reference system is *The Avalanche Atlas*, published by the International Commission on Snow and Ice [UNESCO, 1981]. The classification system is composed of two parts: genetic and morphological. The genetic classification refers to the processes and conditions that cause avalanches; it is not normally used operationally. Instead, the morphological classification is used to form guidelines for what to observe or record as important information about an avalanche. The classification is performed on the basis of the characteristics of three zones identified within the avalanche path:

1. The *starting zone* is the area where the snow becomes unstable and starts to move. Here, the nature of triggering, the position of the sliding surface and the water content of the snow is considered.

2. The *track* is the slope which divides the starting zone from the deposition zone. Here, the avalanche is fully developed and attains its maximum velocity. The form of the path and the form of the movement are the elements used in classification here.

3. The *runout zone* is the area where the avalanche decelerates rapidly and stops. Here, the surface roughness of the deposits, the water content in snow debris at time of deposition and the contamination of deposit are considered as classification features.

The two main general types of snow avalanches are called *loose snow avalanches* and *slab avalanches*, in relation to the manner of triggering (see Section 2.2).

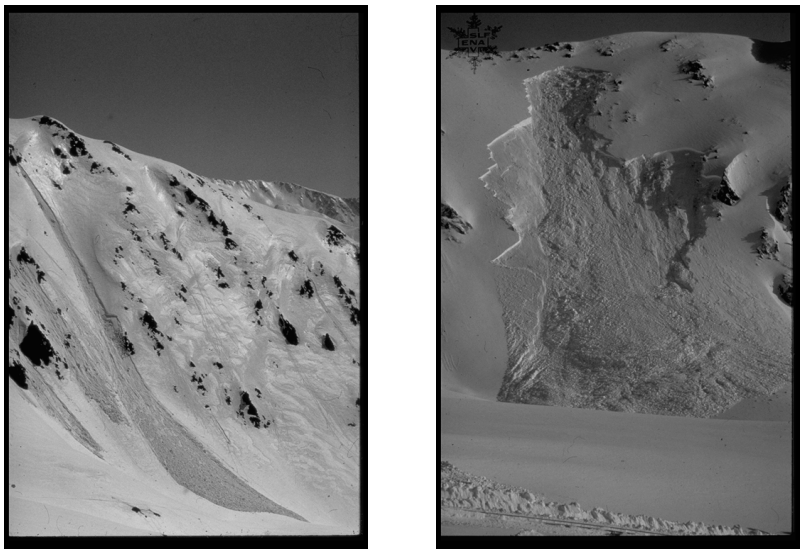

Figure 2.1: Examples of a wet loose snow (left) and a slab (right) avalanche. Photos: SLF archive.

Loose snow avalanches start from a point at or near the surface and collect mass as they move down the slope, assuming a fan-like shape; they have usually small dimensions and can be dry or wet. More dangerous are slab avalanches, which initiate simultaneously over a large area and involve one or more layers of cohesive snow. Figure 2.1 gives two examples of typical loose snow avalanches and slab avalanches, while Figure 2.2 shows the different parts of a slab avalanche.

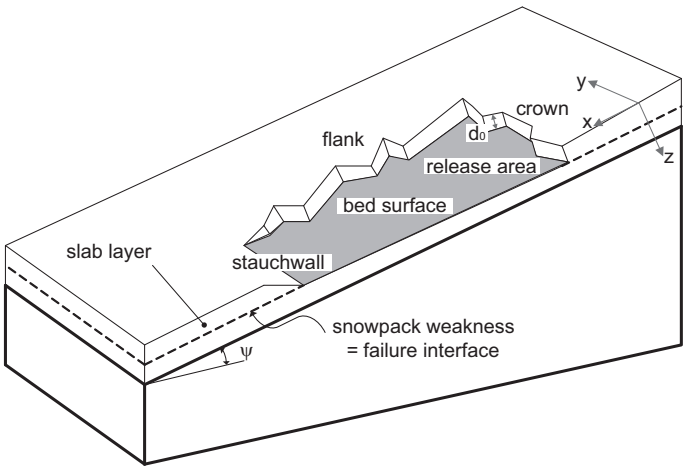

Figure 2.2: Slab avalanche nomenclature. From Schweizer et al. [2003].

The *release area* of a slab avalanche is defined as the area delimited by the *crown* (upper limit), the *flanks*, (lateral limits), and the *stauchwall* (lower limit). After the release, the fracture line is almost always well defined and visible, while the lower limit of the slab is often not recognizable because it is

overridden by the passing avalanche. The *bed surface* is the plane on which the slab slides and lies usually just below the failure plane, which is the plane where the shear failure takes place. The *fracture depth* d_0 is the depth of the fracture at the slab crown, measured perpendicular to the terrain surface.

Based on the form of movement, two types of avalanches are defined: *flowing or dense-snow avalanches*, which move close to the ground with densities around 300-400 kg/m^3, and *powder-snow avalanches*, which are less affected by the topography and have an average density of about 10-30 kg/m^3.

The system proposed by UNESCO [1981] does not take into account avalanche size. In the United States, Atwater elaborated a system to classify the size of the avalanches based on their potential destructive effects [USDA, 1961]. Later, Perla & Martinelli [1976] introduced a classification based on five size classes. An extension of the classification by USDA [1961] was introduced by Perla in Canada and adopted by the Canadian Avalanche Committee in 1977. The Canadian system tried to integrate all the observable variables into a simple estimate of size. More recently, the European Avalanche Warning Services elaborated a glossary of all the words related to snow and avalanches [EAWS, 2003]. This glossary also includes the definition of an avalanche based on its size: a *snow avalanche* is a mass of snow moving rapidly downwards with a volume greater than 100 m^3 and a length greater than 50 m; a mass of snow with volume smaller than 100 m^3 and a length of less than 50 m is called *sluff*. Under the item *avalanche size* in EAWS [2003], there is the official snow avalanche size classification that is suggested for use from now on in Europe (Table 2.1); it is based on the US and Canadian systems.

Extent of the avalanche, classified by runout length, volume and damage potential.

Term		**Runout classification**	**Damage potential classification**	**Quantitative classification**
Size 1	**„sluff“**	Small, harmless snow slide	No eminent danger for humans	Length <50 m, Volume < 100 m^3
Size 2	**small avalanche**	Stops within the slope	Can bury a person, injury or death can occur	Length <100 m, Volume < 1000 m^3
Size 3	**medium avalanche**	Continues to the bottom of the slope	Can bury and destroy cars and damage heavy trucks. Can destroy small buildings and break single trees.	Length <1000 m, Volume < 10000 m^3
Size 4	**large avalanche**	Continues over flat areas (significantly less than 30° slopes) over a distance of at least 50 m. May reach the bottom of the valley.	Can bury and destroy heavy trucks or trains, larger buildings and forested areas.	Length >1000 m, Volume > 10000 m^3

Table 2.1: Avalanche size classification from EAWS [2003].

2.2 Avalanche formation

The release of either a loose-snow or slab avalanche is a complex process that is not yet fully understood. Several contributing factors are involved in the release process, namely terrain, snowpack properties and meteorological conditions. Schweizer et al. [2003] give a good insight into the state of the art of avalanche formation for dry snow slab avalanches, considering both the contributory factors and the failure mechanics at different scales.

What is required for avalanche formation is that the applied shear stress approaches, equals or exceeds the shear strength of the snowpack and that the deformation occurs fast enough to provoke fractures. The shear strength of snow may be seen as composed of two components, cohesion (C) and friction (F), as follow:

$$\tau = C + F = C + \sigma \cdot tan\phi \tag{2.1}$$

where σ is the stress normal to the bed surface and ϕ the static friction angle.

Cohesion in snow refers to how well grains are bound together; it depends on the dimension and shape of grains and crystals and on the density of bonds. *Friction* is related to the resistance to motion of one layer of snow with respect to another; it depends mainly on the snow texture, the water content and the weight of the overlying snowpack [McClung & Schaerer, 1993]. The cohesion is the property which determines which type of avalanche will occur: loose-snow avalanches occur in cohesionless snow, whereas slab avalanches require cohesion high enough to form a snow slab.

For loose-snow avalanches, the cohesion of snow is very low ($C \approx 0$) and the basic release mechanism is that the terrain exceeds the static friction angle ϕ (called also *angle of repose*) until which the snow is in equilibrium. Each type of snow has a characteristic static friction angle which depends on grain geometry, cohesiveness, snow temperature and water content.

For slab avalanches, the release is characterized by a rapid propagation of the fractures underneath and at all boundaries of the slab. The release of a slab occurs when a layer of cohesive snow lies on a weak layer or when it is not well bound to the underlying layer; if the stress applied to these weaknesses exceeds their strength, a shear failure occurs. Failure starts at locations where the shear strength is lower than the average shear strength of the snowpack. These preexisting shear strength deficit zones are named *flaw zones*. There is a critical flaw size to provoke a catastrophic failure of the whole slab [Schweizer et al., 2003]. However, a catastrophic failure alone is not sufficient to release a slab. In fact, if the failure happens slowly, no fracture of the slab avalanche will occur; this slow shear strength failure is named *strain-softening* [McClung & Schaerer, 1993]. To provoke the release of a slab avalanche, a fracture is necessary. A fracture in snow occurs only when both the shear stress approaches the shear strength and the deformation rate is above a critical rate, which is about 1 mm/min for layer thickness as typical of avalanche weak layers (e.g. 10 mm).

For artificially triggered avalanches, the critical rate of deformation into the snowpack is easily produced by skiers or explosives. For natural avalanches, the deformation is usually slower and caused mainly by additional weight due to

new snowfall or blowing snow. Furthermore, in the case of natural avalanches, temperature increase or rain can have great influence on avalanche release.

After a fracture occurs, it propagates upslope and across the slope to form the slab that starts moving downslope. The size of the slab depends on different properties of the snowpack and on the topography of the area. On unconfined planar terrain, field data indicate that the slab width exceeds the slab length, while in confined terrain, such as channels or gullies, the length may exceed the width of the slab [McClung & Schaerer, 1993]. Many studies have been conducted to analyze the dimensions of slabs [Brown et al., 1972; Schweizer & Lütschg, 2001; Perla, 1977].

From the point of view of the physical processes happening in the snowpack after a failure had occurred, some models were developed to describe the release of a slab avalanche and the dimensions of the releasing slab. Johnson et al. [2003] modelled fracture propagation with the hypothesis that the extent of fracturing L_{slab} is entirely controlled by the tensile strength of the overlaying slab. Jamieson & Johnston [1992] studied 13 strictly unconfined slab avalanches and found that the slab width is proportional to an *arrest parameter*, which includes the slab thickness, slab tensile strength and basal shear strength.

All these considerations on the dimensions of avalanche slabs and avalanche releasing mechanism are reported here in order to underline the difficulties of estimating the potential release area of an avalanche, an important parameter in the avalanche hazard mapping procedure.

2.3 Avalanche dynamics

The physical behavior of avalanches is not entirely known yet, but much theoretical and experimental research has been carried out to understand it. With the help of experimental avalanche test sites, such as Vallèe de la Sionne (Canton Valais, Switzerland) and others in Europe [SLF, 1999a], knowledge of the dynamics of avalanches is improving and different mathematical models have been elaborated to model avalanche dynamics.

Increased human activity in mountain regions, mainly due to tourism, in combination with a reduced acceptance of risk from those living in areas exposed to snow avalanches have caused a growing need for protection against avalanches. The first attempt to formulate a general theory of avalanche motion was made by Voellmy [1955], and this theory is still widely used. Since the 1950s, several other studies have been carried out to elaborate empirical and physical models that are able to give information about runout distance and impact pressure of avalanches, important variables for avalanche hazard assessment (see Section 2.4). However, no universal model has so far been developed. A detailed description of all the models developed until 1998 is presented in Harbitz [1998].

A basic distinction can be made between *empirical procedures* and *physical models*. Empirical procedures for estimation of avalanche runout distance use historical records of avalanche runout on documented paths [Bovis & Mears, 1976; Lied & Bakkehoi, 1980; McClung & Lied, 1987] and derive methods to

extend this information to undocumented paths [Bakkehoi & Norem, 1994]. They calculate the runout distance of the simulated avalanche. Physical models consider the physical processes underlying the avalanche dynamics and use mathematical equations to describe the avalanche motion from the release zone to the runout zone. They are then able to calculate dynamical variables, such as runout distance, but also pressure and flow height of the avalanches. Within dynamical models, three groups can be distinguished:

- The sliding block (or lumped mass) dense-snow avalanche models, e.g. Voellmy [1955], describes the avalanche as a rigid body on a linear slope or as a flexible body (*blanket*) following the terrain. Alternatively, the motion can be described by center-of-mass considerations, including the sum of external forces acting on the body.

- Deformable body models, e.g. Bartelt et al. [1999] and Norem et al. [1986], described the dense-snow avalanche as a continuum. In granular models, the avalanche flow is described as a cohesionless material, normally treated as an incompressible Coulomb (dry friction) medium that transmit no tensile but only compressive stresses. The main supporting force is attributed to grain-to-grain interaction.

- Powder-snow avalanche models describe the airborne turbulent particle flow as a block, e.g. Fukushima & Parker [1990], or by other approaches such as density current models or binary (solid-fluid) mixture models, e.g. Naaim & Gurer [1998].

Only a few combinations of these models, i.e. coupled models including both the dense and the powder snow part of the avalanche, exist [Bartelt et al., 2000]. In the present study, the model used in the proposed Monte Carlo approach to avalanche hazard mapping procedure (see Chapter 6) is the dense-snow avalanche model FL-1D, a deformable body model which will be described later in this section.

In order to perform an avalanche simulation, all the models of dynamics require the definition of the initial conditions in term of *release area*, *fracture depth* and *friction coefficients*; their correct definition is a difficult task, subject to uncertainties. Therefore, it is important to investigate how model output varies with respect to variations in initial conditions. Barbolini et al. [2000] made a comparison of two empirical and three physical models at five avalanche sites in Europe and performed a sensitivity analysis to address the aforementioned problem. They found that both runout distance and pressure are remarkably sensitive to both the friction coefficients and the initial conditions, with the friction coefficient μ appearing to influence the model outputs to the greatest extent. A 15% variation of this parameter can produce variations of up to 10% for the runout distance and up to 50% for the impact pressure. These variations, in the case of large avalanches, can produce completely different hazard scenarios. This study highlights the importance of being able to deal with these uncertainties and include them in the avalanche hazard mapping procedure (see Chapter 6).

In the present study, the dense-snow avalanche model "FL-1D", developed at the SLF, is used and briefly described here. "FL-1D" is a numerical, depth-averaged, quasi one-dimensional, continuum model, which tracks the motion of an avalanche from initiation to runout. It is based on the following assumptions:

- Flowing snow is modelled as a fluid continuum of mean constant density.
- The flow width is known.
- A clearly defined top flow surface exists.
- The flow height is the average flow height across the section.
- The vertical pressure distribution is hydrostatic. Centripetal pressures which modify the hydrostatic pressure distribution are not accounted for.
- Flow velocity and depth is unsteady and non-uniform.
- The avalanche mass is constant and no entrainment processes are modelled.

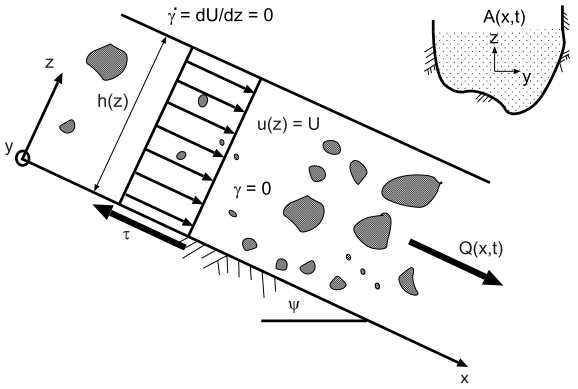

Figure 2.3: Representation of an avalanche as a Voellmy fluid in the FL-1D model. Source: Bartelt et al. [1999].

The fundamental differential equations are based on the principles of conservation of mass and momentum and are solved numerically with finite difference techniques [Sartoris & Bartelt, 2000]:

$$\frac{\partial A}{\partial t} + \frac{\partial Q}{\partial x} = 0 \tag{2.2}$$

$$\frac{\partial Q}{\partial t} + \frac{\partial}{\partial x}\left[\alpha(x,t)\frac{Q^2}{A}\right] + \lambda g A \frac{\partial h}{\partial x} cos\psi = gA(S_0 - S_f) \tag{2.3}$$

where g is the gravity acceleration, $h(x,t)$ is the avalanche flow height at position x along the profile and time t, S_0 and S_f are the acceleration and friction slope respectively, $\psi(x)$ is the inclination of the mountain slope, λ is the passive/active pressure coefficient and $\alpha(x,t)$ is the velocity profile factor. $A(x,t)$

and $Q(x,t)$ are the two scalar fields which describe the avalanche flow: $A(x,t)$ represents the cross-sectional flow area at position x and time t, and $Q(x,t)$ gives the average flow discharge along the mountain profile (see Fig. 2.3). $\alpha(x,t)$ is the velocity profile factor, which is equal to 1 for a rectangular velocity profile.

Volume [m^3]	Topography	Altitude [m.a.s.l.]	300-year		30-year	
			μ	ξ [m/s^2]	μ	ξ [m/s^2]
large avalanche > 60'000	unchannelled	above 1500	0.16	2500	0.17	2000
		1000 - 1500	0.18	2000	0.19	1750
		below 1000	0.2	1750	0.21	1500
	channelled	above 1500	0.2	1750	0.21	1500
		1000 - 1500	0.25	1500	0.26	1500
		below 1000	0.3	1200	0.31	1200
	gully	above 1500	0.3	1000	0.31	800
		1000 - 1500	0.34	750	0.35	600
		below 1000	0.38	500	0.39	400
mean size avalanche 25'000 - 60'000	unchannelled	above 1500	0.2	2000	0.21	1750
		1000 - 1500	0.24	1500	0.25	1500
		below 1000	0.28	1200	0.29	1200
	channelled	above 1500	0.26	1200	0.27	1200
		1000 - 1500	0.29	1200	0.31	1200
		below 1000	0.33	1000	0.34	1000
	gully	above 1500	0.33	1000	0.34	800
		1000 - 1500	0.37	800	0.38	600
		below 1000	0.4	500	0.41	400
small avalanche < 25'000 & wet snow avalanche	unchannelled	above 1500	0.30	1500	0.31	1200
		1000 - 1500	0.32	1200	0.33	1200
		below 1000	0.34	1200	0.35	1000
	channelled	above 1500	0.32	1200	0.33	1000
		1000 - 1500	0.34	1000	0.35	800
		below 1000	0.36	800	0.37	600
	gully	above 1500	0.36	800	0.37	600
		1000 - 1500	0.4	500	0.41	400
		below 1000	0.42	500	0.43	400

Table 2.2: Recommended values for the friction parameters μ and ξ for the application of the FL-1D model. The friction parameters vary in function of the avalanche size, the altitude, the confinement of the terrain and the return period. Source: SLF [1999b].

The model employs a Voellmy-fluid flow law, which assumes no shearing deformations ($\gamma = \tau_{zx}(z) = 0$) in the avalanche body and at the top surface; the avalanche is moving as a plug with a constant velocity $U(x,t)$ over the flow height h. The flow resistance is concentrated at the base of the avalanche (τ in Fig. 2.3) and consists of a dry-Coulomb like friction (μ) and a Chezy-like resistance (ξ). With the assumption of a hydrostatic pressure distribution, the

friction slope S_f and the acceleration slope S_0 for a Voellmy fluid are:

$$S_f = \mu cos\psi + \frac{U^2}{\xi h}. \tag{2.4}$$

$$S_0 = sin\psi. \tag{2.5}$$

The friction parameters μ and ξ are constants whose magnitude varies as a function of the avalanche size, the altitude, the confinement of the terrain and the return period. There exist recommended guideline values for these two friction parameters [SLF, 1999b] based on extensive model calibration with observed field events [Bartelt et al., 1999]. These recommended values are shown in Table 2.2.

Although no shearing deformations occur within the avalanche body, the flow plug undergoes considerable longitudinal strains. The active/passive pressure coefficient λ takes into account these processes and assumes positive or negative values for stretching or compression of the snow plug [Bartelt et al., 1999].

For the purpose of this work, this description is thought to be sufficient to give an overview of the model and to introduce important parameters that are used and discussed in the Monte Carlo approach to avalanche hazard mapping (see Chapter 6). Bartelt et al. [1999], Sartoris & Bartelt [2000] and Christen et al. [2002] describe the FL-1D model in more detail.

2.4 Avalanche Hazard Maps

Avalanche hazard maps identify areas endangered by avalanches of different intensity. In Switzerland, hazard mapping began after the catastrophic winter of 1951 when 98 persons were killed by avalanches and more than 1430 buildings were destroyed. The principle is to prohibit the construction of buildings in an endangered area. The first hazard maps were generated in Gadmen and Wengen, in Canton Bern, in 1954 and 1960, respectively. These first hazard zones were designated according to disastrous events in a rather qualitative way without taking into account climatic factors or avalanche dynamic calculations. In the course of time, the methods have been improved and this development lead to the "Swiss Guidelines for avalanche zoning", issued in 1984 [BBF & SLF, 1984], in order to have a reference to delineate homogeneously different levels of avalanche danger and the consequent land use planning.

The avalanche hazard is a function of the return period T and of the impact pressure p of an avalanche. Table 2.3 describes the different hazard levels as they are defined in Switzerland based on BBF & SLF [1984], while in Figure 2.4 an example of an avalanche hazard map is shown.

The land use planning related to the avalanche hazard states that: in the *red zone*, no new buildings are permitted; in the *blue zone*, only buildings that can resist the possible avalanche impact force are permitted; in the *yellow zone*, the impact forces of possible powder snow avalanches have to be considered and then the structures reinforced in order to resist to them; the *white zone* is

Table 2.3: Definition of different avalanche hazard levels and consequent land use.

Zone	Hazard level	Definition based on T and p
Red	High	$T < 30$ y or $T > 30$ y and $p < 30$ kPa
Blue	Moderate	$30 < T < 300$ y and $p < 30$ kPa or powder avalanches with $T < 30$ y and $p < 3$ kPa
Yellow	Low	$T > 300$ or powder avalanches with $T > 30$ y and $p < 3$ kPa
White	No hazard	no limits

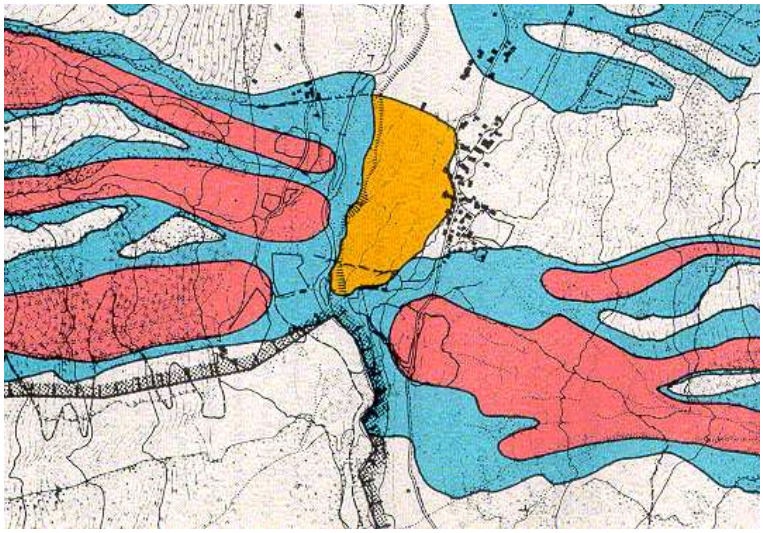

Figure 2.4: Avalanche hazard levels defined as in Table 2.3. Source: BBF & SLF [1984]

considered safe and no limitations are designated for the construction of new buildings.

Avalanche hazard maps are created by the combination of different factors. The procedure includes:

- analysis of the avalanche cadaster, which often provides useful information about historical events;
- analysis of the snow climatology of the region;
- knowledge of the topographical and geomorphological settings of the avalanche path through accurate mapping, aerial pictures and field survey;
- estimation of the possible types of avalanches and their frequency;
- interpretation of the results of avalanche dynamics calculations.

In Switzerland, the year 1999 was a "catastrophic" avalanche winter, which caused the death of 17 persons and damage with a value of about 100 Million

Swiss Francs [SLF, 2000]. This was a valuable test of the avalanche hazard mapping procedure that had been developed since the extreme avalanche winter in 1951. In most cases, the avalanches stopped within the avalanche hazard zones, however 40 of about 1200 large avalanche events surpassed the limits of the existing hazard zones. In most cases, the primary deficiency was the underestimation of the hazard of powder snow avalanches. In other cases, the avalanche release areas were much larger than estimated by the experts for the simulation of 300 and 30yr avalanches. Other reasons for the passing of the hazard zone boundaries were multiple avalanches in single tracks within a short time period, the underestimation of fracture depths and the under-dimensioning of deflecting dams [Gruber & Margreth, 2001; Gruber & Bartelt, 2000].

The avalanche winter of 1999 highlighted deficiencies in the avalanche hazard mapping procedure and underlined the importance of being able to deal with the uncertainties present in avalanche hazard maps. Barbolini [1999] understood the importance of this problem and combined avalanche dynamic calculations with statistical analysis to create a methodology to quantify these uncertainties.

2.5 Geomorphological characterization of the terrain

In this study, an important issue is to define and characterize potential avalanche release areas on the basis of topographical parameters, such as terrain slope, aspect or curvature. The question that arises was therefore how to determine these topographical attributes. The procedure developed here makes use of a Geographical Information System (GIS) where the primary input is a Digital Elevation Model (DEM) (see Chapter 4). As explained in the following, the combination of digital elevation models and GIS permits the extraction of many topographic attributes of the terrain.

2.5.1 Geographical Information Systems

In general, a GIS represents phenomena of the real world in terms of their geographical positions, their properties and their spatial interrelations. In the past many definitions of GIS were formulated. An extensive description of the history of GIS can be found in Coppock & Rhind [1991].

A GIS is a very useful system to analyze geographical databases that attempt to represent reality. Peuquet [1984] explained geographical databases as the results of an analysis considering the following four levels of abstraction:

1. Reality - the real world including all its characteristics.
2. Data model (or conceptual model) - an abstraction of the reality, which includes features relevant for the study that has to be conducted.
3. Data structure (or logical model) - a representation of the data model which reflects implementation issues and is often represented as diagrams or arrays.
4. File structure (or physical model) - the representation of the data in storage hardware.

Therefore, the creation of a geographical database is strongly dependent on many factors, but most of all data structures and storage [Maguire & Dangermond, 1991].

Maguire & Raper [1990] give a good insight into the major types of functions which characterize GIS. There, different types of data storage and structure are given. A regular-gridded DEM, as used in this work, belongs to the class of regular tessellation structures. Other good reviews of data structures are given by [Moore et al., 1991; Weibel & Heller, 1991; Carter, 1988].

A regular-gridded DEM is a representation of the terrain by a regular lattice (or grid) of points at fixed distance (*resolution* of the DEM), with the attributes x and y, which localize a point in a 2D-space, and z, which represents the elevation of the point (Fig. 2.5a). The resolution of the lattice is important to allow representation of terrain features such as gullies or ridges present in the terrain. In order to represent the terrain to a required level of accuracy, the point density must be sufficiently high and problems related to computer memory capacity may arise, in the case of a very large study area.

Another possibility to represent terrain is by a Triangulated Irregular Network (TIN), first introduced by Peucker et al. [1978]. In this case, the irregular network is composed of triangular elements of different size with the vertices at the sample points (see Fig. 2.5b). A TIN is able to describe accurately the terrain complexity using less points, because it can use different point densities, i.e. higher density only where the relief is more complicated. Moreover, structural features, such as sharp ridges, can be inserted into the network, in order to improve the representation of the terrain.

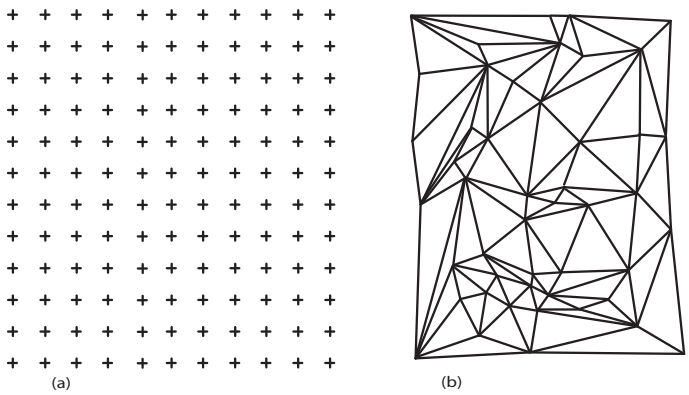

Figure 2.5: The two most commonly used data structures for digital terrain models: (a) regular-gridded DEM, (b) Triangulated Irregular Network. Source: Weibel & Heller [1991].

However, the extrapolation of terrain characteristics such as slope, aspect and curvature, is not so straightforward as it is with regular structures. Not all grid-based algorithms today have an efficient counterpart in TIN [Weibel & Heller, 1991]. Regular-gridded digital elevation models have emerged as the most widely used because they are simple and they are very suitable for several kind of simple computer implementations to obtain terrain characteristics

[Moore et al., 1991; Wise, 1998; Moore et al., 1993]. Most importantly in the context of this work however, regular grids have the distinct advantage that their spatial unit of reference - the grid point or grid cell - is uniform everywhere throughout the DEM. In contrast to TINs with their irregular shaped and sized triangles, this ensures easy and consistent comparison of multiple terrain parameters or between different study areas. This is the reason for the choice of a regular-gridded DEM as input to the procedure of defining and characterizing potential avalanche release areas in this work.

2.5.2 Derivation of topographical attributes from a DEM

From a DEM, several terrain attributes can be derived with GIS. Wilson & Gallant [2000], Moore et al. [1991] and Moore et al. [1993] distinguished between primary topographic attributes that are derived directly from the DEM and secondary topographic attributes that are a combination of primary attributes and provide indices about the spatial variability of physical processes happening in the real world. An example of a secondary attribute is the potential solar radiation, that is computed in a GIS as a function of latitude, slope, aspect, topographic shading and time of year. Slope and aspect are examples of primary attributes; an exhaustive list of primary attributes is given in Wilson & Gallant [2000], where their definition and significance are discussed.

Here, the methods to compute the primary topographic attributes, which are used in Chapter 4 to define and characterize potential avalanche release areas, are described, together with references to works that explain them more in detail. Primary topographic parameters are derived from the DEM computing the derivatives (first and second) of the surface; since the gridded surface is discretized, the derivatives are approximated either by computing difference within a kernel or by fitting a polynomial to the data within the kernel.

Slope and Aspect

Evans [1980] defined slope as the plane tangent to the DEM surface at a given point (center of a cell) and composed of two components: *gradient*, the maximum rate of change in the elevation, and *aspect*, the compass direction of this maximum. Other works, included the present study, use *slope* synonymously for *gradient* as previously defined. Slope can be computed with different methods, for example finite differences or maximum downward slope. Gallant & Wilson [2000] give an overview of different procedures to compute slope and aspect from a gridded DEM. Different studies have been carried out to evaluate the accuracy of several slope calculation methods, e.g. Florinsky [1998], Onorati et al. [1992] and Skidmore [1989].

Here the method implemented in *ArcInfo*, a wide-spread commercial GIS, is used [ESRI, 2001]. The slope function fits a plane to the z values of a 3x3 cell neighborhood around the processing or center cell. The compass direction of this plane is the aspect for the processing cell. The slope of the cell is calculated from the 3x3 neighborhood using a finite difference estimator [Horn, 1981]. This method has also been shown consistently to be among the most accurate by the evaluation studies referred to above.

Curvature

With second derivatives on the surface, curvature is computed. *Plan curvature* is the rate of change of aspect along a contour and *profile curvature* is the rate of change of slope along a flow line. Shary et al. [2002] give a list of different procedures to compute curvature, together with sets of mathematical formulae. In these methods, the surface is represented by a polynomial (of different order in the different cases) fitted to the surface. Schmidt et al. [2003] compared methods that use fitting polynomials of different orders and found that quadratic surfaces give more stable results than higher order surfaces, which can fit more complex landforms but are reliable only for very accurate DEM data.

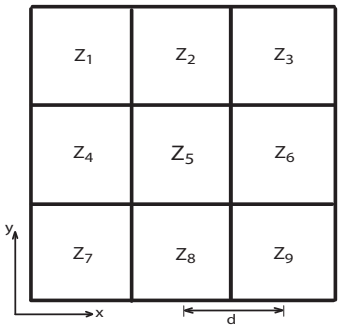

Figure 2.6: 3x3 cells window used to calculate curvature in the central cell: d is the lattice resolution, Z_i the elevation value for the cell i.

Here the method implemented in *ArcInfo* is used [ESRI, 2001] and it is based on the procedure explained in Zevenbergen & Thorne [1987]. Plan and profile curvature are calculated on a cell-by-cell basis. A second-order polynomial in two variables is fitted to a surface composed of a 3x3 window – the central cell plus eight neighbors (see Fig. 2.6) – and has the following expression:

$$Z = Ax^2y^2 + Bx^2y + Cxy^2 + Dx^2 + Ey^2 + Fxy + Gx + Hy + I. \qquad (2.6)$$

The mathematical expressions to derive plan and profile curvature from the second-order polynomial in two variables 2.6 are:

$$Z_{xx} = 100\frac{\frac{z_6-z_5}{d} - \frac{z_5-z_4}{d}}{d} = 100\frac{z_4 + z_6 - 2z_5}{d^2} \qquad (2.7)$$

$$Z_{yy} = 100\frac{\frac{z_8-z_5}{d} - \frac{z_5-z_2}{d}}{d} = 100\frac{z_2 + z_8 - 2z_5}{d^2} \qquad (2.8)$$

In Section 4.2.1, the values -0.2 and +0.2 are used as threshold values for plan curvature to identify concave, "flat" and convex areas. With a lattice resolution d of 50 m, the chosen value of -0.2 corresponds to an elevation increase ($z_6 - z_5$ and $z_5 - z_4$) of 2.5 m within 50 m of both sides of the center position [Schmid & Sardemann, 2003].

2.5.3 Effect of DEM resolution in computing topographical attributes

Two problems are always present when working with gridded digital elevation models in the procedure of identifying different terrain features: the influence of the quality of the DEM data source and the sensitivity to the DEM resolution. Wilson et al. [2000] highlighted the sensitivity of selected primary and secondary topographic attributes to the choice of DEM data source, DEM resolution and algorithm. Here, only the effect of the DEM resolution in deriving terrain features is addressed. Six simple geomorphometric classes are defined by Wood [1996], Evans [1980] and Peucker & Douglas [1975]: channel, pass, peak, pit, plane and ridge (see Fig 2.7). But how well can these features be identified? Fisher et al. [2003] formulated a question: "Where is a mountain?" and made considerations about how a mountain is perceived by humans and how a mountain can be identified within a GIS. While it is relatively clear how a mountain is seen by humans, it is more complicated to be able to identify uniquely a mountain within a GIS. Figure 2.8 shows the different classes which a point belongs to with respect to the scale of the analysis. This is exactly the problem that arises in the classification of a point into one of the six morphometric classes listed above.

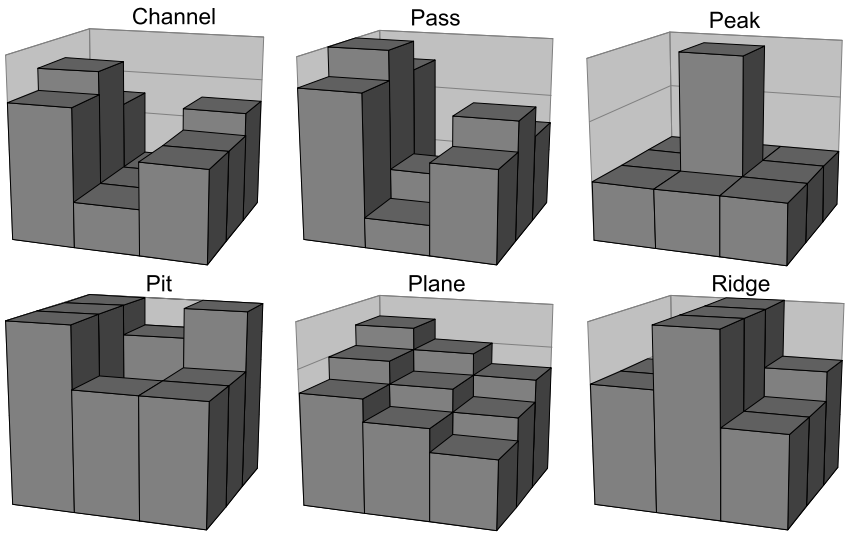

Figure 2.7: The representation of 6 different geomorphometric classes by a gridded digital elevation model. Source: Fisher et al. [2003].

A common result achieved from many past studies, such as Quinn et al. [1991], Panuska et al. [1991], Wolock & Price [1994], Zhang & Montgomery [1994], Moore [1996] and Wilson et al. [2000], is that a coarser DEM resolution tends to have a "smoothing" effect on computed topographic surfaces, therefore short, steep slopes or other small topographic attributes tend to disappear with reductions in the DEM resolution. At higher resolutions, more complex terrain can be described by a gridded DEM, but sometimes all these small scale changes

are not interesting for the analysis at hand. Therefore, when researchers have to address the problem of the classification of terrain features, they should first think about the spatial scale typical of the phenomena under study.

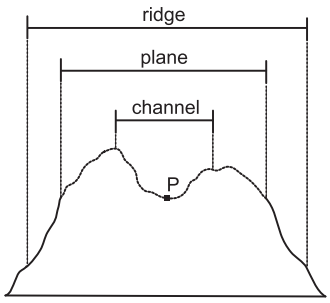

Figure 2.8: Different geomorphometric classes the point P belongs to, with respect to the scale over which the classification is performed. Source: Fisher et al. [2003].

Chapter 3

Study area and database

3.1 Location of the study area

The study area is located in the region of Davos in Canton Grisons in Switzerland. It is a mountain area of about 300 km^2 with altitudes between about 1500 m and 3200 m a.s.l.. The main features are the principal valley with a NE-SW direction and three parallel lateral valleys with a NW-SE direction (Flüelatal, Dischmatal and Sertigtal). Four ski-resorts are present in this area. Since they are located mostly above the tree-line, the ski-patrols of these resorts have a good view of many parts of the Davos area, and therefore they are able to observe many avalanche events.

Figure 3.1: Location of the study area of Davos (Grisons, CH). Map reproduced by permission of swisstopo (BA046644).

The climate in this region is influenced by oceanic and continental regimes with a long winter season. Usually, snow covers the valley bottom from December till April, and it is present at an altitude of 2500 m from October till July (Fig. 3.2). The average winter precipitation is 417 mm (about 70% as snow) and the average winter air temperature is -2.9 °C at an altitude of 1560 m a.s.l.(values taken from [Aschwanden, 1996] for the period November-April).

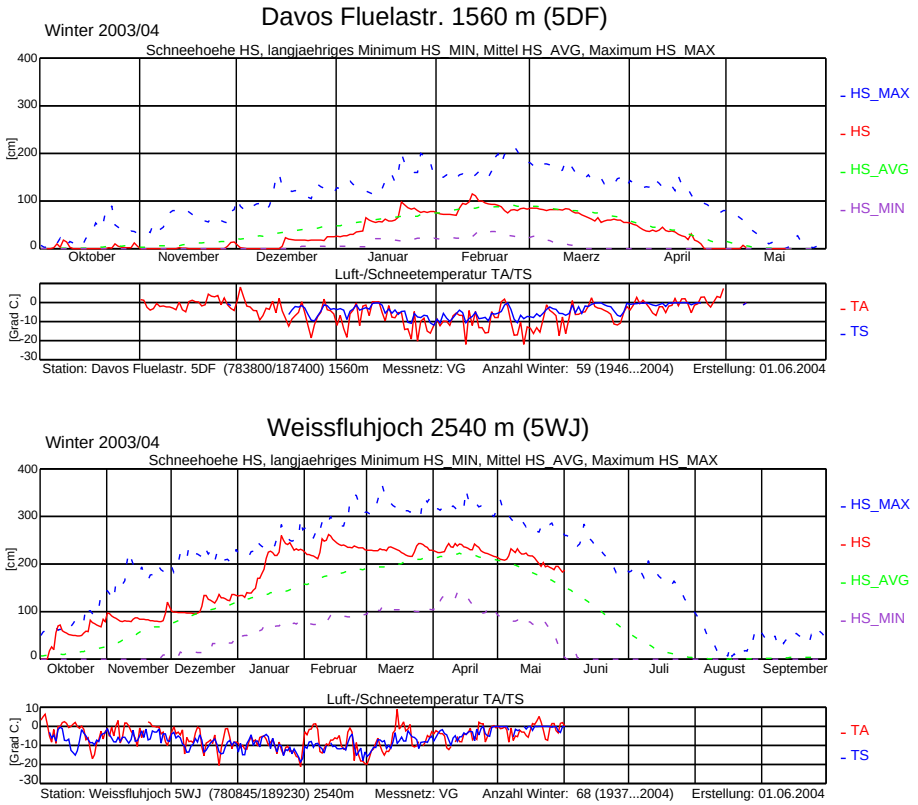

Figure 3.2: Meteo stations Davos Flüelastrasse and Weissfluhjoch operating for 59 and 68 years, respectively: snow height (in red the value for the current year; in green, blue, violet, respectively the value of the mean, the maximum, the minimum over the past years), air (red) and snow (blue) temperature. Source: SLF Database.

In these climatic conditions, avalanches of all types (see Section 2.1) can occur. The avalanche activity is varied: some avalanche paths are characterized by frequent avalanches of small dimension and others by avalanches of large dimension but with lower frequency. There exist areas, mainly in ski-resorts, where the method of artificial triggering is used to keep the ski-runs safe in terms of avalanche danger. Since this procedure is used before a consistent amount of snow can accumulate, the artificially triggered avalanches are usually of small dimensions.

The variety of avalanche type and activity makes this region suitable for this study, which tries to evaluate the influence of topographical features on

the size and frequency of avalanche events. Figure 3.3 shows the frequency of the avalanches in a selected area of the region of Davos.

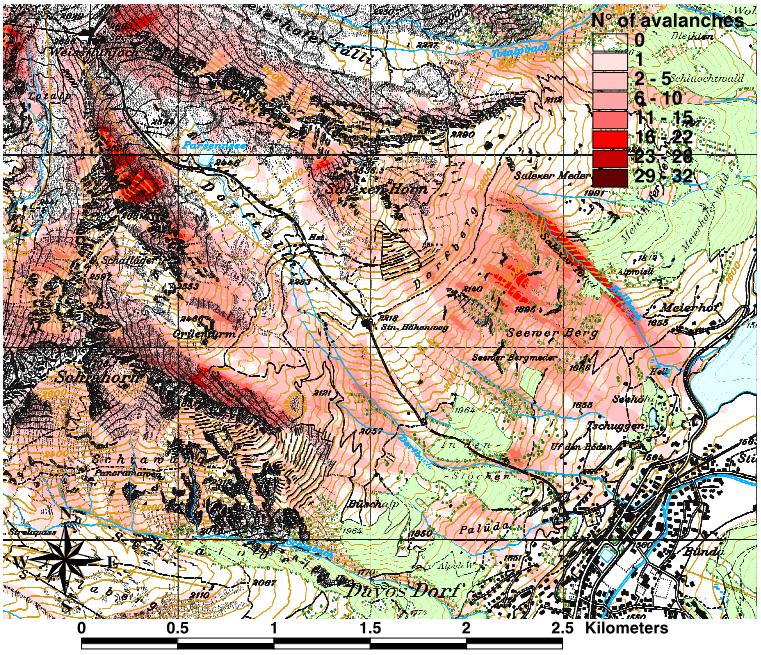

Figure 3.3: Avalanche frequency in the area of Dorftälli in the period 1949 - 1992. Topographic base map reproduced by permission of swisstopo (BA046644).

3.2 Description of the Database

In the region of Davos a large database of about 5000 avalanche events over the last 50 years is available. There are three defined areas where avalanches should be observed by ski-patrols and reported to the Swiss Federal Institute for Snow and Avalanche Research (SLF). They observe large avalanches causing damage or arriving at the valley bottom as well as smaller avalanches in the neighborhood of the ski pistes. The database is also supplemented by avalanche observations from back-country skiers and by avalanche security personel of the community of Davos. For the analysis performed in this research, natural avalanches of any types and dimension are relevant.

Every winter, the avalanches that occurred in this region are recorded in a winter report, *Winterbericht* [SLF, 2002], with annotations about each particular event. Moreover, all the avalanches recorded in these winter reports have been digitized in a GIS to create a digital database. The relevant information for the analysis performed in this study are the avalanche outline, the triggering (spontaneous or artificially triggered) and the width of the avalanche. For this study, the natural avalanches are of the most importance; 3297 natural avalanches are recorded in the Davos database (65% of the total recorded avalanches).

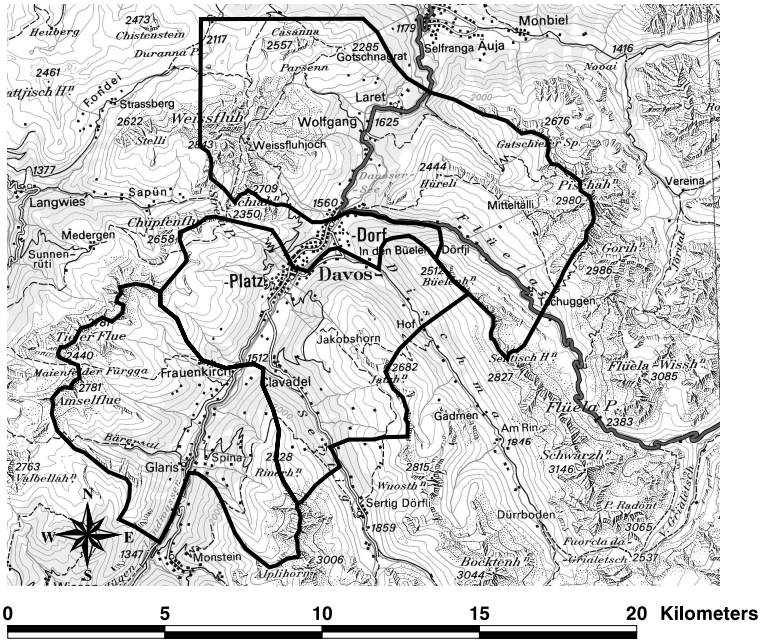

Figure 3.4: Overview of the region of Davos. The areas marked in black are where the ski-patrols should register observed avalanche events. Topographic base map reproduced by permission of swisstopo (BA046644).

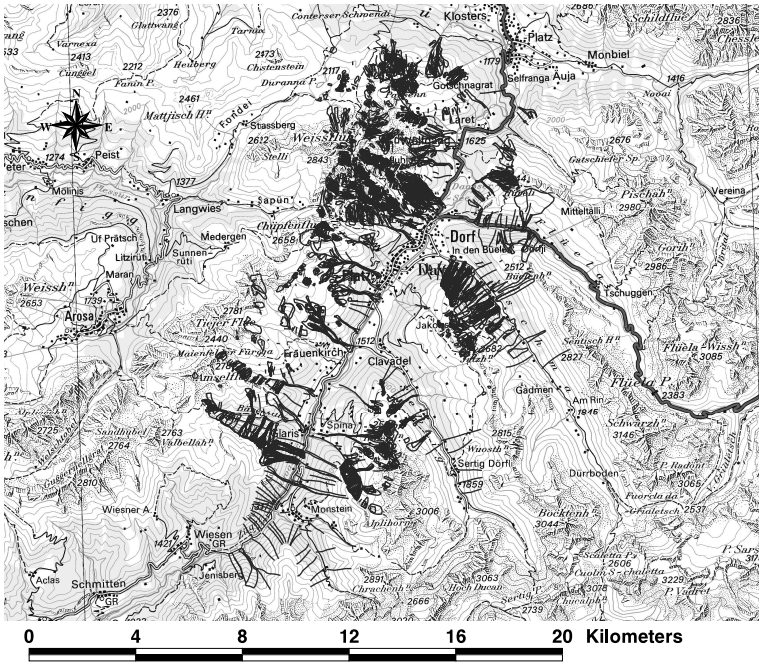

Figure 3.5: Overview of the digital database of Davos: natural avalanches (red lines). Topographic base map reproduced by permission of swisstopo (BA046644).

Unfortunately, precise information does not exist for all the avalanches recorded. As a consequence, the quality of the database is not homogeneous, because avalanches that occurred in areas far from villages or ski resorts or avalanches that happened at night or in a stormy period may not have been recorded or have been recorded with limited detail.

Figure 3.6 shows an example of the uncertainty in recording avalanche events. Most of these avalanches happened outside the controlled areas, but the three avalanches that are located in the right most part of the picture lie inside a ski-resort controlled area and were not reported by the ski-patrols. These avalanches released while it was still snowing slightly and, due to snow deposition, it was not easy to define precisely the avalanche outline. This is a clear example of the problems that influence the quality of the database.

Another study that can give insight as to the quality of the database of Davos was performed by SLF personnel at the end of February 2003 on avalanches that occurred on the days 6th-7th February 2003 [SLF, 2003]. It was a situation of high avalanche activity and many avalanches were not reported by the ski-patrols, who were probably busier with the security of the ski-resorts than with recording avalanches. This is understandable, but it is still an important source of error in the database, which has to be kept in mind while performing the statistical analysis.

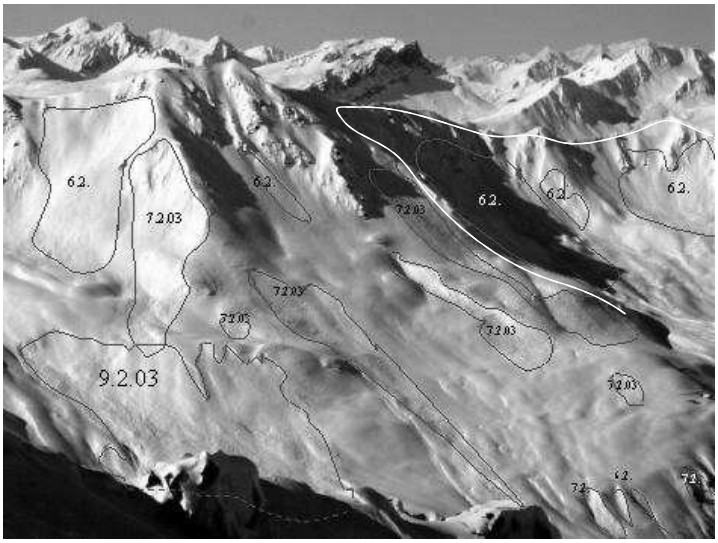

Figure 3.6: View from Sentischorn in the Western direction: avalanches observed on 10th February and not previously registered. The white line on the right delineates the boundary of the ski-area of Jakobshorn. Photo: T. Wiesenger, SLF.

Another example of poor data are the three avalanches that were released somewhere close to Monstein in the winter of 1951, which were recorded simply as a line on the map, even the day of their release is uncertain [SLF, 1952]. On other occasions, the person who recorded the avalanche event drew only the boundary of the deposition zone or of the upper limit of the release zone.

However, high quality data are also available; there are cases when even the lower limit of the release area (*Stauchwall*) was visible and recorded in the *Winterbericht*.

An example of such accurate data is the recording of the avalanche which naturally released on 26th January 1968 from the East side of Schiahorn at an elevation of about 2640 m a.s.l. (Fig. 3.7). This avalanche was well recorded and much detail is given in the *Winterbericht* [SLF, 1969], including pictures, information about the damage (see Fig. 3.8) and details of the rescue action and preventive measures adopted due to the critical meteorological conditions.

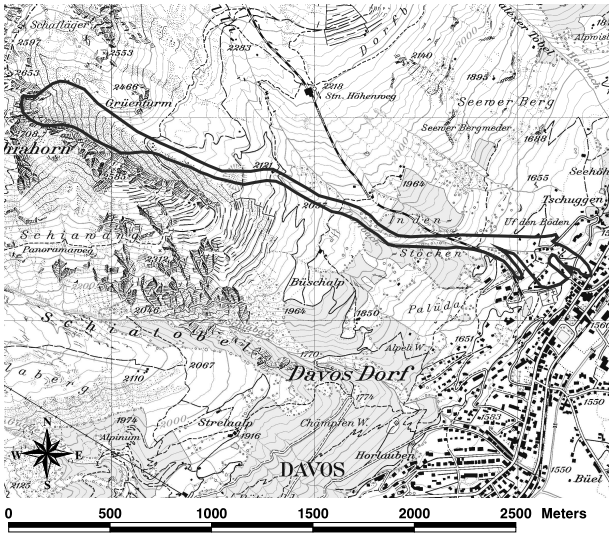

Figure 3.7: Perimeters of the Dorfbach avalanche in Davos Dorf on 26th Januar 1968. Example of a well recorded avalanche. Topographic base map reproduced by permission of swisstopo (BA046644).

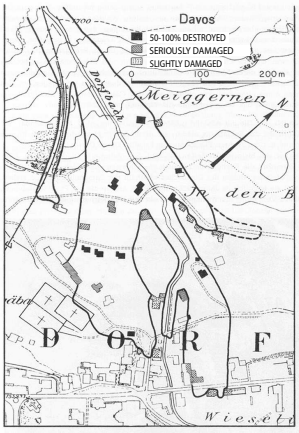

Figure 3.8: Dorfbach avalanche in Davos Dorf: one of the avalanches that in Winter 1968 produced most damage. Source: SLF [1969], p.97-98.

In summary, in Davos there exists a good but imperfect database. Unfortunately, there is no possibility to derive a measure of the quality of the recording of every avalanche, because the data cannot be anymore compared with the corresponding historical avalanche events.

3.3 Choice of the analysis and validation area

On the basis of all the considerations explained in this Chapter, a selection was made in order to consider only those areas which are easily visible from ski-resorts or from villages, i.e. areas where there is a good chance that all the avalanche events have been recorded (see 4.2.2). The region selected as study area for the analysis covers about 70 km^2 including the ski-resort of Jakobshorn, a part of the Parsenn ski-resort, the area around Hüreli and around Strelapass. The regions further north, from Gotschnagrat/Casanna down to Klosters, and the region further south, from Amselfluh on the Western side to Monstein on the Eastern side, were used as test areas to validate the whole procedure (Fig. 3.10). These three areas are similar: in all of them ski-resorts are present, the forest covers about the same proportion of the landscape and the topography is similar. Figure 3.9 shows that the distributions of the values of the slope-angle and of the plan-curvature have very similar patterns for the three regions, whereas, with respect to the aspect, the northerly validation area presents more northern aspect than southern one.

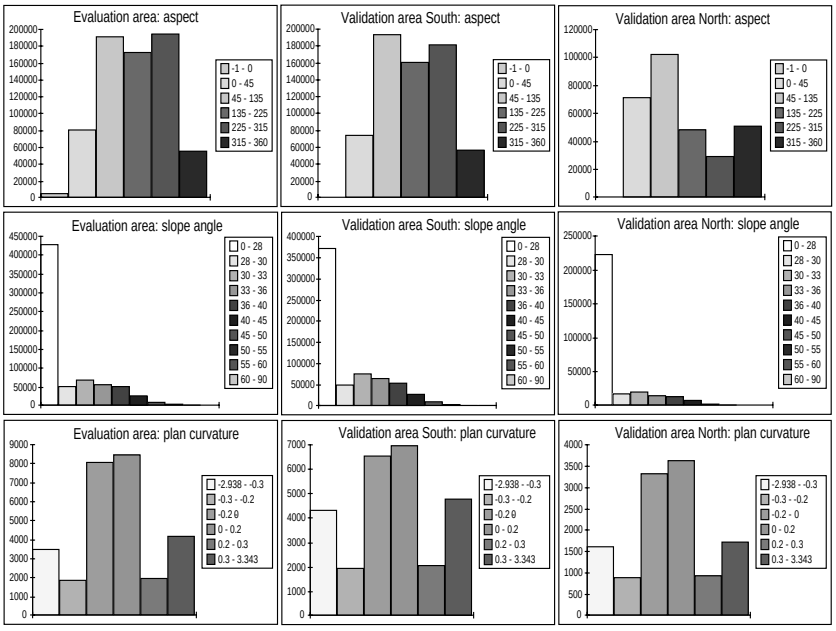

Figure 3.9: Distributions of the values of the slope angle (in degrees), of the aspect (in degrees clockwise from North, -1 - 0 means horizontal terrain (lake)) and of the plan curvature (in 1/100m) for the evaluation area, the validation area South and the validation area North (as in Fig. 3.10).

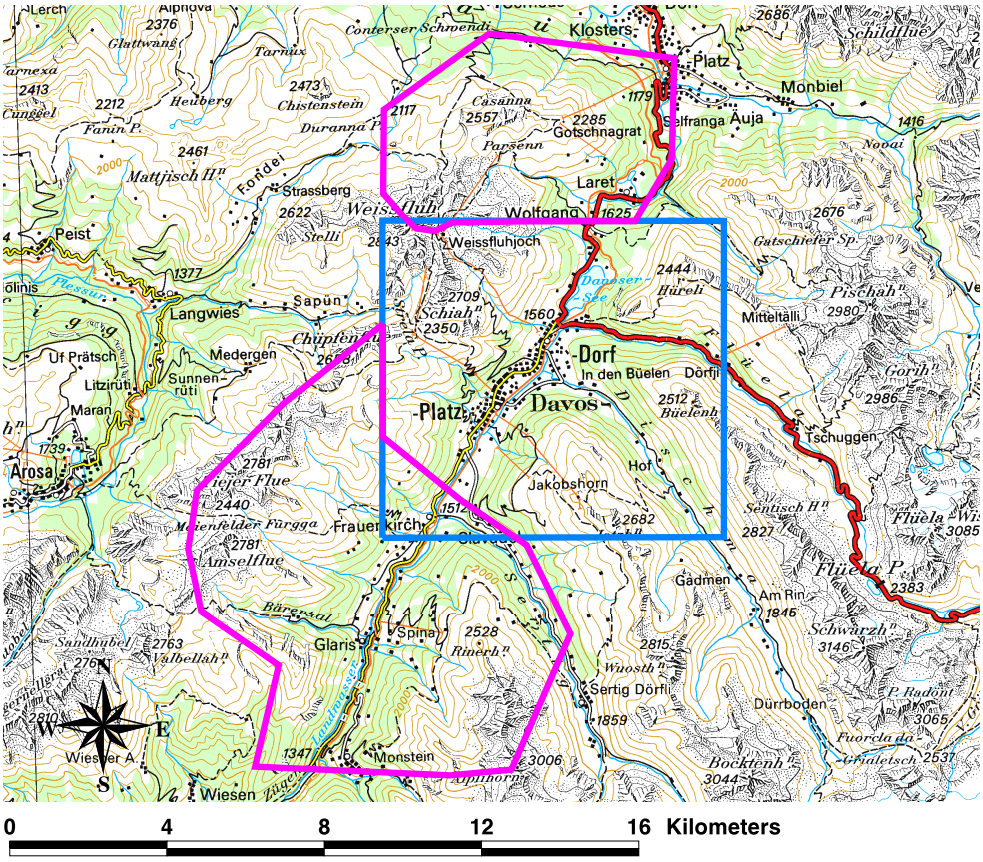

Figure 3.10: Selected areas for the evaluation area (blue box) and for the validation areas (pink polygons). Topographic base map reproduced by permission of swisstopo (BA046644).

Chapter 4

Potential avalanche release areas

4.1 Introduction

In this chapter three key questions about potential avalanche release areas are addressed:

1. Where are they found?
2. What are their topographic characteristics?
3. How are they related to avalanche frequency and extent?

With respect to the first two questions, many studies have already been done to try to localize potential avalanche release areas, some with respect to the avalanche hazard related to land use planning or safety of traffic roads [Margreth et al., 2003], others with respect to avalanche hazard related to recreational activities such as skiing, ski-touring, etc. [Jamieson & Geldsetzer, 1996; Weir, 1989]. Schmid & Sardemann [2003] developed a method to define release areas for very frequent avalanches (return period 3 years), to simulate those avalanches with a two-dimensional model, and to study the influence of the avalanche depositions on the presence of permafrost. McClung & Schaerer [1993] discuss in detail the characteristics of the starting zone of an avalanche.

In reality, whenever the avalanche hazard has to be assessed, the release area is one of the most important parameters that has to be determined. Until now, the common procedure for estimating avalanche release areas was based on critical slope angles and on site evaluation of avalanche paths. This study aims to develop a consistent and reproducible method to identify potential avalanche release areas on the basis of more topographical parameters, such as for example slope together with curvature and aspect. The combination of GIS techniques with an elevation model (DEM) is the most important characteristic in making this method a reproducible tool which can be used in different areas, provided a DEM is available.

The third question is an important point of this research, because here the avalanche activity is defined not only as the frequency of the avalanches [Stoffel

et al., 1998; Gleason, 1995; Glazovskaya, 1998], but as the frequency and also the extent of the release area of past events with respect to the total potential release area (PRA). The avalanche activity is represented by a release area distribution that describes how many avalanches occurred in a PRA and with what extent (see Section 4.4).

The initial three questions are taken to delineate the structure of this Chapter, which is divided into three parts giving detail descriptions of these steps:

1. Definition of PRAs based on rules related to topographical parameters (Section 4.2).

2. Characterization of the PRAs with more detailed topographical parameters (Section 4.3).

3. Analysis of real past avalanche events with respect to the defined PRAs (Section 4.4).

The goal of the first step was to identify all potential release areas and to split them into smaller coherent units that could be considered as standard to be the PRA of one single avalanche event. In theory, it is possible that all these slopes may release at the same time, but usually, avalanches occur on smaller portions that (a) are distinguished from each other by topographical features, such as ridges, and (b) show a certain topographical homogeneity within their extent. Yet, a general definition of the criteria that separate neighboring release areas from each other is not available. The goal of this step is to propose such a definition for a standard potential release area - remaining aware that this definition might fail in some extreme cases. However, for the purpose of this research, such a definition is essential in order to be able to automatically delineate potential release areas and to have an objective basis on which to carry out the analysis of the topographic parameters in the various PRAs. The PRA definition procedure is made of three steps which are referred to as (a), (b) and (c) in Section 4.2.

In the second step, small scale topographical parameters were derived from the DEM to characterize each PRA. Finally, in the third step, the release areas of the past avalanche events were analyzed with respect to their extent and frequency.

All the steps are based on automatic procedures using macro language AML (Arc Macro Language) of the GIS software ArcInfo [ESRI, 2001] so that they can be easily transferred to other areas. The DHM25 of the Swiss Federal Office of Topography was used as a DEM (resolution of 25 m). This also enables the transfer of the procedure to other areas in Switzerland, since this DEM is available for the whole Switzerland. With some adjustments, these procedures should also be usable in other regions outside Switzerland.

4.2 PRA definition

4.2.1 Method

A rule-based method was created in a GIS to define potential avalanche release areas. The rules are based on expert considerations about topographical parameters influencing avalanche release and on past studies of avalanche release. In this research, the following criteria were used: forest cover, slope, curvature, main ridges, size, aspect and altitude difference.

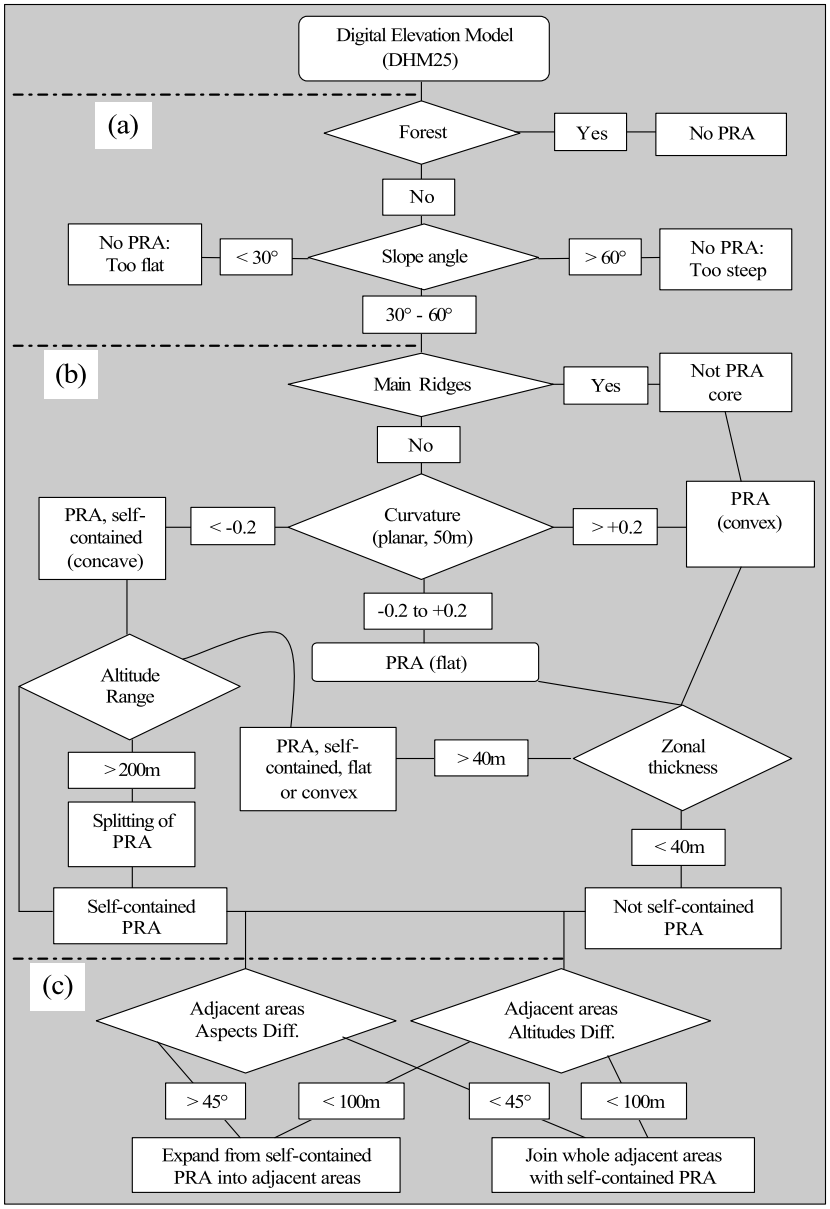

Figure 4.1: Procedure for the definition of Potential Release Areas: (a) Defining potential release areas, (b) Separating potential release areas, (c) Merging and expanding potential release areas.

Figure 4.1 gives an overview of the procedure, which is described in this chapter. The original input is the TIN of the region of Davos, derived from the DHM25 with the ArcInfo command *latticetin*, from which lattices with different cell size are derived, and a layer with the information about the forest cover (reproduced by permission of swisstopo (BA046644)). Some steps of the procedure were performed working with raster data and some others working with vector data, depending on the current need. The output is a raster where all the cells defined as belonging to any identified PRA take the identity value of that PRA and the remaining space is flagged as null. Then, this raster file is transformed to a vector file with polygon topology to analyze the results and to perform further analysis.

(a) Defining potential release areas

Here, the parameters forest and slope are used to define a large unique potential release area, that is then split using other parameters.

Forest

In general, avalanches can initiate on any slopes with a certain inclination unless dense forest is available to prevent avalanche initiation [Munter, 1997; SLF, 2000; Gubler & Rychetnik, 1991]. The use of forests as active avalanche protection is well known and much research has been done to identify the characteristics that make forest good avalanche protection [Frey et al., 1987; Schneebeli & Meyer-Grass, 1993].

The regions covered by forest are excluded from the potential release area simply subtracting the raster file representing the forest from the DEM.

Slope angle

Slope angle is the most important topographical parameter for avalanche formation. Systematic identification of release areas considers slope angles with values between 30° and 50°, occasionally 60°, to be ideal for avalanche initiation. Salm et al. [1990] suggested considering as release area, for dense avalanche calculations, regions with a slope angle between 30° (eventually 28°) and 50°. Schweizer et al. [2003], Butler & Walsh [1990], LaChapelle [1985] considered values between 30° and 45°. Perla [1977] found that the mean slope angle for 194 slab avalanches was 38° with a standard deviation of 5°; Schweizer & Jamieson [2001] analyzed 809 skier-triggered avalanches and found a mean slope angle of 38.8° ± 3.8°.

In the present study, only natural avalanches are considered and the hypothesis is that they can initiate on slopes with an inclination between 30° and 60° (Fig. 4.2). Below 30° the gravitational force is too weak to initiate an avalanche, whereas on slopes steeper than 60° avalanches are very frequent but of small dimensions, since avalanches occur before deep snow accumulates on such slopes.

The slope angle is derived from the digital elevation model, that has first been resampled to a cell size of 10 m, and only areas with slope angles between 30° and 60° are selected. The resampling procedure did not add any uncertainty because the distribution of the difference between the slope angle calculated

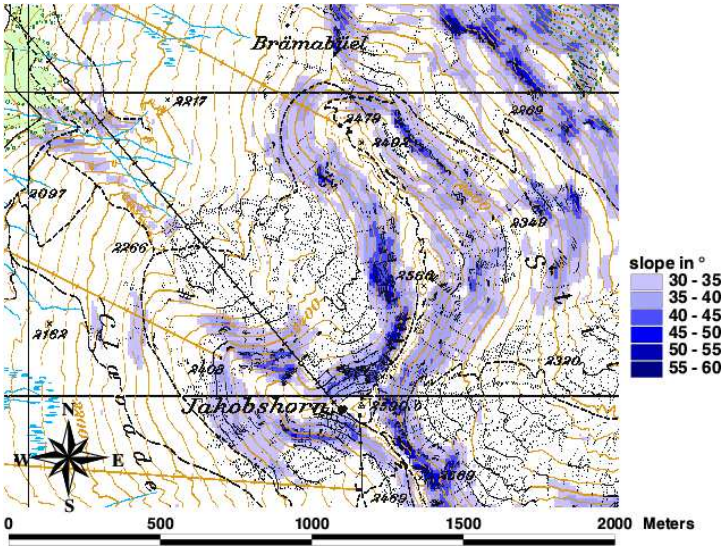

Figure 4.2: Selection of a potential avalanche release area based on the considered slope-angle condition. Topographic base map reproduced by permission of swisstopo (BA046644).

from a 10 m lattice and the slope angle calculated from a 25 m lattice has a standard deviation of 3.15°, which is of the same order of the uncertainty of the slope values calculated from the original DHM25.

(b) Separating potential release areas

The following parameters are used to separate the large unique potential release area into smaller units that can be related to single avalanche events.

Main ridges

Ridges are important terrain features which separate different cirques or areas with different aspect. Their importance is related to the phenomenon of snow-drift. Wind contributes to snow loading and is often considered the most active avalanche contributing factor after new snow [Schweizer et al., 2003]. Gauer [1999] measured the snow deposition and erosion pattern on both sides of a mountain ridge and found that, averaged over the whole slope, 20-30% more snow was deposited on the lee side compared to a study plot placed on flat terrain. For avalanche calculations, Salm et al. [1990] suggested an increase of the fracture depth by a factor linked to snow-drift for release zones that are influenced by this phenomenon.

Main ridges are excluded from a potential release area selected with the two previous criteria and used as separating feature. They are automatically derived from the DEM using a procedure which is the combination of the two methods explained briefly in the following:

1. Areas with large aspect change (>40°) and highly positive values of curvature (>1 1/100m) are selected with ArcInfo GRID commands, in order

to identify potential ridges (the corresponding part of the AML program is given in the footnote[1], in order to make the description of this method clearer for GIS specialists).

2. In this method, first, the original DHM25 is converted to a TIN (Triangular Irregular Network) with the ArcInfo command *latticetin* with the default values for the necessary parameters. Secondly, from this TIN, two lattices with different resolutions (10 m and 50 m) are derived with the ArcInfo command *tinlattice*. Then, the cell size of these two lattices is set to the same value (10 m). Finally, the difference between the z-coordinate of the two lattices is computed identifying regions with positive or negative values (Fig. 4.3). The regions with positive, respectively negative, values are considered as ridges, respectively gullies [Bertogg, 2001].

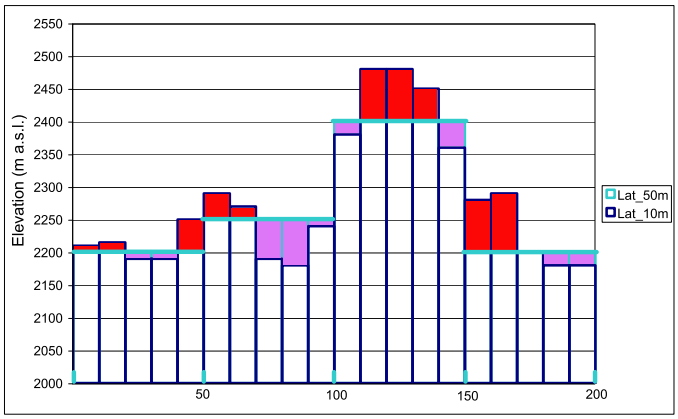

Figure 4.3: Determination of ridges and gullies with the method of the difference between lattices at different resolutions. The dark blue histogram represents the elevations of the points of the lattice at 10 m resolution, the light blue the elevation of the points of the lattice at 50 m resolution, resampled to a cell size of 10 m. Violet areas are gullies and red areas ridges.

The intersection of those two regions delineates the main ridges. In Figure 4.4 the results of the ridge definition for Bräemabüel show the quality of the procedure: sharp ridges were very well defined, whereas separation areas between a steep slope on one side and a flat slope on the other side could not

[1]First part of the AML code to define ridges. In bold is the condition already explained by words in the text; the last four operations have the goal of excluding ridges of small dimension. The inputs are two lattices with resolution of 10 m and 50 m):

```
aspect = aspect(lattice10)
der_asp = slope(aspect)
curv_50 = curvature(lattice50,prfcu50a,pcu_50a)
curv50_10 = resample(curv_50,10)
ridges = con(der_asp GT 40 and curv50_10 GT 1,1)
ridges_sum = focalsum(ridges)
ridges_sum1 = con(ridges_sum GT 0,1)
ridges_reg = regiongroup(ridges_sum1)
ridges_sel = con(ridgesreg.count GT 300,1)
```

be recognized as ridges. Changing the threshold values for the aspect change (45°, 50°) and for the curvature (1.5, 2) did not improve the results.

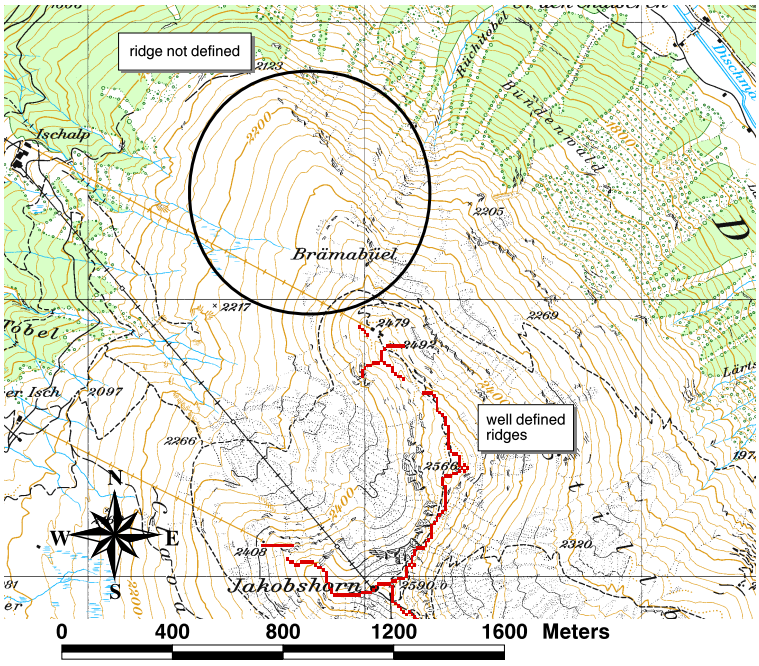

Figure 4.4: Result of the definition of main ridges. Topographic base map reproduced by permission of swisstopo (BA046644).

Curvature

Profile and plan curvature are determining factors for the acceleration/deceleration and convergence/divergence of near-surface flows [Gallant & Wilson, 2000; Mosley, 1974; D'Souza & Morgan, 1976]. They also affect the distribution of stresses in the ground and in any snow or ice cover. The shape of the slope influences deposition and depth of snow [Luckman, 1978]. Those paths that have a concave plan curvature, such as a bowl or a cirque, are able to trap blowing snow from several directions in relation to the wind direction [Armstrong & Williams, 1986], while on those paths that have convex plan curvature the snow is often blown away resulting in a thinner snow-pack. Gleason [1995] and McClung [2001] found that avalanches are more frequent in starting zones with concave plan curvature.

The plan curvature is used to separate concave areas from "flat" and convex ones. It is computed in GRID with the function *curvature* as explained in Section 2.5. The following criterion is adopted (Fig. 4.1):

- concave areas: plan curvature $\leq$ -0.2 1/100m
- "flat" areas: -0.2 1/100 $<$ plan curvature $<$ +0.2 1/100m
- convex areas: plan curvature $\geq$ +0.2 1/100m

The cell size of the DEM is reduced to 50 m so that only the large scale variations in curvature are considered, since the smaller scale topographical curvature changes are not capable of separating neighboring release areas from each other. The chosen value of -0.2 1/100m corresponds to an elevation increase of 2.5 m within 50 m of both sides of the center position [Schmid & Sardemann, 2003]. Areas with a value of plan curvature lower than -0.2 are considered concave PRA [Schmid & Sardemann, 2003; Maggioni & Gruber, 2003]. Independent of size, they are considered *self-contained*, i.e. they are classified as the core of one single potential release area. A sensitivity analysis on the threshold values for the plan curvature was performed and is discussed in Section 4.2.4.

Size

This research is oriented to avalanche hazard maps and therefore small release areas are not relevant for this work. The size of the areas is taken as a criterion for determining whether the "flat" and convex PRA (plan curvature higher than -0.2 1/100m) are big enough to be considered *self-contained*. A value of 5000 m^2 is taken as threshold value. Smaller areas are classified as expansion areas in which the *self-contained* PRA can be expanded (Fig. 4.6).

Altitude range

A *self-contained* PRA is split if its altitude range is more than 200 m. This differentiation is necessary since on steep and long slopes, where the critical slope angle never falls below 30° except for near the run out zone, the whole area would be assigned as one single PRA. This is not reasonable, since important criteria for the determination of avalanche frequency may vary along this distance, leading to a very inhomogeneous characterization of the PRA. The value of 200 m was arbitrarily introduced by visual comparison of the results to observed avalanche events. In the SLF experimental test site of Vallèe de la Sionne, very large avalanches were triggered and the altitude difference inside the release area (mean slope angle of 35°) was never more than 200 m, corresponding to an avalanche release length of about 350 m [Sovilla, 2004].

This separation is again performed in ArcInfo GRID. The maximum altitude inside each PRA is calculated and only cells with a value of altitude greater than *(maximum altitude - 200m)* are considered to belong to that PRA.

(c) Merging and expanding potential release areas

Aspect and altitude difference

Two additional criteria are used to arrive at the final potential release areas. Adjacent areas are merged if the altitude difference is less than 100 m and the mean aspect difference is less than 45°. In the remaining expansion areas the self-contained PRA can linearly expand.

These last steps are also performed working with raster data. A neighboring procedure is applied to check the values of aspect and altitude for those areas close to the considered PRA; the same identity number is given to PRAs that fulfill the merging criteria. After the merging, a recursive geometrical expansion of all the self-contained PRAs is performed, to fill the expansion areas (see

Fig. 4.5). The effect of the expansion of the self-contained PRAs into the expansion areas is clear in Figure 4.6.

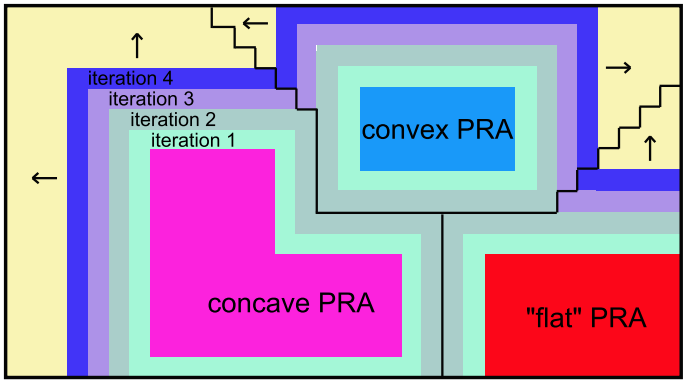

Figure 4.5: Geometric expansion procedure: the initial self-contained PRAs can expand recursively into the expansion area (yellow), resulting in the final PRAs drawn with thick dark boundaries.

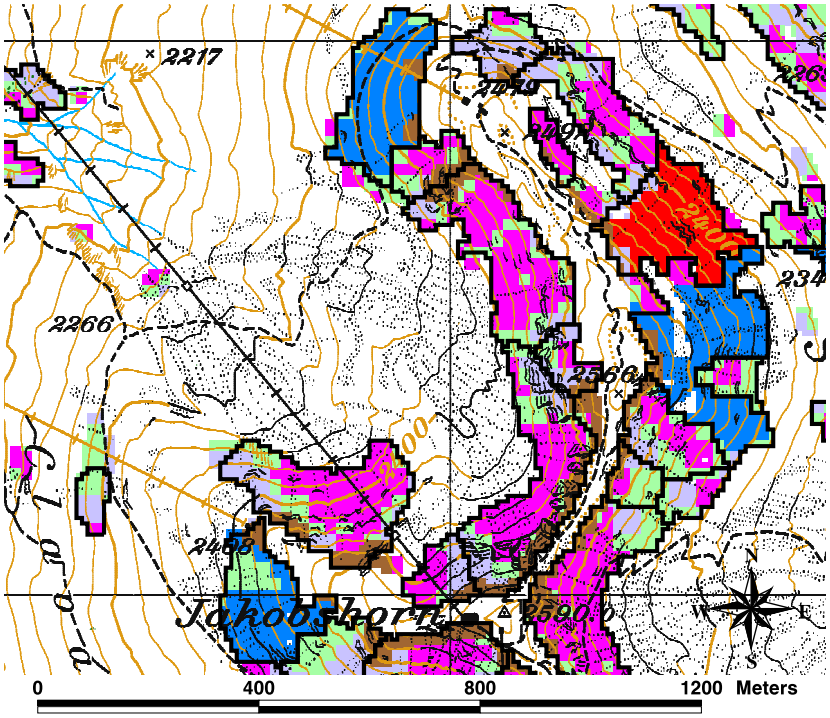

Figure 4.6: The black lines represent the boundaries of the PRAs resulting after the expansion procedure: pink, blue and red represent concave, convex and "flat" self-contained PRAs respectively, the other colors represent expansion areas. Topographic base map reproduced by permission of swisstopo (BA046644).

4.2.2 Results

The potential release areas defined by the automatic procedure applied in the selected area in Davos are shown in the following figures. Figure 4.7 gives an overview of the whole region. It shows the percentage of the evaluation area that is prone to avalanches, but the boundaries of single PRAs are not drawn. A more detailed view of Jakobshorn, with each individual PRA delineated, is given in Figure 4.8. Here, it is possible to recognize some release areas that were well defined and some others that were not. Therefore, five additional rules were introduced at the end of the automatic procedure to eliminate potential release areas that, for different reasons, are not relevant to definition of PRAs for the purposes of avalanche hazard mapping.

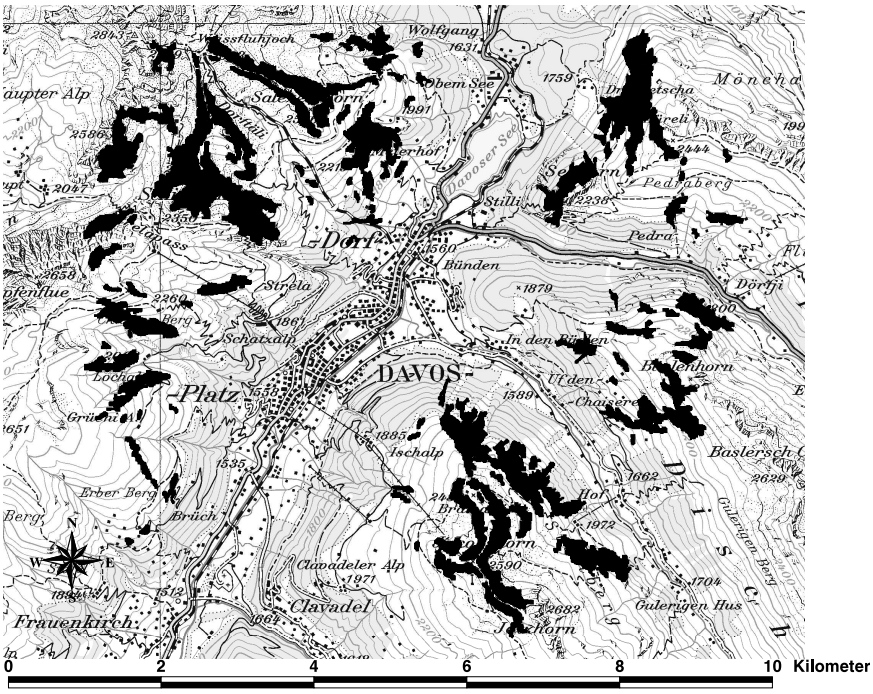

Figure 4.7: Overview of the potential avalanche release areas in the whole region of Davos (black areas). This figure gives a global overview and does not show the separation between each single PRA. Topographic base map reproduced by permission of swisstopo (BA046644).

The following PRA have been eliminated, those which:

- are smaller than 5000 m^2;
- contain avalanche protection measures;
- are between forest and belonging to the track of other avalanches;
- are below the forest, on the valley floor;
- are not visible from ski-resorts or villages.

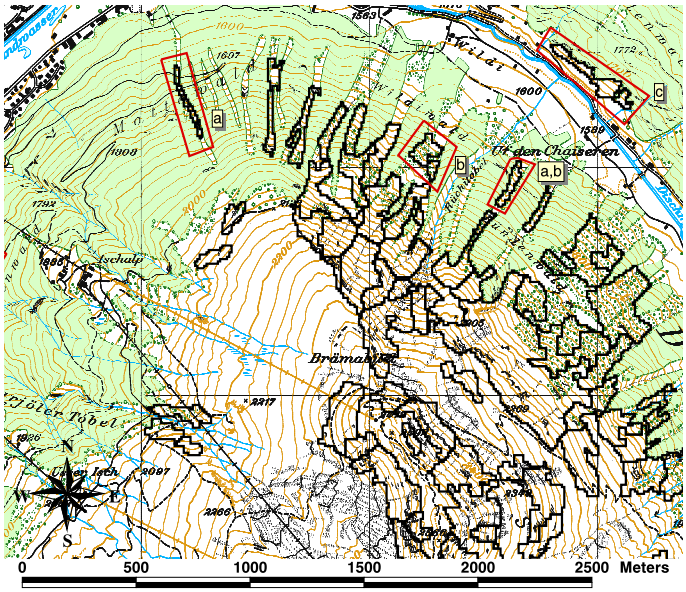

Figure 4.8: Result of the automatic definition of the potential avalanche release areas in a part of the selected area in Davos: Jakobshorn (before the expert selection). Outlined in red are examples of PRAs within forest (a), on the avalanche track of avalanches that initiate above (b), below the forest close to the valley floor (c). Topographic base map reproduced by permission of swisstopo (BA046644).

Many PRAs were deleted due to the first rule. It often happened that small areas with a slope angle greater than 30° were detected inside wider regions with overall flatter inclination. These areas are usually very small and really related to local changes in the topography, small scale changes not interesting in comparison to the scale of common avalanche release areas. As this research focuses on avalanches that are relevant for avalanche hazard maps, small release areas are not of interest since they are not able to produce avalanches belonging to a category important for avalanche hazard assessment (see Chapter 2.4).

Figure 4.9 presents a good example of automatically defined PRAs that cover exactly a zone where avalanche retaining structures have been built. The fact that this procedure is able to delineate such protected areas is an indication of the quality of the procedure. These areas cannot be included in the analysis of past avalanche events (Section 4.4), because the terrain was disturbed and the consequent avalanche activity is not comparable with that of other PRAs or with the activity before the defence structures have been built.

The PRAs defined in the region of Brämabüel are a good example of areas between forest and along the track of other avalanches. The slope north of Brämabüel is always above 30° and with an altitude difference of about 1000 m, therefore the rule of the 200 m is applied there to separate different PRAs. As Figure 4.10 shows, there exist steep channels in the forest which were defined as PRAs, but in reality are avalanche tracks. Based on these considerations, they were not included in the final PRA database.

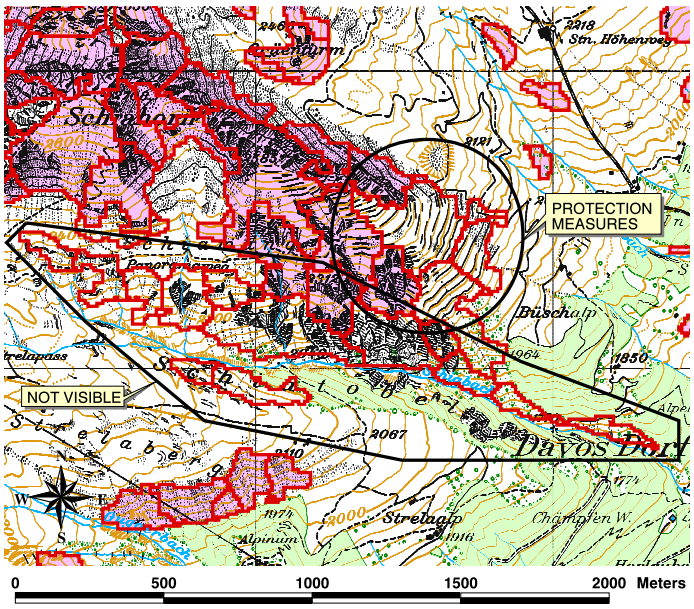

Figure 4.9: Example of expert selection of PRAs. The filled areas are considered as valid PRAs. The unfilled ones are not considered as PRAs, because the areas are not visible (Schiatobel) or because of the presence of avalanche protection measures (end of the South-East ridge of Schiahorn). Topographic base map reproduced by permission of swisstopo (BA046644).

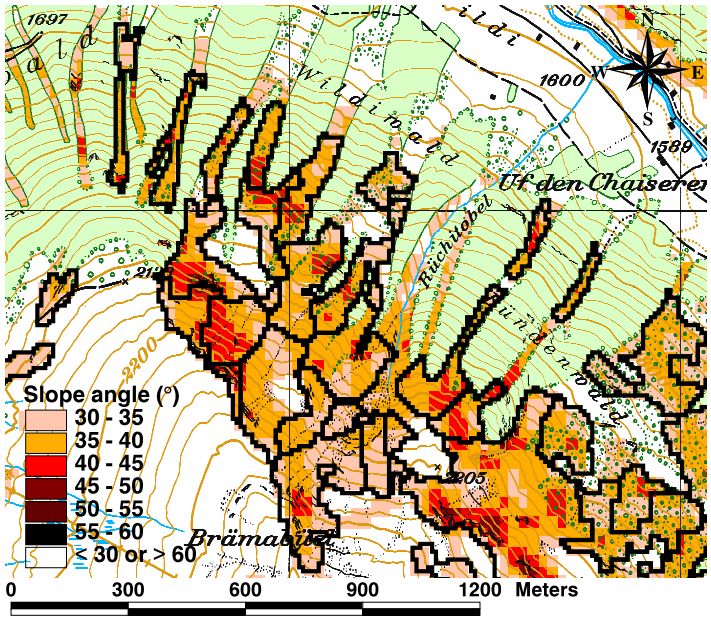

Figure 4.10: Map of Brämabüel: clearly visible are the steep channels between the forest, automatically delineated as PRAs but subsequently deleted because they are considered as avalanche tracks. Topographic base map reproduced by permission of swisstopo (BA046644).

With the proposed automatic procedure, areas close to the valley floor and/or below the lower limit of the forest were defined. In these locations, no avalanches have been observed and if any were observed, they would be only sluffs and thus not of interest with respect to avalanche hazard maps. Therefore those PRAs are excluded from the database.

The evaluation area was chosen around the village of Davos and includes parts of the ski-resorts. In Chapter 3, it was said that only areas visible from the villages or the ski-resorts are considered, but the evaluation area must be chosen as a rectangle because of some operations to be performed on the DEM. Therefore, most of the evaluation area is visible, but there also exist small portions within it which are not visible either from the ski-resorts or from the valley floor (see e.g. the Schiatobel area in Fig 4.9). The PRAs within these regions are eliminated because, even if well defined as PRAs, avalanches that occurred there might not have been recorded.

After this selection, the initial number of PRAs within the evaluation area of Davos reduced to 294, with areas ranging from 5000 m^2 to more than 100000 m^2. The attribute "size" was introduced to divide the PRAs database into smaller classes where the characterization procedure and the statistical analysis of past events were calculated separately. Since in Switzerland, previous to EAWS [2003], there existed no classification based on the size of the avalanche, as is the case in Canada [McClung & Schaerer, 1993], the classification shown in Table 4.1 was adopted.

4.2.3 Validation

The verification of the methodology was carried out by comparison of the automatically defined PRAs with the historical avalanche database, described in Section 3.2. The following were analyzed: areas with historical avalanches where PRAs were defined, areas with no avalanches where PRAs were defined and areas with historical avalanches where no PRAs were defined. In 83% of the defined PRAs, avalanches were recorded, while in 17% they were not. In Table 4.1 the number of PRAs with and without avalanches is shown, divided per PRA size class.

Table 4.1: Classification of the total 294 PRAs based on their size; PRAs with and without avalanches, for different PRA size classes.

Size-class	Area (m^2)	Number of PRAs	PRAs without ava	PRAs with ava
1	5000 - 10000 m^2	81	25	56
2	10000 - 30000 m^2	130	20	110
3	30000 - 50000 m^2	55	3	52
4	50000 - 100000 m^2	22	2	20
5	$>$ 100000 m^2	6	0	6

To check the areas where avalanches were recorded in the historical database but not defined as PRAs the following simple statistical analysis was performed. Out of the avalanche database (containing 3297 natural avalanches in total and

2082 in the evaluation area), avalanches that do not cross defined PRAs were extracted (440, 21% of the avalanches in the evaluation area). Then, some characteristics such as size, avalanche crossing forest, maximum slope angle and mean slope angle, were derived in the GIS and a statistical analysis was performed.

In Table 4.2, the distribution of these 440 avalanches between the different size classes is given. The size of the avalanches was computed in the GIS, taking the value of the area of the polygon when the avalanche was stored as a polygon, otherwise, if the avalanche was stored only as a line in the database, a buffering procedure was applied to build a polygon. The buffer distance was taken to be equal to the avalanche width given in the database, when this information was available, otherwise equal to 20% of the length of the line. This buffering procedure is also used in the statistical analysis of the historical data in Section 4.4.

Table 4.2: Size distribution for the 440 avalanches that released where no PRA was defined (21% of the total number of natural avalanches that occurred within the evaluation area). Size classes defined as in Table 4.1.

Avalanche Size	Number of avalanches	Percentage
1	300	68.2%
2	72	16.4%
3	12	2.7%
4	29	6.6%
5	27	6.1%

The analysis of how many avalanches started inside forested areas was performed manually on the map. There are 26 avalanches (out of those 440 which are in areas where no PRAs were defined) with release area in the forest (5.9%) and 18 just above the forest (4%), giving a total of around 10%.

The analysis of the release areas of avalanches with respect to their mean and maximum slope angle was performed in S-Plus:

- 326 avalanches (74%) released from areas with a mean slope of less than 30° (Fig. 4.11 (a)).
- 176 avalanches (40%) started from an area with a maximum slope angle smaller than 30° (Fig. 4.11 (b)).

In summary, within those 440 avalanches which released from areas not delineated by the procedure presented in this research, 10% released within areas that were mapped as forest and 74% had the release area within regions with a mean slope angle of less than 30°. Within those 440 avalanches, 59 belong to size class 4 and 5 and 29 of these released from areas with a slope angle of less than 30°. The avalanches of large dimension are important with respect to avalanche hazard mapping, therefore it is important that they are identified. There are several possible reasons why they were not properly identified. Most importantly, these problems might be related to the quality of the database, as discussed in Section3.2. In fact, many of those avalanches are drawn as lines

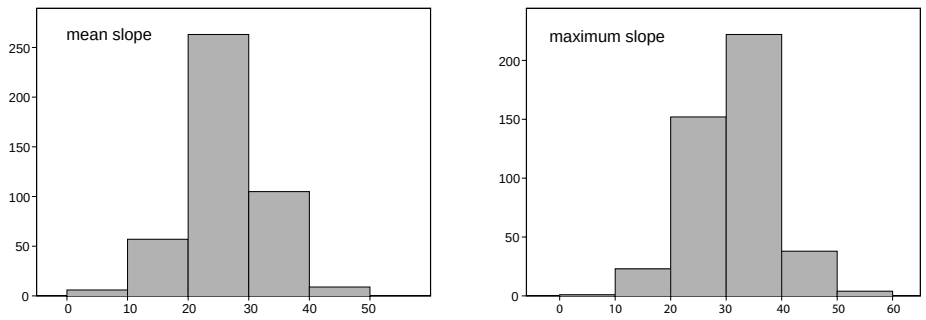

Figure 4.11: Mean slope (a) and maximum slope (b) distributions for the avalanches that occurred where no PRAs were defined.

starting from areas with a slope angle of less than 20°, a slope angle that is considered too low for avalanche releasing. Perhaps this might be due to an oversight or lack of care of the observers when drawing the lines on the map.

The value of 30° was taken as threshold value for avalanche releasing on the basis of many past studies carried out on the same topic. It is a well accepted value in avalanche literature. Figure 4.23 in [McClung & Schaerer, 1993] shows the distribution of the values of the mean slope angle for the release area of dry slab avalanches and shows that 5% of the analyzed avalanches released within regions with a mean slope angle smaller than 30°. Perla [1977] found that less than 5% of 194 dry slab avalanches had a release area less steep than 30°. In the present research, on 2082 avalanches, a percentage of 15% released within regions with a mean slope angle of less than 30° (Table 4.3).

Table 4.3: Avalanches which released within regions with a mean slope angle smaller than 30°.

Slope angle	Number of avalanches	Percentage
$< 20°$	63	3%
20° - 24°	124	6%
25° - 29°	138	6%

Combining the conditions "mean slope angle smaller than 30°" and "crossing forest avalanche", implies that a total of 80% of the avalanches that started where no PRAs were defined by the automatic procedure, have the release area with at least one parameter that breaks the rules used to define the PRAs. This means that only 20% of the historical avalanches that released where no PRAs were automatically defined (440), started within regions that fulfill the rules of the automatic procedure but were not defined as PRAs. On the total number of the avalanches in the evaluation area (2082), these 20% of 440 avalanches mean about 90 avalanches which should have been identified from the proposed procedure, because they released within areas with a slope angle greater than 30° and not within forest, but they were not. Because of this fact, an analysis of the avalanches which started where no PRAs were identified was performed manually on the map.

This manual analysis highlighted again some problems related to the quality of the database (see Section 3.2). Some avalanches have been recorded on the map in regions with a slope angle of less than 25° (in one case only 12°), values considered too low for avalanche release (unless they were wet avalanches, but this was not the case: they released in high winter season). The other problem is the accuracy of the DEM. Some small avalanches had a release area comparable to or even smaller than the cell size (10 m) of the lattice used in the analysis. In this case, their detection is almost impossible and it would result in an area composed of one single cell which would be deleted anyway, due to the selection rules included in the procedure (see Section 4.2.2).

Another analysis was conducted manually on the maps to check the length of these 440 avalanches. Except for 49 avalanches that have a length of more than 500 m, the other avalanches are of small size and therefore are not interesting in terms of avalanche hazard maps. The fact that the corresponding PRAs were not defined by the proposed procedure seems to be not a problem for the purpose of this research.

In conclusion, the percentage of historical avalanches that released outside the PRA identified by the procedure presented in this work is 21% of the total; this means that this method identified about 79% of the release areas of past avalanche events.

Another analysis was carried out to study in detail the 79% of historical avalanche release areas which were identified by the proposed procedure of defining potential release areas. By means of an AML procedure, a count is made of how many avalanches released within a single defined PRA and how many avalanches have a release area covering more than one single PRA. This gives additional information about the procedure of separating the big initial potential release area, defined with the common rules related to the forest cover and to the slope angle (Section 4.2.1(a)), into smaller units that can be related to single avalanche events (Section 4.2.1(b)). These results indicate that some 40% of these avalanches released from more than one PRA, and some 60% released from single PRAs. In other words, individual PRAs are related to individual avalanches in slightly more than half of the historical database. The procedure to check avalanches within multiple PRAs was done automatically and anytime an avalanche started from more than one PRA the related count increased by 1. No difference is considered whether an avalanche released 99% inside one PRA and only 1% inside another other PRA or if an avalanche has a release area covering two PRAs with almost the same percentage. This analysis is seen as a further possible check and may give better information on the quality of the procedure.

4.2.4 Discussion

The definition of potential avalanche release areas with methods that consider several topographical features was a first attempt to improve the common rule related only to the slope angle of the terrain. The resulting PRAs were not perfectly defined, however, the results show that 79% of the release areas of past avalanche events were identified by the proposed procedure.

This analysis was performed in an automatic way, with the help of a GIS, in order to have a reproducible and objective tool which could be helpful in delineating the possible release area for a specific avalanche site. An expert who has to assess the avalanche danger in a specific site could find such a tool a valuable addition. Buisson & Charlier [1989] have already indicated the importance of a knowledge-based or expert system to help specialist consultants in avalanche path analysis.

This study is another approach along the same lines as that suggested by Buisson & Charlier [1989]. However, topographical attributes as used in this procedure to identify PRAs are not the only ones that may be used. Further research could be done to find other attributes, e.g. surface roughness, that might improve the procedure of defining potential avalanche release areas presented in this work. From statistical analysis of past events, it is widely accepted that slope angle is one of the most important factors influencing avalanche release [Schweizer et al., 2003; Salm et al., 1990; Munter, 1997; Ghinoi, 2003]. This work is the first that has tried to identify potential avalanche release areas with a systematic procedure that combines more topographical factors.

For many steps of the procedure threshold values were used to separate different cases and perform the appropriate operations (Fig. 4.1). For the slope angle, 30° was taken as the lower limit and 60° as the upper limit. When these limits were changed to 28° and 50° [Salm, 1982], the results changed only slightly (Fig. 4.12). Therefore the values 30° and 60° were kept in the procedure proposed in this research. The same sensitivity analysis was done with respect to the parameter plan curvature and also in this case, the results showed only small differences (Fig. 4.13). The initial values of $\pm$ 0.2 1/100m were thus kept. The results of the sensitivity analysis with respect to the choice of the threshold values for slope angle and plan curvature were also checked directly on the map and the choice of 30°-60° for slope angle and of $\pm$ 0.2 1/100m for plan curvature resulted in better defined potential release areas in comparison to the results related to the choice of other threshold values.

Another point of discussion is which is the best DEM resolution to detect terrain features that can influence the frequency of avalanches of a certain size. For some parameters, for example curvature, a resolution of 50 m is acceptable or even better than a smaller one, in order to get a global view of the curvature of a PRA and not to consider small scale terrain changes. In addition, in the winter season, the natural terrain is often smoothed by wind transported snow. Since most avalanches glide on existing snow cover layers and not on the natural terrain itself (except for full-depth avalanches), a slight smoothing of the digital terrain model should not influence the accuracy of the procedure.

Another approach to detect terrain features is discussed by Wood [1996], who introduced a way to extract terrain characteristics from a DEM taking into account scale dependence. He used always a digital elevation model with a constant resolution of 50 m and varied the moving window from 3x3 cells to 69x69 cells; then he distinguished locations that are consistently classified as the same feature from locations that have a high degree of scale dependency in their classification. As Figure 2.7 shows, what may be a channel at one scale may be a ridge at another scale. This underlines the importance of the choice

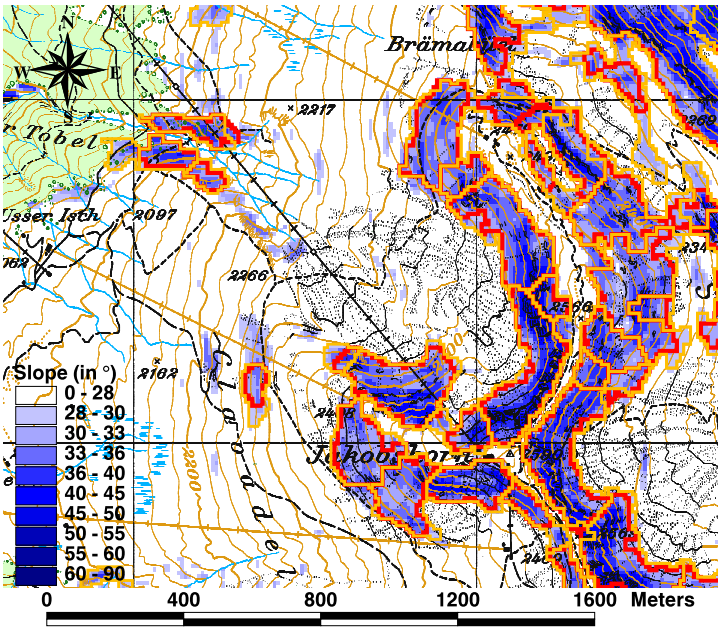

Figure 4.12: Results of the PRA definition procedure using two different selection criteria for the slope angle: 30° and 60° (red line) or 28° and 50° (orange line). Topographic base map reproduced by permission of swisstopo (BA046644).

of the dimension of the moving window with respect to the scale of the problem that is addressed. What could also have been used in the proposed procedure to get a global view of the curvature of the terrain, and not all the small terrain changes, is a moving windows of 9x9 cells (instead of the standard 3x3 cells window used in ESRI [2001]), which has the effect of smoothing the terrain. However, in this research, the approach of Wood [1996] is not used, but the one described of degrading the resolution of the DEM from 25 m to 50 m.

For the global procedure of defining PRAs the resolution of 25 m of the Swisstopo DHM25 is considered good enough if compared to the scale of avalanche release areas. Moreover, the idea was to be able to apply this procedure to other areas in Switzerland, where a DEM with a resolution higher than 25 m is not always available, whereas the DHM25 covers the extent of the whole of Switzerland. However, the DHM25 is sometimes insufficient to recognize correctly small features and release areas.

The validation shows that about 80% of the release areas of past events were correctly defined with the PRA definition procedure that used as input the DHM25 (Section 4.2.3). Most of the avalanches whose release areas were not identified correctly, were either small or released on slopes where the DEM shows a slope angle of less than 30°. This can be related either to the inaccuracy of the avalanche recording or to the inaccuracy of the DEM. For the purpose of this work, the quality of the PRA definition procedure is considered sufficient.

Another possible approach to validating the model would be the approach

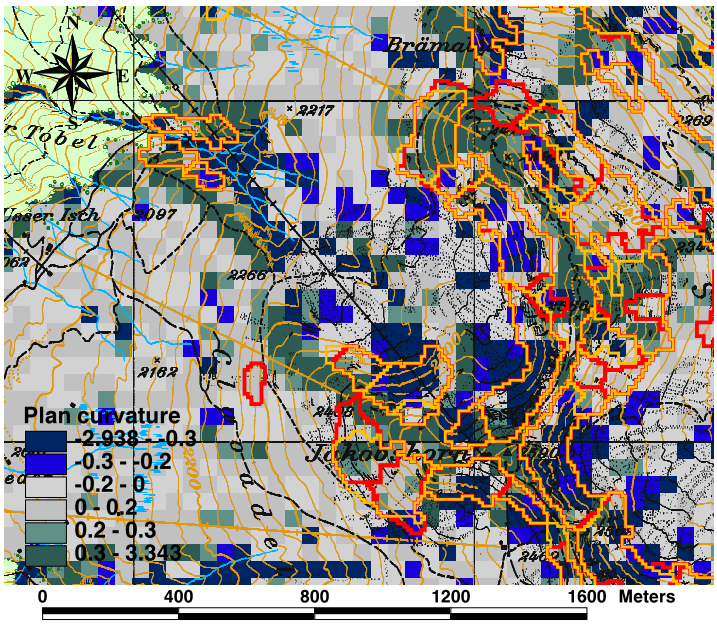

Figure 4.13: Results of the PRA definition procedure using two different selection criteria for the plan curvature: ± 0.2 1/100m (red) or ± 0.3 1/100m (orange) to delineate concave, "flat" and convex areas. Topographic base map reproduced by permission of swisstopo (BA046644).

of Ghinoi [2003]. In that study, the past avalanche events occurred in Alta Badia (Dolomites, Italy) and in Tyrol (Austria) were analyzed with respect to their topographical characteristics. Based on the most common topographical parameters within the release area of those recorded avalanches, a model was created to predict new potential avalanche release areas, in terms of susceptibility. It is a pixel-based analysis, where each pixel of the DEM of the considered region is described by a combination of its topographical characteristics and a value of susceptibility. The application of the model by Ghinoi [2003] in the region of Davos could be used to check if the areas with higher susceptibility fall inside the PRA defined with the proposed procedure. Such an approach is recommended for the future.

4.3 PRA topographical characterization

4.3.1 Method

After the PRA definition, the second step of the procedure is to perform a detailed topographical characterization of the automatically defined potential release areas. The aim is to find the most representative topographical parameters, in order to characterize each PRA and try to link these characteristics to different avalanche activities (Chapter 5). The characterization procedure is applied inside each size class (defined as in Table 4.1).

During the first step of the definition of PRAs, some expansion procedures were applied in order to assign the maximum extent of a potential release area. However, for the topographic characterization of the PRA, only the core of the PRAs is considered. It is better to consider only the most representative area of the PRAs and to neglect their boundaries because they may differ significantly from the core area and therefore can influence some of the characterizing parameters. For example, the expansion of a concave self-contained PRA into an expansion area which has values of plan curvature around of 0 would lead to a characteristic value of the plan curvature for that PRA that is not representative of its core.

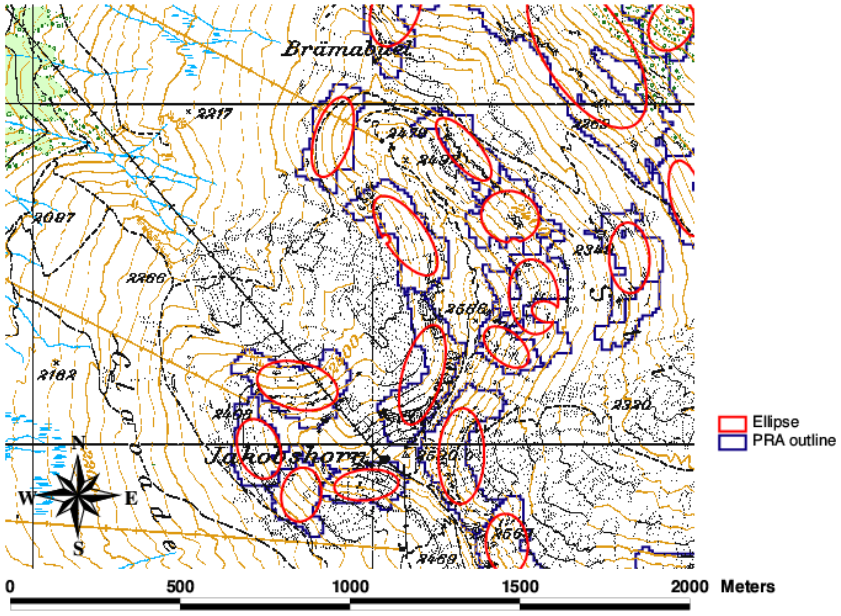

Figure 4.14: Ellipses related to the core area of the PRA in which the characterization is performed. Topographic base map reproduced by permission of swisstopo (BA046644).

The idea was to represent the core of each PRA with an ellipse fitted to its boundaries. The center of each PRA was identified and the geometrical parameters related to the ellipses that best fit the PRAs were determined. With this information, an AML program was written to build the ellipses for every PRA. In Figure 4.14, the ellipses in the area of Jakobshorn are shown. The intersection between each PRA and the related ellipse gives the area in which the topographical characterization is performed. Another justification for using ellipses is that they give further useful information, e.g. the main orientation of the PRA (see later in this section), for the characterization procedure.

The following terrain parameters are considered to represent the characteristics of every PRA:

1. Mean slope angle (in degrees)

2. Standard deviation of slope angle (in degrees)
3. Maximum slope (in degrees)
4. Mean aspect (in degrees clockwise from North)
5. Distance to the next ridge (in meters)
6. Shape
7. Plan curvature (in 1/100m)
8. Profile curvature (in 1/100m)
9. Maximum profile curvature (in 1/100m)

In Section 2.2 and 4.2.1, many reasons for considering slope angle as an important parameter with respect to avalanche release have already been given. However, in the characterizing procedure, not only the mean slope angle, but also the variation of the slope angle within a PRA and the maximum slope angle are considered. These are also important parameters to characterize a potential release area because they give information about the distribution of the value of the slope angle and therefore the homogeneity of the PRA in this respect. *Mean slope angle*, *Standard deviation of slope angle* and *Maximum slope angle* are calculated in GRID from the raster of the slope angle of the evaluation area.

Mean aspect is derived from the grid of the aspect of the evaluation area. Because of the circular nature of this variable, the initial grid of aspect was transformed in order that a 0° aspect is considered equal to a 360° aspect.

The feature *Distance to the next ridge* is important because of the influence of snow drift, which is much more relevant for areas close to ridges (see Section 2.2 and 4.2.1). *Distance to the next ridge* is calculated computing the euclidean distance between the ridges and each cell belonging to the PRA and taking the minimum value.

The feature *Shape* gives an indication of the orientation and of the shape of a PRA; it defines the PRA's length/width ratio and how the PRA is oriented in respect to the mean aspect (the *length* of the PRA is defined along the direction of the mean aspect and the *width* along the perpendicular direction to the mean aspect). *Shape* is calculated using the ratio between the major and the minor axis of the ellipse in combination to the mean aspect of the PRA; three classes are distinguished (Fig. 4.15):

- Class 1: the ratio between the major and the minor axis is greater than 1.5 and the orientation of the major axis is equal to an angle that does not differ more than 45° from the mean aspect (the PRA is longer than it is wide).
- Class 2: the ratio between the major and the minor axis is less than 1.5. The orientation with respect to the mean aspect has no importance.

- Class 3: the ratio between the major and the minor axis is greater than 1.5 and the orientation of the major axis is equal to an angle that differs more than 45° from the mean aspect (the PRA is wider than it is long).

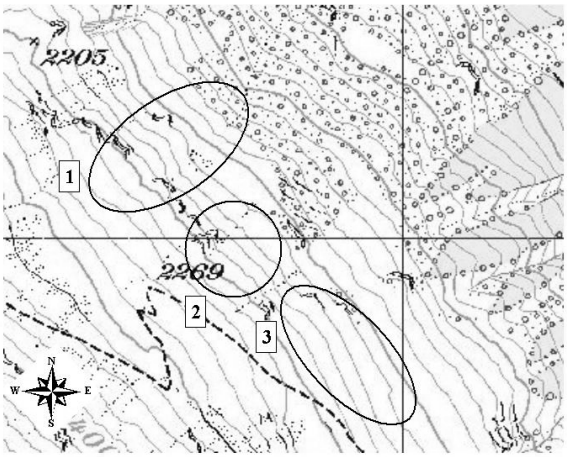

Figure 4.15: The three different classes for the parameter *Shape*, related to the ratio between the major and minor axis and to the orientation of the ellipse with respect to the mean aspect of the PRA. Topographic base map reproduced by permission of swisstopo (BA046644).

Plan curvature and *profile curvature* are important to describe the shape of the terrain of the potential release areas (Section 4.2.1). They can be calculated in different ways (see Section 2.5). In this study, they are calculated using the GRID function *curvature* combined with the information related to the ellipses. The idea is to find the right resolution of the lattice to be used to compute the plan and profile curvature for each PRA depending on the size of the PRA itself. The size of every PRA is related to the length of the axis of the corresponding ellipse. To explain better the procedure, a single PRA is taken as an example (Fig. 4.16). First, the relation between the mean aspect and the orientation of the corresponding ellipse is considered – the orientation is defined as an angle between the x axis and the major axis of the ellipse. The values of the orientation increase counterclockwise starting from 0° in the East (horizontal, to the right) and going through 90° when the major axis is vertical (mathematical definition of direction angles, ESRI [2001]). For the example in Figure 4.16, the mean aspect is equal to 351° and the orientation of the ellipse is equal to 168°. The orientation has first to be transformed to azimuth values, in order to be able to compare it to the mean aspect, which is calculated from the North and increasing clockwise. The value of the orientation in the mean aspect reference system is equal to 282°. The difference between the orientation and the mean aspect is 69°. Therefore, in this case, the major axis is considered as the width of the PRA (equal to 245 m) and the minor axis is considered as the length of the PRA (128 m). The next step is the choice of the resolution of the lattice in relation to the width and the length of the PRA to compute the plan and the profile curvature, respectively. Since plan and profile curvature are calculated

on a 3x3 window in ArcInfo GRID (see Section 2.5), the choice of the correct lattice resolution is important in order to have 3 cells inside the ellipse. In the example, a lattice with a resolution of 100 m is chosen to compute the plan curvature and a lattice with a resolution of 50 m is chosen to compute the profile curvature (see Fig. 4.16b). All the different possibilities are taken into account and implemented in an AML program which operates internally on all the PRAs.

The *Maximum profile curvature* is a very local characteristic, which says if there is a point where the slope angle is changing considerably. There exists more stress in the snowpack in the proximity of abrupt changes in the slope. For example, Föhn et al. [2002] state that a change from 28° to 40° (positive value of the profile curvature) produces local tension in the snow cover, resulting in a likely triggering point for avalanches. *Maximum profile curvature* is calculated as follows. The mean aspect of each PRA is used to build a gridded line that starts from the center of the related ellipse and ends at the boundary of the ellipse (or at the boundary of the PRA, if this is reached earlier), following the direction given by the mean aspect (red line in Fig 4.16a). Along this line, the profile curvature is computed using a DEM with a resolution of 10 m. This is done for all the PRAs and the result is a grid composed of 294 lines, one for each PRA. On this grid, the maximum profile curvature for every PRA is calculated.

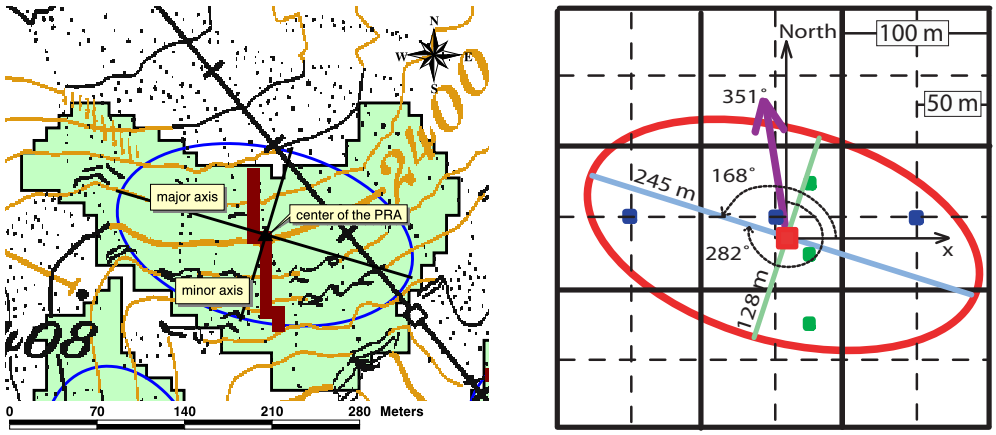

(a) (b)

Figure 4.16: Example of a PRA with the related ellipse: (a) the red thick line crossing the center of the PRA is the gridded line on which the maximum profile curvature is computed (Topographic base map reproduced by permission of swisstopo (BA046644)); (b) the blue and green points are the center of the cells used for the computation of the plan and profile curvature, respectively.

4.3.2 Results and Discussion

After the characterization procedure, a database with all the potential release areas defined for the region of Davos and their topographical characteristics (as described in Section 4.3.1) is available. The results are stored in a table of

294 rows and 9 columns for the topographical parameters. An extract from the database is shown in Table 4.4.

pranumber	Maspect	Mslope	Std-slope	Maxslope	Dist-ridge	plc-curv	prf-curv	Maxprf	shape
20255	104	37	5.223	49	57	-0.157	-0.153	4.747	3
21094	88	36	3.415	45	184	-0.674	0.305	1.875	3
20110	59	36	2.698	42	0	-0.125	0.116	1.025	3
22979	29	40	3.056	46	20	-0.180	0.221	1.214	2
7961	26	38	2.432	42	0	0.276	-0.347	1.521	3
20905	74	40	5.305	53	25	-0.012	0.624	2.67	3
20270	123	35	3.185	41	5	-0.437	0.934	2.822	3
20516	213	40	3.58	47	0	-0.221	0.687	1.754	3
21623	152	36	3.03	41	993	-0.709	-1.533	1.427	3
21415	38	44	11.281	59	0	-0.101	4.273	7.789	3

Table 4.4: Extract of the final table with the values of topographical parameters used to characterize the PRA. Mean and maximum slope angle are in degrees, mean aspect is in degrees starting from the 0° of the North and going clockwise, distance to ridges is in meters; the others are unitless.

The stratification of the database according to PRA size was adopted since *size* is important in defining avalanche size and therefore hazard. The characterization according to topographical parameters is performed separately inside each size class.

Related to the resolution of the lattice is the fact that the values of some topographical parameters such as mean and maximum slope angle or mean aspect may vary if a different cell size is used in the characterization procedure. Simple sensitivity analysis was performed to see what differences resulted if a lattice with a cell size of 50 m was used to compute the above mentioned parameters. In Table 4.5, the summary of this analysis shows that the mean value of the difference is 5° for the mean aspect, 3° for the mean slope and 8° for the maximum slope, values which are unlikely to produce a significant difference in the characterization of the PRA with respect to the statistical analysis of the topography and avalanche activity (Chapter 5).

Table 4.5: Summary statistics for the distributions of the difference between the mean aspect, the mean slope and the maximum slope calculated with lattices with cell size of 10 and 50 m, respectively.

Statistical attribute	Mean aspect	Mean slope	Max slope
Min:	0.00	0.00	0.00
1st Qu.:	1.00	1.00	5.00
Mean:	4.99	2.77	7.92
Median:	2.00	2.00	7.00
3rd Qu.:	4.00	4.00	10.00
Max:	97.00	14.00	30.00
Std Dev.:	12.64	2.35	3.93

In this study, nine topographical parameters are used for the characterization of the PRA. The basic idea was to start considering several topographical

parameters to characterize potential avalanche release terrain in order to analyze the possible relation between them and the associated avalanche activity (Chapter 5).

4.4 Analysis of the past avalanche activity

4.4.1 Method

The last step of the procedure is the analysis of past avalanche data and the derivation of the release area distributions for each defined PRA.

The size of the release area of each recorded avalanche is compared to the total extent of the corresponding PRA. For each avalanche event, the percentage of the PRA that avalanched during this event is stored and used to derive, for each PRA, the release area-frequency distribution over 10 classes of percentage of the total PRA (class1: 0-10%, class2: 10-20%,..., class10: 90-100%).

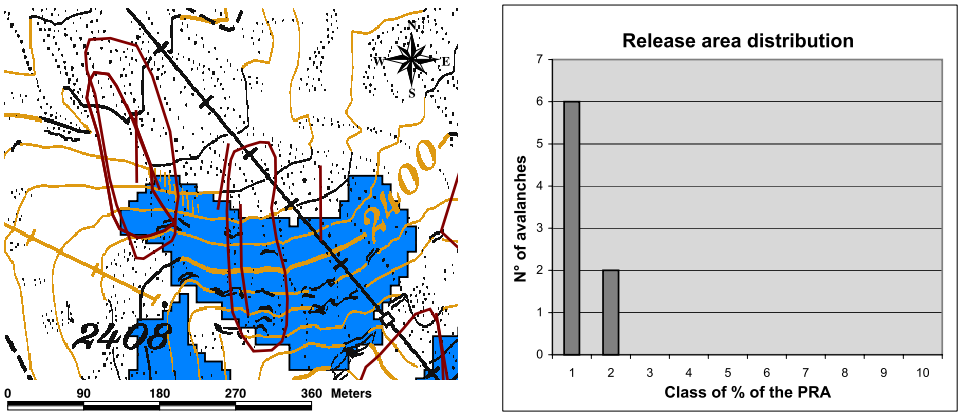

(a) (b)

Figure 4.17: Example of a PRA with past avalanche events (red lines) (a) and the related release area distribution (b). Topographic base map used with permission of swisstopo (BA046644).

As in the previous two steps of the procedure, this step is also implemented in ArcInfo GRID. An AML program was written to consider separately each PRA and the related avalanches. Each PRA is selected iteratively and only the avalanches which intersect it are considered. Then, iterating on polygons representing avalanches, each avalanche in turn is taken into account to calculate the intersection between the polygon representing the PRA and the polygon representing the current avalanche. Prior to this step, a selection was made to exclude those avalanches which only pass through the PRA, but start above it. The extension of the intersection area is stored in a table, which, at the end of the loop on the PRAs, contains 294 rows as the number of the PRAs and 12 columns – ten for the 10 classes of percentage of the total PRA, one for the total area of the PRA and one for the ID number of the PRA (Fig. 4.18).

As discussed in Chapter 3, some avalanches are stored only as lines in the database. Therefore, before intersecting them with the related PRA, a buffering

procedure is necessary. The line representing the avalanche is buffered to create a polygon which has a width either equal to the value recorded in the database by the observer or equal to 20% of the length of the line.

4.4.2 Results and Discussion

A database with the release area distribution of every defined PRA in the study area of Davos was created. An extract of the final table with these results is shown in Figure 4.18.

Analyzing the resulting release area distributions, it seems that many of them are skewed to the left (see Fig. 4.18). This means that it was common that small percentages of a PRA released. It is not surprising that the most frequent avalanches were small. Big catastrophic avalanches have a much longer return period, probably longer than the 50 years covered by the database. There are also PRAs with avalanche activity characterized by a homogeneous distribution of the release area over all the percentages of the total potential release area. In most of these cases, the PRAs are of small area and belong to size class 1 or 2 (see Table 4.1).

PRAnumber	PRAarea	Pra_10	Pra_20	Pra_30	Pra_40	Pra_50	Pra_60	Pra_70	Pra_80	Pra_90	Pra_100
20255	17200	10	8	4	2	0	2	0	1	1	0
21094	12200	7	4	5	3	0	2	4	0	1	0
20110	27700	12	8	1	0	0	0	0	0	0	0
22979	22400	2	8	3	3	2	0	3	0	0	1
7961	21000	11	5	4	3	0	3	1	3	0	0
20905	18300	8	12	5	2	1	1	0	1	0	0
20270	17100	17	7	2	1	1	1	0	1	0	1
20516	25300	23	6	5	1	2	0	0	0	0	0
21623	11800	32	1	8	0	0	0	0	0	0	0
21415	23700	20	16	7	5	2	3	1	0	0	0

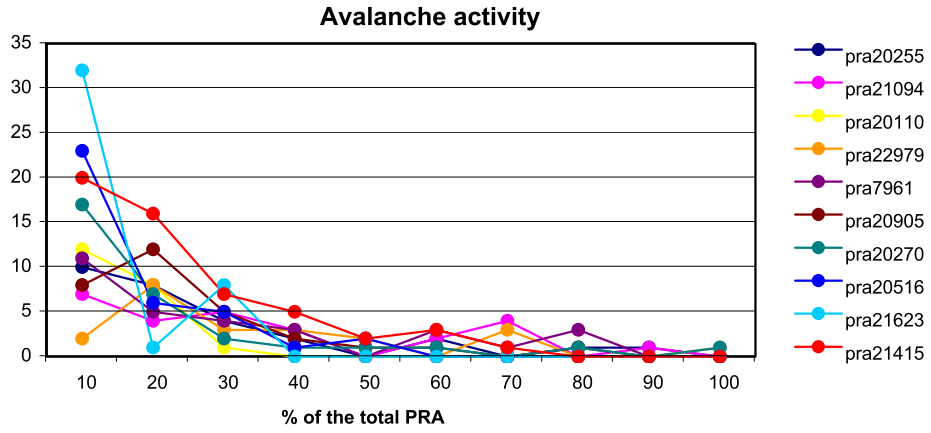

Figure 4.18: Extract of the final table with the release area distribution for the PRAs and the related graphs.

Chapter 5

Topography and avalanche activity

5.1 Introduction

In Chapter 4, 294 potential release areas (PRAs) were calculated and stored in a database, characterized, on one side, by topographical parameters and, on the other side, by the related historical avalanche activity. This chapter investigates the basic question *"Is there a statistical relationship between topographical features and avalanche activity?"*.

Different methods to find this link were examined and are presented in this chapter. Before going into the details of the procedure, it is important to recall the definition of avalanche activity used in this study and to compare it to other definitions of avalanche activity that can be found in literature.

Here, as determined in Section 4.4, avalanche activity is defined on the basis of frequency and extent of the release area of past avalanche events with respect to the total potential release area. In the literature, the most common definition of avalanche activity is related only to frequency of avalanches and the terms *avalanche activity* and *avalanche frequency* are often used synonymously. Figure 3.3 in Chapter 3 is an example of how avalanche activity is often addressed: with the help of a GIS, each pixel (grid cell of the DEM) is characterized by the number of avalanches crossing it. This is the most common approach, because what is important for avalanche hazard assessment are information on the frequency and the impact pressure in the runout zones, especially if they are close to settlements or traffic routes. An area reached by avalanches with a high frequency is assigned to the high level of hazard in the avalanche hazard map, with the appropriate consequences on land use planning (see Section 2.4).

Besides avalanche frequency, other variables have been used by different authors for the definition of avalanche activity. Davis & Elder [1995] defined avalanche activity by the total number of avalanche releases on a given day, the sum of the sizes of avalanches and the maximum size. The authors stated: "Our premise for specifying these avalanche activity characteristics was that the number of releases may provide an indication of how widespread the aval-

anche hazard (i.e. spatial dispersion), the sum of sizes may indicate the overall intensity of the activity, and that the maximum size may provide an index of local intensity of hazard.". In Schweizer et al. [1998], the avalanche activity index is introduced to represent daily avalanche activity as the mass of released avalanche snow; it is the sum of all observed avalanches and includes weights accounting for the nature of triggering and for the size of avalanche (following the Canadian classification USDA [1961]). Stoffel et al. [1998] proposed a classification of avalanche activity per day based on frequency of occurrence and area covered by avalanches on that day. They analyzed the relation between the portion of terrain covered by avalanches and the avalanche occurrence and found that it can be described by an exponential function with negative exponent. This behaviour seems to be typical of natural hazard in general. In the present study, the distributions resulting from the analysis of historical avalanches within the automatically defined potential release areas are often skewed to the left (see Fig. 4.18), that is in the past, the most frequent avalanche events released only from small areas. This is a characteristic which can be seen to be similar to what Stoffel et al. [1998] described. However, the basic concept is different, because there the avalanche activity is related to the frequency and extent of the total avalanche, whereas here it is related only to the frequency and extent of the release area.

Many studies have been conducted to analyze the influence of terrain, snow and meteorological variables on avalanche activity (see Schweizer et al. [2003] for a good literature review). The main issue of avalanche forecasting methodologies is to be able to predict avalanche activity on the basis of relevant variables that can be measured efficiently and reliably. Table 5.1 gives an extract of research made on this topic; it is useful to illustrate the different avalanche parameters that have been used for the definition of avalanche activity.

Table 5.1: Extract of studies about avalanche forecasting methodologies, with the avalanche parameters used there to define avalanche activity. Modified from Davis & Elder [1995]; references as in that work.

Study	Avalanche parameters
Bovis (1977)	avalanche day (local)
	magnitude
	total number
	(wet/dry avalanches)
Föhn (1977)	avalanche day (local/regional)
Obled and Good (1980)	avalanche day (local/regional)
Judson and Erickson (1983)	total number (local/regional)
Buser (1983, 1987, 1989)	avalanche day (local)
Jaccard (1990)	total number (local)
Davis et al. (1992)	avalanche day (local)
McClung and Tweedy (1993)	sum of sizes (local)

Note that there is an important difference between this work and the aforementioned studies. There, the main purpose was to predict *daily* avalanche

activity distributed over a large region (an example are avalanche bulletins to predict the avalanche hazard level for the next day). Here, the purpose is to estimate the avalanche activity on single avalanche paths with respect to the avalanche hazard over the long term (an example of this long-term forecasting are the avalanche hazard maps - see Section 2.4). Related to this consideration is also the fact that the present work concentrates on topographical features, which are constant in time, being aware that avalanche formation is a combination of terrain, snow and meteorological conditions.

Much effort has been made to analyze avalanche paths or avalanche starting zones in respect to terrain characteristics. In Chapter 4, the importance of some topographical parameters, e.g. slope, aspect and curvature, in the evaluation of potential avalanche release areas was discussed. In this chapter, these and others topographical features are analyzed regarding their relation to the avalanche activity.

McClung & Schaerer [1993] found that the main contributing factors to avalanche frequency, when analyzing the total avalanche extent, include slope angle, shape and roughness of the track, vegetative cover, exposure to wind and sun, as well as size and slope angle of the starting zone. They found that the average slope angle of the track is the most important influencing factor: in the case of large avalanches, an increase of the average inclination of the path leads to an increase of avalanche frequency. Judson & King [1984] analyzed 99 avalanche paths crossing roads in Colorado and Utah, U.S.A., and found that the frequency of the avalanches crossing the road was strongly correlated to the average inclination of the avalanche paths and to the inclination of the paths in the final 100 meters to the roads. Though this study focused on the avalanche frequency in the runout zone and not in the release area, it indicated that slope angle is an important terrain parameter. Gleason [1995] found that altitude and aspect with respect to the dominant wind direction are the most significant terrain parameters that influence the frequency of natural avalanches. Together with the geometry and slope angle of the starting zone, they are able to explain 62% of the variance correlating the terrain parameters to avalanche frequency. In the study of Schaerer [1977], it was shown that roughness, wind exposure, slope angle of the fracture-point and of the track are significantly correlated with avalanche frequency. In the case of natural avalanches, Smith & McClung [1997] analyzed the events recorded over 24 years on 43 avalanche paths in the area of Rogers' Pass, British Columbia, and built up a regression model to predict avalanche frequency on the basis of terrain and other parameters. Their regression model includes roughness, 30 year maximum water equivalent, path length and elevation of the starting zone, which turned out to be the most significantly correlated parameters to avalanche frequency.

Research about which factor have most influence on avalanche activity and about the quantitative relation between them is still ongoing. In conclusion of this literature review, the following citation of Gleason [1995] is well worth quoting

> "The overall conclusion one may draw from literature regarding the importance of factors that affect avalanche occurrence is that there is

> no general consensus as to which parameters are most influential for indicating the probability of avalanche release, identifying potential avalanche slopes or quantifying predicted avalanche frequency. Most of sources indicate a need for further research."

In this chapter, the following topographical characteristics of avalanche release areas are considered: mean slope angle, standard deviation of slope angle, maximum slope angle, mean aspect, distance to the next ridge, shape, plan curvature, profile curvature and maximum profile curvature.

In order to relate the topographical parameters to avalanche activity, different statistical approaches were used: linear regression models, Classification and Regression Tree models (CART) and cluster analysis. Note that, in the course of the work, the number of topographical parameters used in the analysis was changed to improve the description of the PRAs. Therefore, some statistical methods involved less than 9 parameters, for example the linear regression.

The statistical analysis was carried out within each size class separately. Table 5.2 recalls the definition of the size classes, already given in Table 4.1, and gives the number of PRAs and the total number of avalanches within each size class for the considered evaluation area (defined as in Section 3.3).

Table 5.2: Area, number of PRAs and total number of avalanches within each size class.

Size class	Area (m^2)	Number of PRAs	Number of avalanches
1:	5000 - 10000	81	238
2:	10000 - 30000	130	1009
3:	30000 - 50000	55	577
4:	50000 - 100000	22	331
5:	$>$ 100000	6	174

5.2 Methods

In this section the three different statistical approaches to analyze the relation between avalanche activity and topography are explained. All analyses were carried out for every size class, but note that here only size class 3 is taken as example to explain the procedure and the results in detail.

Before applying any methods, the relation between the topographical parameters (the independent variables in the following statistical analysis) was explored. The scatterplot matrix in Figure 5.1 shows the relation between every possible combination of the nine topographical parameters for size class 3.

Two examples are taken from the scatterplot matrix to explain better what is a 'relation' between variables. An example of no relation is given by the scatterplot for *distance to ridge* and *plan curvature* (Fig. 5.2a): no pattern can be found, all the values are spread out randomly, i.e. for a value of *distance to ridge* of 50 m, any value of *plan curvature* is possible. Instead, the scatterplot

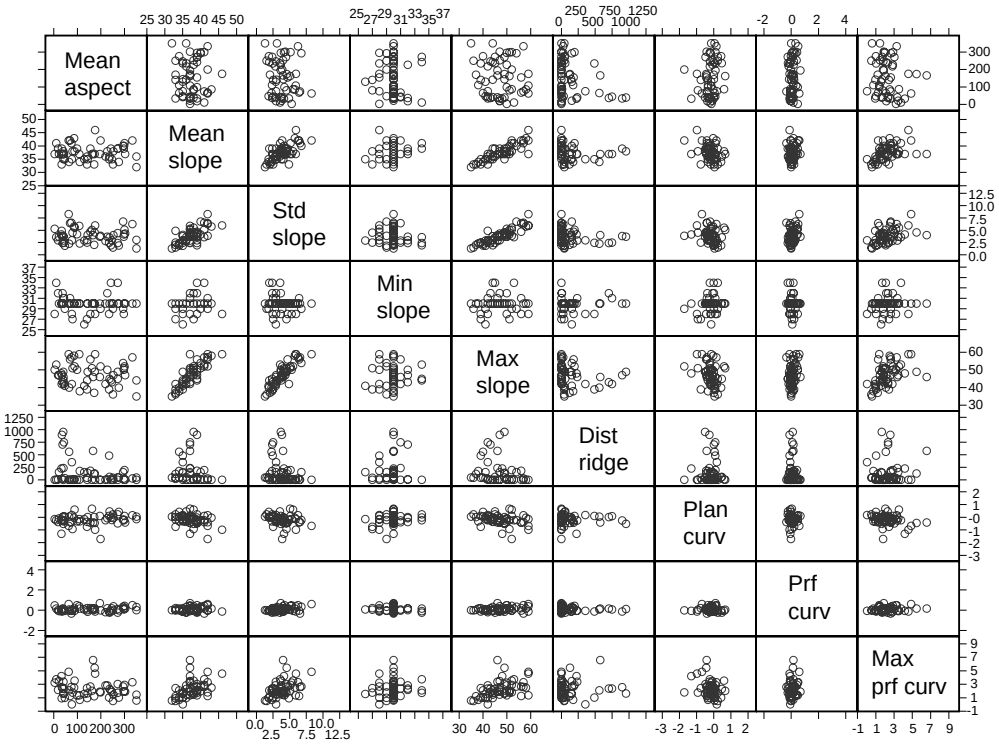

Figure 5.1: Scatterplot matrix for nine topographical parameters for size class 3.

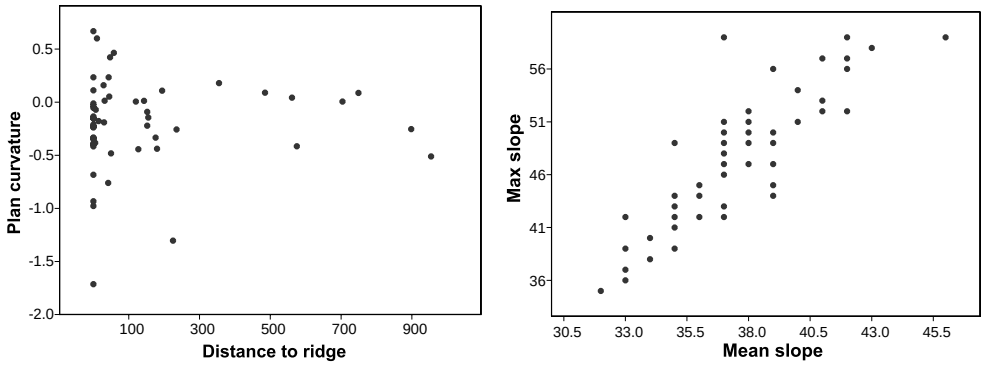

(a) (b)

Figure 5.2: Scatterplots for *distance to ridge* and *plan curvature* (a), and for *mean slope* and *maximum slope* (b) in size class 3. Extract of Fig. 5.1.

for *mean slope* and *maximum slope* (Fig. 5.2b) is an example of a relationship between variables: a linear pattern can be found, i.e. the higher the *mean slope*, the higher the *maximum slope*.

In general, there is no clearly recognizable pattern in most of the scatterplots, which means no clear relation between the variables, with the exception of values derived from slope, where as expected a correlation is evident.

5.2.1 Linear regression

The first approach used to relate avalanche activity and topographical parameters was linear regression. In general, it is the first statistical method that is commonly used to find relations between variables, because it is simple to understand and to apply and it gives clear results [Wonnacott & Wonnacott, 1972]. Linear regression methods assume a linear relation between the dependent variable and the independent variables. Here a linear regression model based on topographical parameters (independent variables) to predict avalanche activity (dependent variables), was defined. The null hypothesis is that there is no statistically significant association between these variables.

In this study, avalanche activity is represented by a vector of 10 elements as:

$$y = (y_{10}, y_{20}, y_{30}, y_{40}, y_{50}, y_{60}, y_{70}, y_{80}, y_{90}, y_{100}) \tag{5.1}$$

where y_i represents the number of avalanches that released with an area of $i\%$ of the total extent of the PRA (Pra_i in Fig. 4.18).

The independent variables are the seven topographical parameters represented by x_j $\{j = 1, ..., 7\}$: mean, maximum and standard deviation of slope angle, distance to ridge, plan, profile and maximum profile curvature.

The assumption was that the elements y_i are independent. This assumption was confirmed by the scatterplots created for the five size classes (in Figure 5.3, the scatterplot for size class 3 is given as an example). The scatterplots also show that the data are skewed to the left, therefore a logarithmic transformation was applied. The new independent variables are $\widetilde{y}_i = \log(y_i + 1)$. Ten linear regression equations were used:

$$\widetilde{y}_i = a_{i,1}x_1 + a_{i,2}x_2 + ... + a_{i,7}x_7 + c + \epsilon_i \tag{5.2}$$

where i stands for 10, 20,..., 100, $a_{i,j}$ and ϵ_i stand for the regression coefficients and for the error for the i^{th} equation, respectively, and c is a constant.

The linear regression model was applied separately inside each size class, defined as in Table 5.2. The resulting coefficients $a_{i,j}$ were used to build the linear regression equations and predict the values of $\widetilde{y}_i$. Figure 5.4 shows the predicted versus the observed values for $\widetilde{y}_{10}$, $\widetilde{y}_{20}$, $\widetilde{y}_{40}$ and $\widetilde{y}_{90}$ for the case of size class 3. In case of perfect prediction the points would lie on a line with slope equal 1 (predicted = observed).

The fact that linear regression models did not perform well can also be seen from the values of R-square (R^2) and 'Significance F' given in Table 5.3. R^2 is an indicator of how well the model fits the data. The smaller the variability of the residual values around the regression line relative to the overall variability,

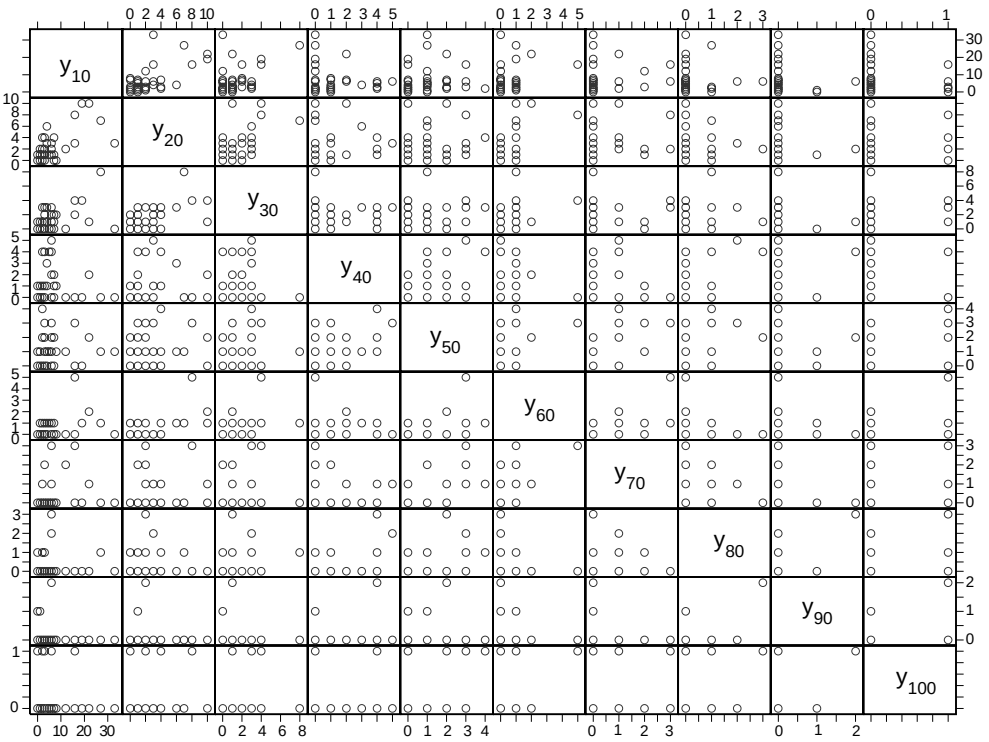

Figure 5.3: Scatterplot matrix for the ten elements of the vector representing avalanche activity for size class 3.

	R^2				Significance F			
	size1	**size2**	**size3**	**size4**	**size1**	**size2**	**size3**	**size4**
y10	0.22	0.18	0.32	0.55	0.008 **	$9{\cdot}10^{-4}$ **	0.009 *	0.071
y20	0.10	0.22	0.27	0.32	0.368	$4{\cdot}10^{-5}$ **	0.031 *	0.501
y30	0.15	0.11	0.18	0.36	0.100	0.033 *	0.180	0.386
y40	0.07	0.13	0.15	0.22	0.552	0.014 *	0.336	0.763
y50	0.12	0.09	0.29	0.29	0.212	0.104	0.016 *	0.593
y60	0.05	0.24	0.18	0.18	0.802	$1{\cdot}10^{-5}$ **	0.203	0.868
y70	0.17	0.09	0.21	0.47	0.051	0.099	0.121	0.174
y80	0.03	0.07	0.35	all 0	0.950	0.239	0.004 **	all 0
y90	0.07	0.09	0.11	all 0	0.618	0.091	0.546	all 0
y100	0.12	0.10	0.19	0.21	0.215	0.057	0.151	0.803

Table 5.3: Linear regression models applied inside each size class: R-square R^2 and 'Significance F'. "All 0" means that all the data for the corresponding y_i are missing (i.e. null). Size class 5 contains not enough data to perform statistics. With * and ** are highlighted the values of $p \leq 0.05$ and $p \leq 0.01$, respectively, which mean significant correlations.

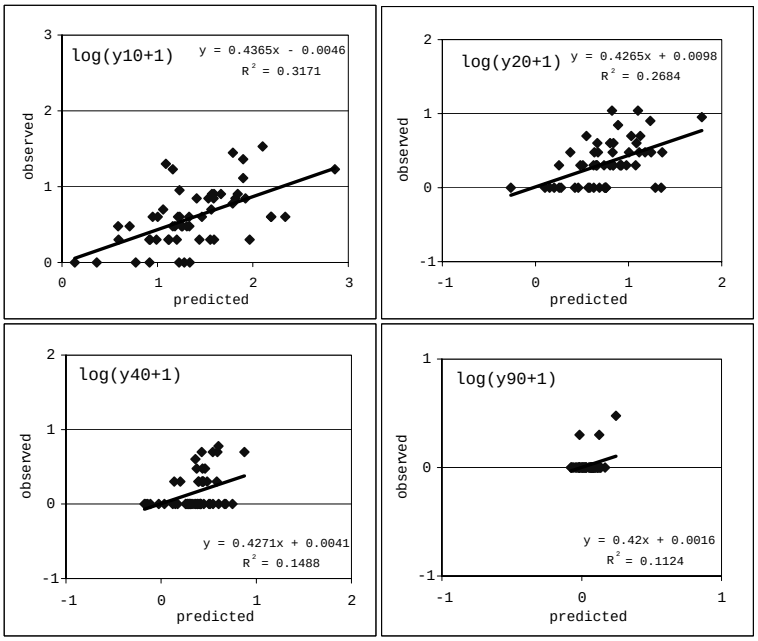

Figure 5.4: Predicted versus observed avalanche activity for size class 3.

the better is our prediction. R^2 is a measure of this variability and assumes values between 0 and 1, being 1 in the case when the model fits perfectly the data. 'Significance F' is the associated P-value for the F test, which determines whether the association between the variables is statistically significant. Its value depends on the results of the regression analysis and the chosen confidence level. For a confidence level of 95%, if 'Significance F' is smaller than 0.05, then the null hypothesis is rejected (there is a statistically significant association between the variables). Conversely, if 'Significance F' is greater than 0.05, then the null hypothesis is accepted (there is no statistically significant association between the variables).

To be able to confirm a statistically significant relation between avalanche activity and the considered topographic parameters, it is necessary that the values of 'Significant F' are smaller than 0.05 for all the y_i inside the same size class. However, the values of 'Significance F' are not always smaller than 0.05. Indeed, except for a few exceptions, they are greater than the threshold value of 0.05.

The small value of R^2 means that, under the assumption that the linear regression model is correct, there is no strong relation between the independent and the dependent variables. A reason for the small values of R^2 might be that the assumption of linearity is not correct, one of the basic assumptions for the use of linear regression. In this case, it would be difficult to get high values of R^2. Scatterplots to visualize the relation between avalanche activity (represented by the variables y_i) and topographical parameters (x_j) were derived; the scatterplots in Figure 5.5 show the distributions of the values of y_{10} and y_{40}

with respect to distance to ridge, mean slope angle and plan curvature for size class 3. As the scatterplots show, the y_i do not have a linear relation with the considered topographical parameters. The same non-linearity was also found for the other parameters and within the other size classes.

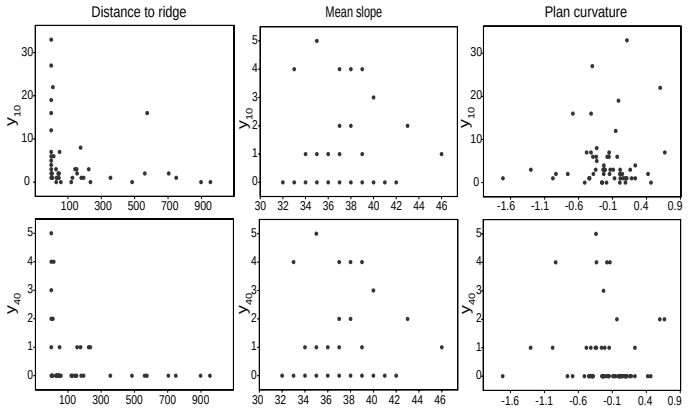

Figure 5.5: Scatterplots for y_{10} and y_{40} with respect to distance to ridge, mean slope and plan curvature for size class 3.

The other basic assumption for the use of linear regression is that the residuals (predicted minus observed values) must be distributed normally (i.e., follow the normal distribution). This was not the case for the results of the application of the linear regression model to the database used here.

In conclusion, the linear regression model was not appropriate to predict avalanche activity on the basis of the considered topographic characteristics. No statistically significant linear relation was found between the dependent variables y_i describing the avalanche activity and the independent variables x_j representing the topographic features.

5.2.2 Classification and regression tree

A second method used to analyze the relation between topographical parameters and avalanche activity was the Classification And Regression Tree (CART) [Breiman et al., 1984]. CART builds classification trees to predict the values of a *categorical* dependent variable (class, group membership, etc.) from one or more continuous and/or categorical predictor variables. CART builds also regression trees to predict the values of a *continuous* dependent variable from one or more continuous and/or categorical predictor variables. The CART methodology is technically known as binary recursive partitioning. The process is called binary because parent nodes are always split into exactly two child nodes and recursive because the process can be repeated by treating each child node as a parent. The process of splitting is based on two basic steps: first, to look at all possible splits for all variables included in the analysis and, second, to chose the best splitting rule, on the basis of a quality-of-split criterion [Venables & Ripley, 1997]. On each node, a variable is selected to divide the population into two sub-populations at a selected breakpoint of that variable.

The chosen variable is the one which better performs this division and which therefore has more importance in differentiating different groups. Therefore, by analyzing the splitting procedure, information about which variables create more homogeneous (i.e. better) groups are derivable. Davis & Elder [1995] used the CART methodology to rank critical variables in terms of their sensitivity to avalanche activity. In this study, CART is used for the same purpose: to rank topographical parameters regarding their importance with respect to avalanche activity, in this case coincident with avalanche frequency and represented by the number of avalanches that occurred within the PRAs.

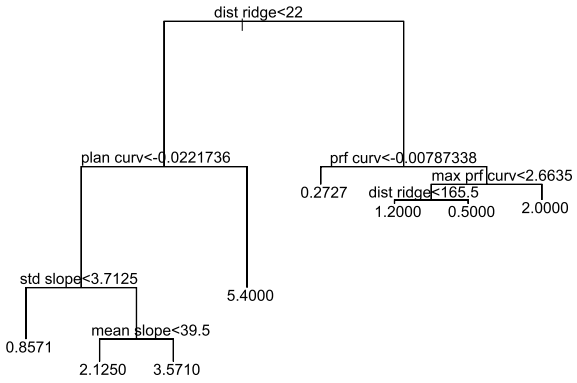

Figure 5.6: Regression tree built for y_{20} in size class 3 starting from the seven topographic parameters listed in Table 5.4. At each node the splitting rule is shown and at the end of each branch of the tree the predicted y_{20} is given.

In this section, the same notation used in Section 5.2.1 is adopted, representing with y_i the number of avalanches that released with an area equal to $i\%$ of the PRA. As in Section 5.2.1, for size classes 1, 2, 3 and 4 and for y_i $\{i = 10,$ 20, 30, 50, 70, 100$\}$ a regression tree was built. The tree was not built for size class 5 as it contains only six PRAs. The purpose of this CART analysis was to analyze which parameters were the cause of each splitting and not to predict the final y_i. Figure 5.6 gives an example of the regression tree built for y_{20} in size class 3. Table 5.4 is a summary of how many times each topographical variable was chosen in the CART procedure as splitting variable, in the case of first, second or following splits in the trees built for the four size classes. As first splitting variable, profile curvature was chosen for size class 1, mean slope for size class 2, distance to ridge for size class 3 and standard deviation of slope for size class 4. In general, standard deviation of slope, plan and profile curvature and distance to ridge are most frequently used as splitting variables. The results obtained from the CART applied to the data for the region of Davos suggest that the aforementioned variables have the most important influence on avalanche activity. Distance to ridge, plan and profile curvature have been already considered in the literature as important topographical parameters for avalanche activity, because they are related to the combined effect of wind and terrain shape on snow accumulation and therefore related to stress in snow (see Section 4.2.1 and 4.3.1). Standard deviation of slope did not received the same

Table 5.4: Frequency of the different topographical parameters chosen as splitting variable, for the first, the second and the following splits in the regression trees of the four considered size classes.

	mean slope	std slope	max slope	plan curv	prf curv	max prf curv	dist ridge
first:	0	0	0	1	3	1	1
second:	0	2	0	2	1	1	2
following:	1	11	0	6	5	3	4
tot. size1:	1	13	0	9	9	5	7
first:	2	1	1	1	0	0	1
second:	0	2	0	1	3	2	2
following:	4	13	7	8	13	5	10
tot. size2:	6	16	8	10	16	7	13
first:	0	1	0	1	0	0	4
second:	1	0	0	4	2	1	1
following:	2	5	0	3	1	7	3
tot. size3:	3	6	0	8	3	8	7
first:	0	4	0	2	0	0	0
second:	0	0	0	0	1	2	2
following:	0	0	0	0	0	0	0
tot. size4:	0	4	0	2	1	2	2

attention in previous works. It is related to the variation of slope angle within a potential release area. The fact that standard deviation of slope is shown to be important in relation to avalanche activity can be explained by the fact that low values represent homogeneous slopes, whereas high values represent irregular slopes with possible abrupt changes, e.g. cliffs or other undulations, which create stress zones in the snow cover.

In conclusion, CART was a valuable tool to explore the importance of topographical parameters in relation to avalanche activity. The most important topographical parameters were shown to be: distance to ridge, standard deviation of slope, plan and profile curvature. However, CART is known to be unstable with respect to the choice of the input variables [Hastie et al., 2001], therefore the results of this analysis must be considered with care. Nonetheless the aforementioned topographical parameters should be analyzed further when studying avalanche activity and topography.

The next step is to group PRAs with clustering procedures in order to make further considerations about the possible relation between topography and avalanche activity.

5.2.3 Cluster analysis

A common method for data mining is cluster analysis [Hartigan, 1975; Gordon, 1981; Venables & Ripley, 1997]. Cluster analysis is an exploratory data analysis tool for solving classification and grouping questions. It sorts objects based on

the similarity of their attributes into groups or clusters, so that the degree of association is strong between members of the same cluster and weak between members of different clusters. Most cluster analysis techniques are hierarchical, i.e. the resultant classification has an increasing number of nested classes. There exist also non hierarchical methods, for example *k-means* clustering. In this chapter, an agglomerative hierarchical tree is used as clustering method. Agglomerative clustering works by taking all the data objects as if they were clusters of one item. Then the closest clusters are joined together to form a bigger cluster and so on until eventually only one big cluster including all data objects accumulates. The first step of the procedure consists in merging the two closest objects. To decide which objects to merge, a measure of their similarity or difference is needed. There exist several distances that can be used for this purpose [Torgrip, 2002]. The most common one, Euclidean distance, was used in this study:

$$d(x,y) = |\underline{x} - \underline{y}| = \left[\sum_{i=1}^{N} (x_i - y_i)^2\right]^{1/2} \tag{5.3}$$

where $\underline{x}$ and $\underline{y}$ are vectors composed by i components.

The distance between two individual objects is easy to compute, whereas computing the distance between a cluster of objects and another one involves more considerations about the way to carry out this step (*linkage method*). There exist different linkage methods: *single linkage*, *complete linkage* and *average linkage* are the most common ones [Torgrip, 2002]. With *single linkage*, the distance between two clusters is considered to be equal to the shortest distance from any member of one cluster to any member of the other cluster. With *complete linkage*, the distance between two clusters is considered to be equal to the longest distance from any member of one cluster to any member of the other cluster. With *average linkage*, the distance between two clusters is considered to be equal to the average distance from any member of one cluster to any member of the other cluster. Figure 5.7 helps to visualize the meaning of the different linkage methods. In this research, the *complete linkage* method is

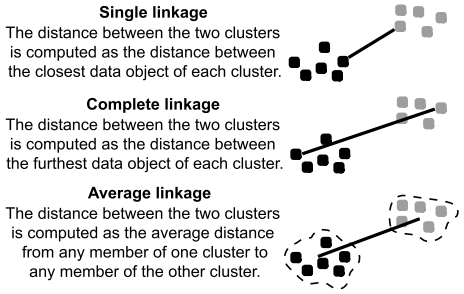

Figure 5.7: Different linkage methods to compute the distance between two clusters.

used. This method reduces dissimilarity within a cluster because it joins clusters on the basis of the distance between the furthest members and therefore the other members are sure to be closer, that is they have higher similarity.

The result of the agglomerative hierarchical clustering (AHC) procedure can be presented by a dendrogram such as the one in Figure 5.8 [Venables & Ripley, 1997]. In the lower part of the tree, all the objects are considered as clusters of one item (each PRA is identified by its identity number) and at the top of the tree they are all joined together. The vertical axis (Height) denotes the linkage distance, thus, at each node of the tree, the distance between the members of the newly created cluster is known. When the data contains a clear structure in terms of clusters of objects that are similar to each other, then this structure is often reflected in the hierarchical tree as distinct branches. To identify individual clusters in a hierarchical tree, it is necessary to decide where to *cut the tree*, i.e. which distance to use to stop the agglomerative procedure. Obviously, the lower the tree is cut, the higher the homogeneity within a cluster, which contains conversely few objects. The higher the tree is cut, the more objects are included in a cluster but more dissimilarity is present. The best compromise has to be chosen; this is important, because different thresholds lead to different results.

AHC was used as a tool to explore the potential relationship between topography and avalanche activity in the different size classes. If, as hypothesized, topography is a determining factor in avalanche activity, then the cluster of PRAs defined by topographical parameters should have similar avalanche activity. Conversely, clusters of PRAs defined by avalanche activity, should also have similar topographic characteristics. If similarity both in avalanche activity and topography was found, the conclusion that a certain combination of topographical parameters leads to a certain type of avalanche activity could be drawn. In the following sections the two aforementioned analyses are described.

Cluster analysis on topography

Agglomerative hierarchical clustering was applied to the database composed of 294 PRAs characterized by their topographical parameters. An extract of the database is given in Table 4.4. The different variables are measured in different units, e.g. degrees for slope, meters for distance to ridge, 1/100m for curvature, dimensionless number for shape, and have different range, e.g. very big for distance to ridge (0 - 1250 m) and much smaller for curvature (-3 - +4 1/100m). The range of the initial data has a large impact on computing distance. In order to avoid this problem, the variables are rescaled to the same range [0, 2].

The distance used to calculate similarity or differences between clusters is the Euclidean distance for mean slope angle, standard deviation of slope angle, maximum slope angle, distance to ridge, shape, plan curvature, profile curvature and maximum profile curvature, whereas for aspect this distance cannot be used because of the circular nature of this variable. Instead, the distance along a circle is used as in equation 5.4:

$$d(asp_1, asp_2) = \rho \cdot min\{|\theta_1 - \theta_2|, |2\pi - |\theta_1 - \theta_2||\} \tag{5.4}$$

where ρ is the radius of the unit circle, therefore equal to 1, and θ_1 and θ_2 are the angles representing the aspect of the two members in question. In computing

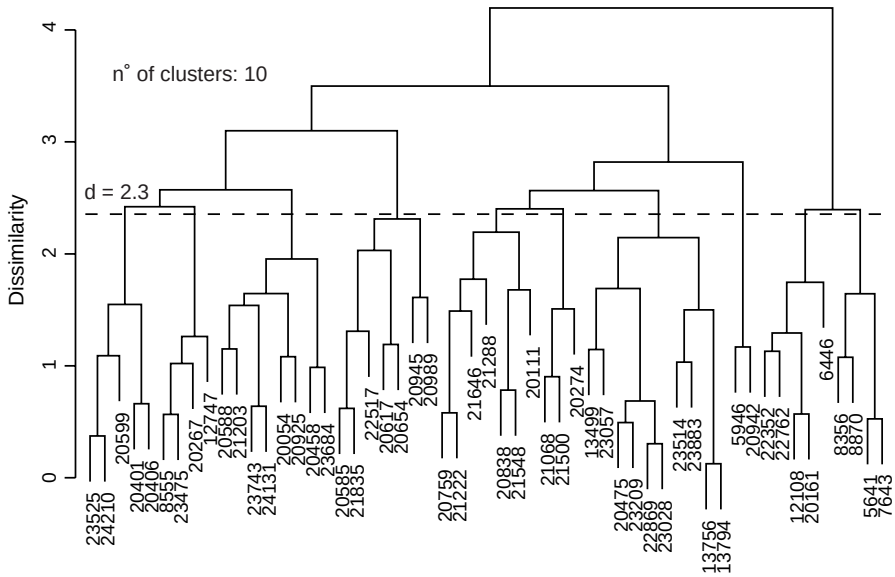

Figure 5.8: Agglomerative hierarchical tree on the basis of topographical parameters for the PRAs in size class 3. Each PRA is labelled by a number written at the end of each branch. The dashed line shows the distance used to cut the tree.

this circular distance, a rescaling procedure to the interval [0, 2] is included, in order to give the aspect the same weight as the other parameters.

To create the agglomerative hierarchical trees, a specific program in C++ was written, where both the Euclidean and the circular distance could be implemented. Then, the dendrogram was drawn using S-Plus procedures [MathSoft, 2000]. The resulting hierarchical trees are shown in Figure 5.8 and 5.9. Size class 5 contains only six PRAs, which are considered as insufficient to perform significant statistical analysis. In Figure 5.8 the original output from S-Plus is given, to show all the information available, including the PRA number at the end of each branch. An horizontal dashed line is added in the graphs to represent the threshold distance used to cut the tree. All the four trees were cut with the goal of obtaining around ten clusters. This number was considered to be optimal to have, within each cluster, enough, but not too many, PRAs to perform statistical analysis.

In order to check if the clustering methodology, combined with the chosen threshold distance, was able to identify homogeneous groups, the topographical parameters of the PRAs belonging to every cluster were analyzed. As an example, Table 5.5 shows the mean value, the standard deviation and the range (rescaled values) of the nine topographical parameters for the whole size class 3 and for the ten clusters in size class 3. Small values for the range and the standard deviation indicate homogeneity with respect to the considered topographical parameter within the considered cluster.

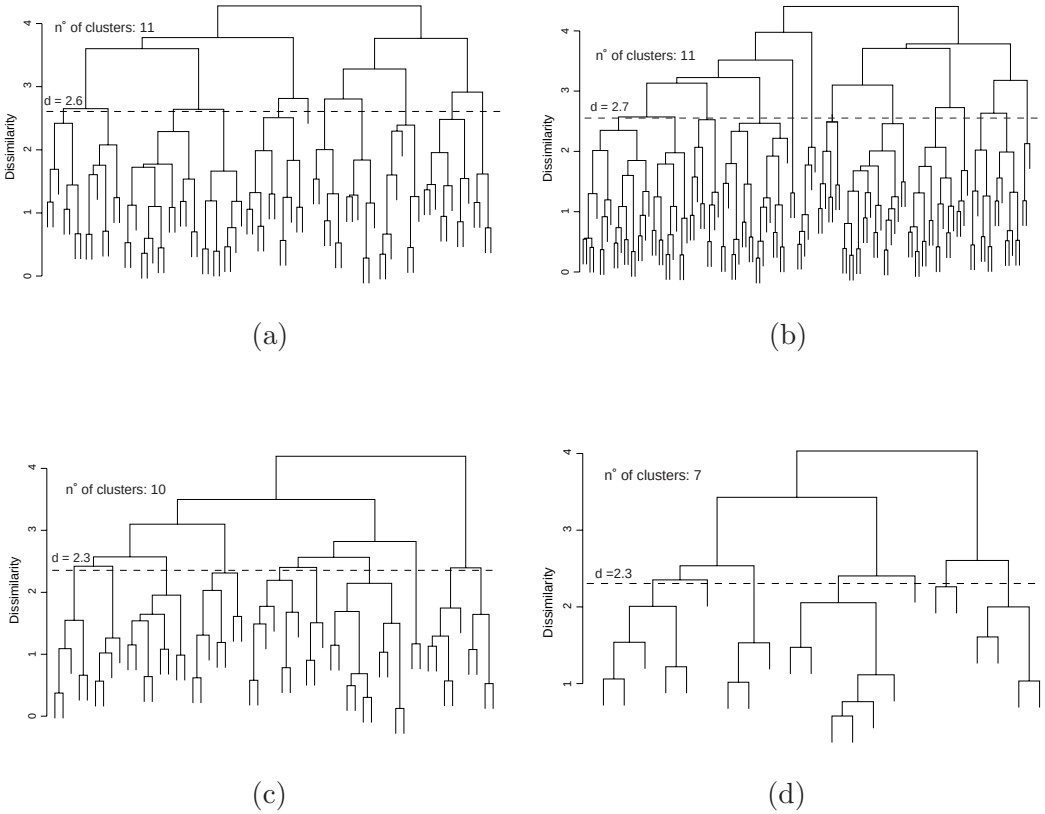

Figure 5.9: Agglomerative hierarchical tree on the basis of topographical parameters for the PRAs in size class 1 (a), size class 2 (b), size class 3 (c) and size class 4 (d). The dashed lines show the distances used to cut the trees.

The plots in Figure 5.10 help to visualize the distribution of the values of the nine topographical parameters within each cluster of size class 3 and in the whole size class 3. The plots for Cluster1, Cluster3 and Cluster6 show clusters of points (PRAs) around certain values of the topographical parameters, while the values of the topographical parameters for Cluster4 and Cluster5 are spread along a wider range. This is confirmed by the values of standard deviation and range in Table 5.5. The former clusters (Cluster1, Cluster3 and Cluster6) can be represented by the mean value of the topographical parameters, while for the latter (Cluster4 and Cluster5) the mean values are not meaningful alone, because the standard deviation and the range are large.

		Mean slope	STD slope	Max slope	Dist ridge	Plan curv	Prf curv	Max prf curv	Shape
Cluster1 5 PRAs	mean:	0.78	0.39	0.69	0.00	1.22	0.60	0.45	2.00
	std:	0.14	0.13	0.13	0	0.06	0.12	0.11	0.00
	range:	0.35	0.34	0.30	0	0.15	0.30	0.30	0.00
Cluster2 4 PRAs	mean:	0.57	0.31	0.48	0.45	1.27	0.52	0.35	2.00
	std:	0.18	0.17	0.30	0.37	0.05	0.03	0.33	0.00
	range:	0.43	0.39	0.73	0.83	0.12	0.05	0.74	0.00
Cluster3 8 PRAs	mean:	0.98	0.68	1.09	0.08	1.19	0.64	0.58	1.75
	std:	0.20	0.21	0.25	0.13	0.08	0.05	0.17	0.46
	range:	0.52	0.61	0.79	0.31	0.25	0.12	0.49	1.00
Cluster4 7 PRAs	mean:	0.89	0.64	1.08	0.07	1.10	0.55	0.42	2.00
	std:	0.36	0.27	0.49	0.13	0.13	0.10	0.29	0.00
	range:	1.04	0.70	1.27	0.31	0.43	0.28	0.83	0.00
Cluster5 7 PRAs	mean:	0.89	0.71	1.08	0.21	1.00	0.59	0.78	0.43
	std:	0.27	0.31	0.42	0.33	0.09	0.07	0.44	0.53
	range:	0.78	0.96	1.21	0.92	0.23	0.22	1.15	1.00
Cluster6 3 PRAs	mean:	1.04	0.55	1.05	0.04	0.91	0.54	0.50	0.00
	std:	0.15	0.06	0.09	0.04	0.35	0.02	0.15	0.00
	range:	0.26	0.13	0.18	0.08	0.66	0.04	0.27	0.00
Cluster7 10 PRAs	mean:	0.76	0.43	0.72	0.61	1.12	0.53	0.49	0.20
	std:	0.16	0.15	0.17	0.64	0.17	0.03	0.22	0.42
	range:	0.52	0.50	0.48	1.53	0.61	0.10	0.71	1.00
Cluster8 2 PRAs	mean:	1.09	0.81	1.33	0.01	1.38	0.55	0.67	0.00
	std:	0.31	0.03	0.26	0.01	0.19	0.06	0.16	0.00
	range:	0.43	0.05	0.36	0.02	0.28	0.08	0.22	0.00
Cluster9 5 PRAs	mean:	0.66	0.42	0.64	0.25	1.30	0.54	0.39	1.00
	std:	0.17	0.20	0.39	0.32	0.14	0.04	0.16	0.00
	range:	0.43	0.50	0.85	0.78	0.35	0.10	0.39	0.00
Cluster10 4 PRAs	mean:	0.65	0.27	0.52	0.06	1.40	0.48	0.31	1.75
	std:	0.23	0.15	0.26	0.04	0.05	0.05	0.17	0.50
	range:	0.52	0.33	0.55	0.09	0.10	0.08	0.38	1.00
ALL 55 PRAs	mean:	0.82	0.52	0.87	0.22	1.17	0.56	0.50	1.15
	std:	0.25	0.25	0.38	0.38	0.18	0.07	0.27	0.87
	range:	1.22	1.15	1.45	1.53	1.04	0.35	1.42	2.00

Table 5.5: Summary of the topographical parameters for the 10 clusters identified on the basis of topographic parameters for size class 3 and for the whole size class; rescaled values to range [0 - 2]. On the left of the table the name of the cluster and the number of the PRAs belonging to it are given. Cluster8 contains only 2 PRAs and is therefore excluded from the analysis.

Within each cluster identified by the AHC, the avalanche activity of the PRAs was analyzed. In Figure 5.11 the graphs for the avalanche activity grouped by clusters, for the case of size class 3, are shown. These graphs were carefully analyzed in relation to the characterizing topographical parameters (shown in Table 5.5). The first evidence is that within each homogeneous

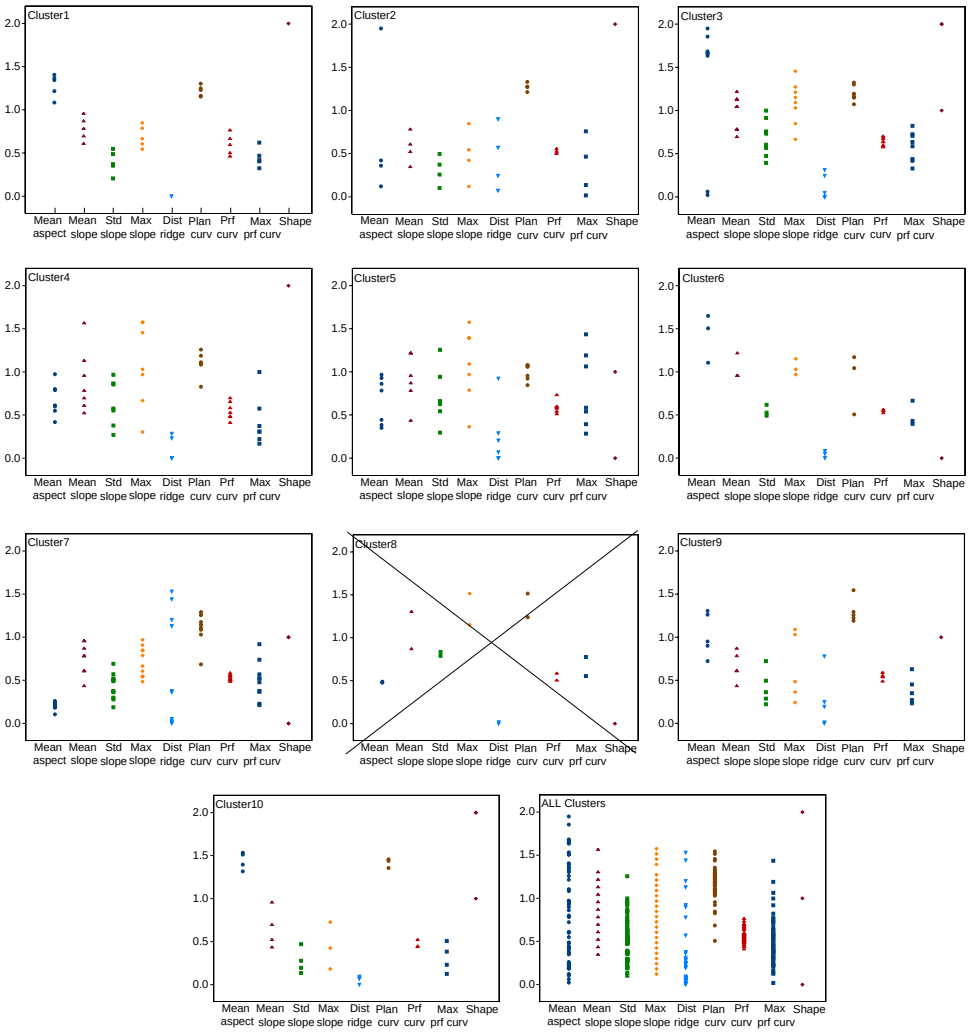

Figure 5.10: Scatterplots for the nine topographical parameters within the 10 clusters identified on the basis of topography for size class 3 and for the whole size class; rescaled values to range [0 - 2]. Cluster8 contains only 2 PRAs and is therefore excluded from the analysis.

topographical cluster, different kinds of avalanche activities are present. In the ideal case, the avalanche activity of all the PRAs belonging to a cluster would be similar (all the lines of one plot of Figure 5.11 would overline). Although this is not the case, some typical characteristics are found in each plot. For example, Cluster1 and Cluster5 contain PRAs with an avalanche activity characterized by many avalanches, mostly with small release areas (around 10-20% of the total PRA), but covering also higher percentages of the total PRA. Cluster4 and Cluster7 show avalanche activities with less avalanches, with a maximum on the 10% of the PRA too, but covering also percentages of PRA until 100%. Cluster6, Cluster9 and Cluster10 join PRAs that released rarely and with release areas of only up to 50% of the total.

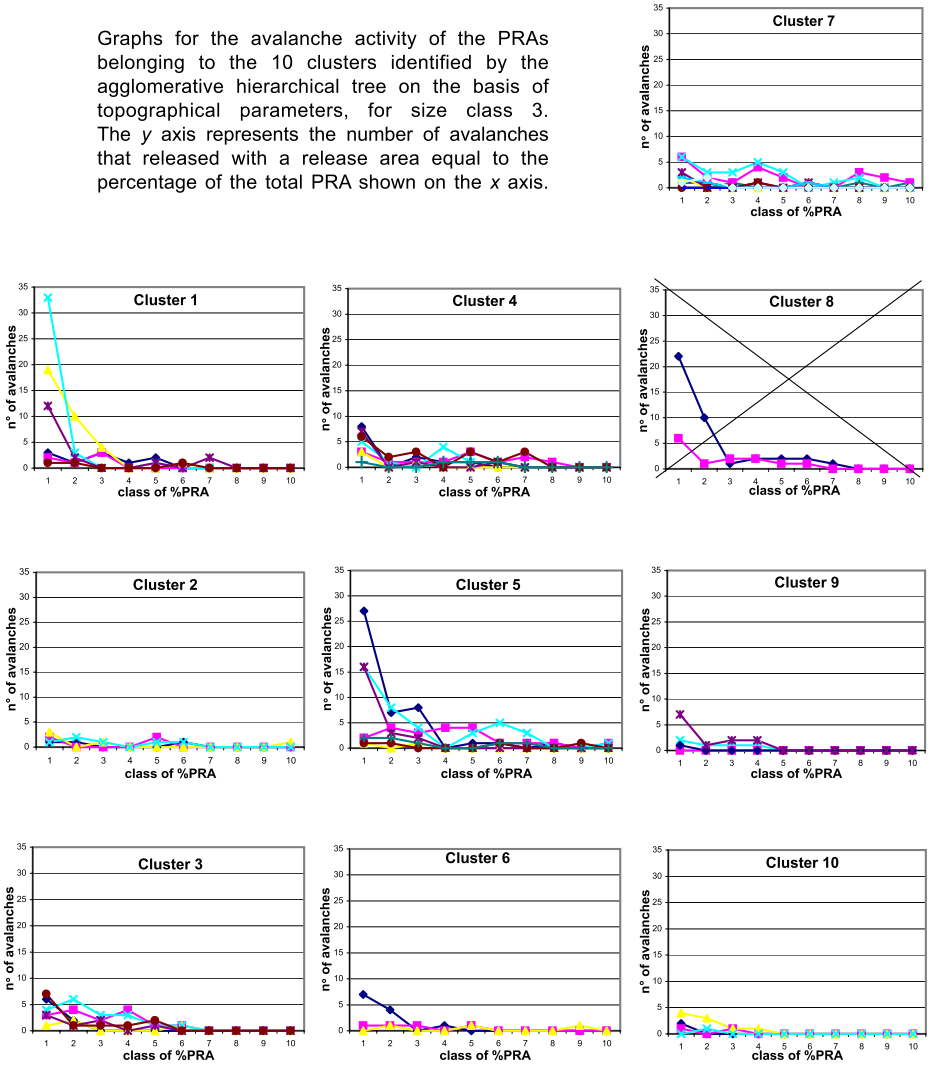

Figure 5.11: Avalanche activity for the PRAs (size class 3). Cluster8 contains only 2 PRAs and is therefore excluded from the analysis.

The aforementioned groups of clusters with similar avalanche activity were reexamined with respect to their topographic parameters, in order to identify potential topographic similarities that may have not been detected by the previously applied AHC method on topography. Further potential similarities were sought between clusters represented by the mean value of the topographic parameters, recalling that comparing mean values makes sense only when the clusters are well defined (small range and standard deviation for the topographic parameters). This reexamination provided no additional similarities: for example, the mean values of *mean aspect* and *distance to ridge* of Cluster6 are closer to the ones of Cluster1 than to the ones of Cluster9, and the mean values of *mean slope*, *STD slope* and *max slope* of Cluster9 are closer to the ones of Cluster1 than to the ones of Cluster6, although Cluster6 and Cluster9 have a similar avalanche activity.

Graphs and Tables like Figures 5.10 and 5.11 and Table 5.5 were prepared for each size class. In their analysis , as in the case of size class 3, well-defined clusters in terms of topographical parameters were found. Again, the reexamination of the topographical parameters of clusters with similar avalanche activity was performed. Unfortunately, also in these cases no additional similarities were identified.

The following general comments can be drawn for all the size classes. Agglomerative hierarchical clustering performed well in identifying homogeneous clusters with respect to topographical parameters. Although in analyzing the avalanche activity inside each cluster examples of similarity could be found, it was not possible to find a clear association between a specific combination of topographical features and a particular type of avalanche activity.

Cluster analysis on avalanche activity

Agglomerative hierarchical clustering was applied to the database composed of 294 PRAs with the related avalanche activity. An extract of the database is given in Figure 4.18. In order to apply the clustering procedure, a way to compute the distance between the avalanche activity of two different PRAs had to be found. The initial problem was how to characterize avalanche activity, namely to find variables to describe the distributions representing it.

An appropriate method was found to be the combination of the area and the shape of the distributions describing avalanche activity. The former represents the frequency of avalanches, while the latter expresses how the distribution is skewed. The area of the distribution was represented by the variable *numava*, that is the total number of avalanches for a PRA. To describe the shape of the distribution the equation to compute the skewness of a distribution was modified as follows:

$$skew = \frac{n}{(n-1)(n-2)} \left[\sum_{i=1}^{5} \frac{(-y_i) - \overline{y}}{s} + \sum_{i=6}^{10} \frac{(y_i) - \overline{y}}{s} \right] \tag{5.5}$$

where n is equal to 10 (number of components of the vector $\underline{y}$), y_i is the i^{th} component of the vector, $\overline{y}$ is the mean value and s is the standard deviation. Figure 5.12 shows how two distributions are described by *numava* and *skew*.

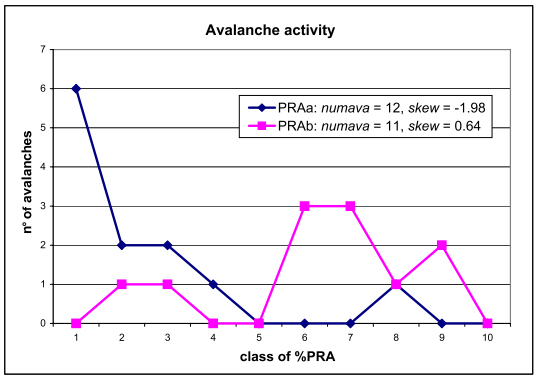

Figure 5.12: Distributions representing the avalanche activities for two PRAs and the related values for *numava* and *skew* used to describe them.

For each size class, *numava* and *skew* were used as variables to which the AHC was applied in order to find homogeneous clusters in terms of avalanche activity. The results of the agglomerative hierarchical tree are represented by dendrograms such as the one in Figure 5.13. Analyzing the plots, clusters were identified cutting the trees at different distances; in Figure 5.13 the dashed lines represent where the tree for size class 3 was cut to results in nine clusters.

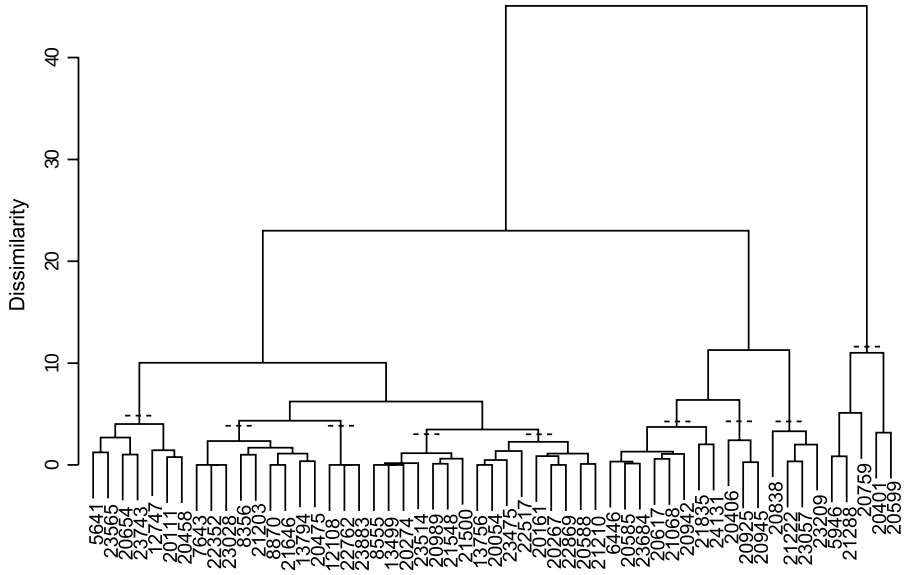

Figure 5.13: Agglomerative hierarchical tree on the basis of *numava* and *skew*, for the PRAs in size class 3. Each PRA is labelled by a number written at the end of each branch. The dashed lines show the distances used to cut the tree.

The avalanche activities of the PRAs grouped by clusters are represented in the graphs of Figure 5.14. Table 5.6 gives in the last two columns the total number of avalanches and the 'skewness', whose mean value, standard deviation

and range were computed. These mean values will be used later in a graphical visualization of the results of the analysis of avalanche activity and topography (see Fig 5.17). The nine clusters are all characterized by a negative mean 'skewness', that means more avalanches with a small release area, as it can also be seen from the graphs in Figure 5.14; only Cluster3 has *skew* and *numava* equal zero, because it contains PRAs with no avalanches.

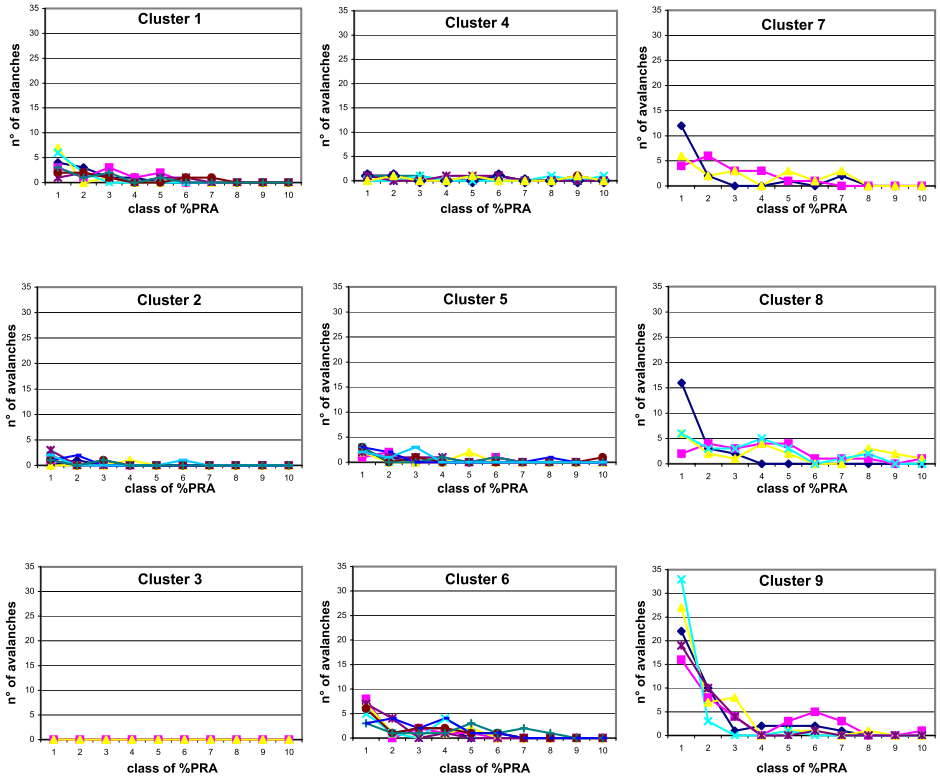

Figure 5.14: Avalanche activity of the PRAs within each of the nine clusters identified by AHC on the basis of *numava* and *skew*, for size class 3.

Within each cluster identified by the AHC, the topographical parameters of the PRAs were analyzed. Table 5.6 shows the mean value, the standard deviation and the range (rescaled values) of the nine topographical parameters for the whole size class 3 and for the nine clusters in size class 3. As discussed in the previous section regarding Table 5.5, small values for the range and the standard deviation indicate homogeneity with respect to the considered topographical parameter within the cluster in question. This is not the case: apart from some exceptions, e.g. Cluster7, these values are large - examples over all are Cluster2 and Cluster4. The plots in Figure 5.15 help to visualize the distribution of the values of the nine topographical parameters within each cluster in size class 3 and in the whole size class 3. The points in the plots are spread along a wide range of the possible values and not concentrated in clusters.

From Table 5.6 and Figure 5.15 it is evident that there is no homogeneity in terms of topographical parameters within each cluster.

		Mean slope	STD slope	Max slope	Dist ridge	Plan curv	Prf curv	Max prf curv	Shape	numava	skew
Cluster1 7 PRAs	mean:	0.71	0.40	0.75	0.02	1.18	0.58	0.42	1.71	8	-1.50
	std:	0.28	0.23	0.49	0.03	0.13	0.07	0.22	0.76	1.4	0.97
	range:	0.78	0.75	1.45	0.07	0.43	0.21	0.68	2.00	4	2.52
Cluster2 9 PRAs	mean:	0.80	0.43	0.82	0.24	1.26	0.55	0.50	1.00	2	-2.62
	std:	0.24	0.24	0.42	0.38	0.15	0.07	0.21	0.87	0.9	0.66
	range:	0.78	0.78	1.27	1.19	0.39	0.26	0.61	2.00	2	1.38
Cluster3 3 PRAs	mean:	0.67	0.34	0.48	0.80	1.23	0.50	0.36	1.00	0	0
	std:	0.27	0.16	0.32	0.62	0.08	0.03	0.18	0.00	#	#
	range:	0.52	0.30	0.61	1.25	0.15	0.05	0.34	0.00	#	#
Cluster4 7 PRAs	mean:	0.94	0.51	0.96	0.34	1.03	0.53	0.52	0.71	3	-0.08
	std:	0.35	0.21	0.37	0.56	0.28	0.03	0.42	0.95	0.5	0.20
	range:	0.96	0.68	1.09	1.53	0.83	0.09	1.17	2.00	1	0.62
Cluster5 9 PRAs	mean:	0.77	0.51	0.80	0.41	1.17	0.55	0.58	1.33	5	-1.73
	std:	0.20	0.24	0.30	0.36	0.19	0.07	0.18	0.87	0.8	0.47
	range:	0.61	0.74	0.85	1.13	0.62	0.21	0.57	2.00	2	1.48
Cluster6 8 PRAs	mean:	0.85	0.59	0.93	0.05	1.18	0.60	0.44	1.38	13	-1.76
	std:	0.23	0.19	0.35	0.10	0.16	0.06	0.20	0.92	1.1	0.93
	range:	0.78	0.57	1.21	0.28	0.50	0.17	0.54	2.00	3	2.48
Cluster7 3 PRAs	mean:	1.01	0.69	1.13	0.00	1.16	0.56	0.44	1.67	18	-1.39
	std:	0.13	0.24	0.31	0.00	0.07	0.13	0.13	0.58	0.6	1.21
	range:	0.26	0.42	0.61	0.00	0.15	0.25	0.25	1.00	1	2.22
Cluster8 4 PRAs	mean:	0.67	0.59	0.77	0.24	1.05	0.55	0.60	0.25	22	-0.96
	std:	0.19	0.09	0.23	0.46	0.14	0.03	0.56	0.50	1.0	1.31
	range:	0.43	0.19	0.55	0.92	0.33	0.08	1.22	1.00	2	2.76
Cluster9 5 PRAs	mean:	1.01	0.74	1.12	0.00	1.22	0.60	0.60	1.00	39	-2.25
	std:	0.20	0.41	0.39	0.01	0.21	0.13	0.31	1.00	4.1	0.62
	range:	0.43	1.05	0.91	0.02	0.56	0.26	0.78	2.00	11	1.72
ALL 55 PRAs	mean:	0.82	0.52	0.87	0.22	1.17	0.56	0.50	1.15	10	-1.52
	std:	0.25	0.25	0.38	0.38	0.18	0.07	0.27	0.87	11.0	1.09
	range:	1.22	1.15	1.45	1.53	1.04	0.35	1.42	2.00	45	3.29

Table 5.6: Summary of the topographical parameters for the nine clusters identified on the basis of *numava* and *skew* for size class 3 and for the whole size class; rescaled values to range [0 - 2]. The last two columns are the number of avalanches and the 'skewness' for the clusters. On the left of the table the name of the cluster and the number of the associated PRAs are given.

Class	mean aspect (°)	mean slope (°)	std slope (°)	max slope (°)	dist ridge (m)	plan curv	prf curv	max prf curv	shape
1	315-135	>= 40	<= 2	> 50	<= 50	<= -0.2	>= 0.2	>= 4	1
2	226-314	35-39	2-4	40-50	50-400	-0.2-0.2	-0.2-0.2	2-4	2
3	136-225	<= 35	> 4	< 40	> 400	>= 0.2	<= -0.2	<= 2	3

Table 5.7: Classification table for the topographical parameters. The three classes are represented by shades of grey as in Figure 5.17: black for 1, dark grey for 2 and light grey for 3.

To better visualize the results of the AHC analysis on the basis of *numava* and *skew*, plots like the one in Figure 5.17 for every size class were drawn. The x and y axis represent the variable *skew* and *numava*, respectively. Each PRA is represented by a pie where each sector represents one of the nine to-

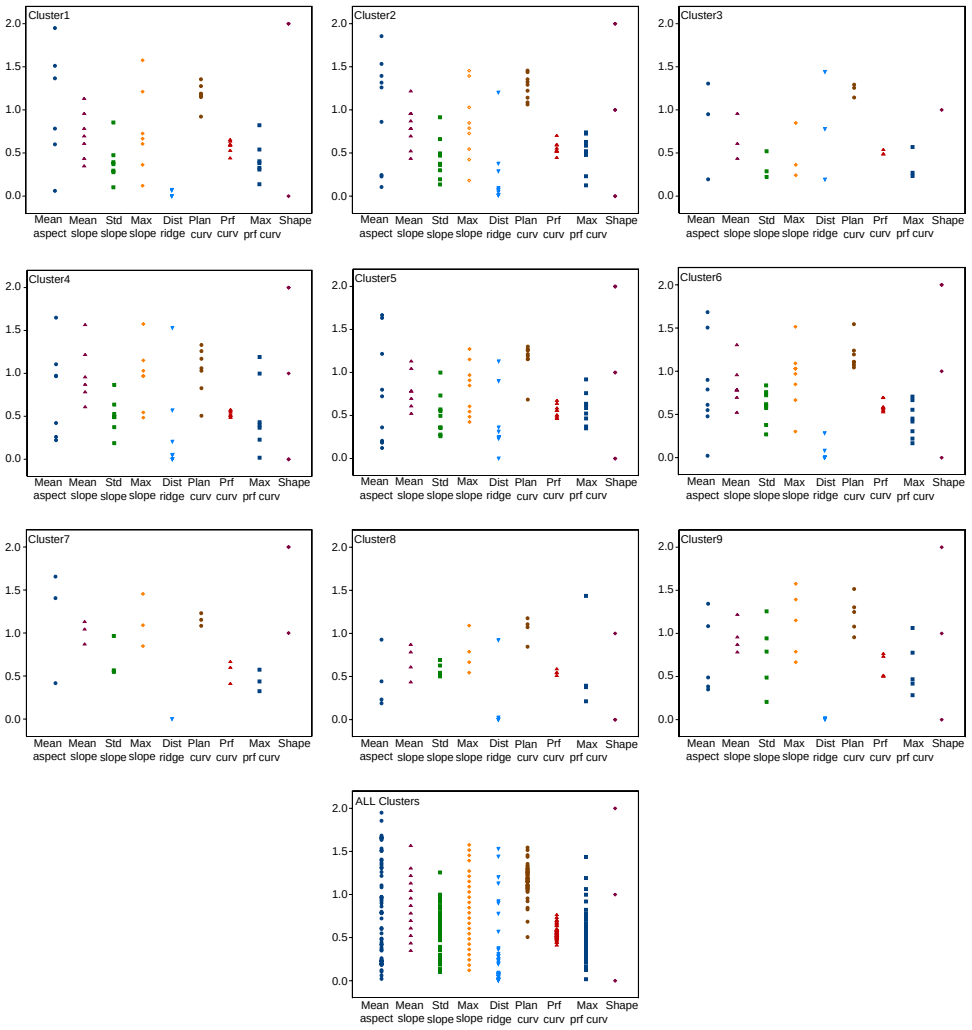

Figure 5.15: Scatterplots for the nine topographical parameters within the nine clusters identified on the basis of *numava* and *skew* for size class 3 and for the whole size class; rescaled values to range [0 - 2].

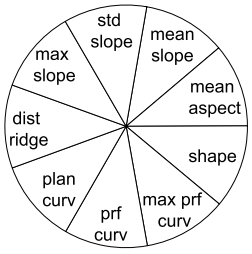

Figure 5.16: Sectors representing the topographical parameters of a PRA in the pie charts used in Figure 5.17.

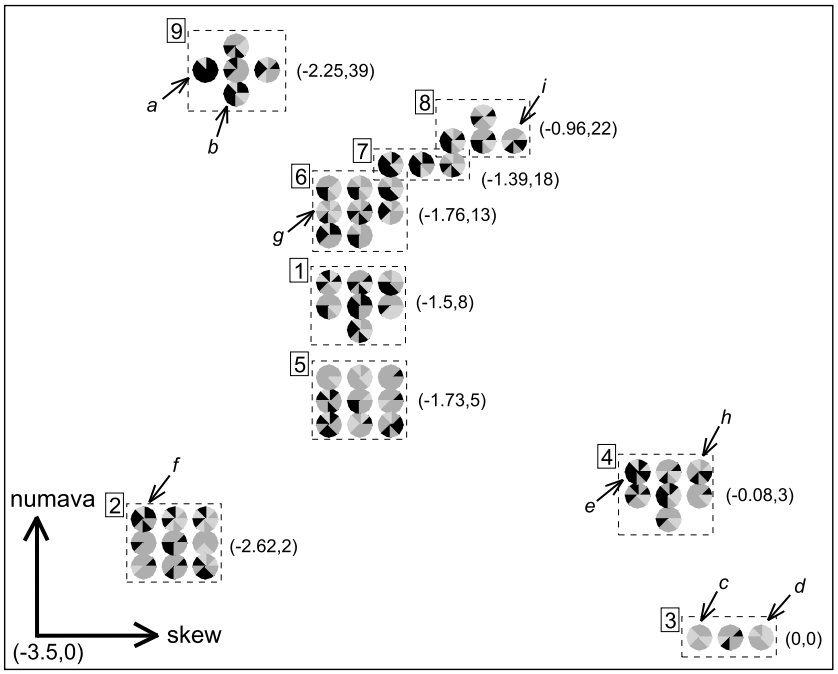

Figure 5.17: Position of the clusters of PRAs on a 2d space defined by *numava* and *skew*. See the text for explanations.

pographical parameters characterizing the PRA (see Fig. 5.16). The shade of grey of each sector is defined according to the classification shown in Table 5.7. This classification considers three classes which indicates the possible influence of the considered parameters on avalanche activity. The classes are defined according to the literature for parameters such as distance to ridge, slope angle and curvature [Munter, 1997; Gleason, 1995; McClung, 2001] and based on expert considerations (U. Gruber, personal communication) for cases where no literature was present about the topic. Class 1 (dark) is the most dangerous class, Class 3 (light gray) the least dangerous and Class 2 (dark grey) in between. For example, a distance to ridge of a few meters is more dangerous than a distance to ridge of hundreds of meters, therefore Class 1 is defined for distances of less than 50 m and Class 3 for distances of more than 400 m. The aim was to verify if this 'expert scheme' was correct and to ascertain whether similar pies belong to the same cluster in Figure 5.17. What is expected is that pies dominated by dark sectors are placed in the top-right corner of the plot (high number of avalanches distributed over all the percentages of PRA), while pies dominated by light gray are placed in the bottom-left corner of the plot (low number of avalanches with small release areas). The analysis of the plot does not fully support the 'expert scheme', since black sectors do not dominate the upper part of the plot. But, there are good examples supporting it: pies *a* and *b*, characterized by at least five dark sectors, that belong both to the Cluster9 placed in the upper part of the plot, or pies *c* and *d*, characterized by no dark sectors and mostly light grey sectors that belong to Cluster3 placed in

the lower part of the plot. On the other hand, pies e and f should be placed higher in the plot, as they have many dark sectors, or pie g is placed too high for having only one dark sectors. There are also cases of little difference in the topographical parameters, e.g. pie h and i, but large difference in the avalanche activity. Good examples could be found to support the 'expert scheme', but no general rules could be derived.

In conclusion, no homogeneity in terms of topographical parameters could be found within the clusters identified on the basis of variables describing avalanche activity.

5.3 Discussion

The initial assumption for this part of the work was that a relationship between avalanche activity and topography exists. Unfortunately, the results presented in this chapter did not support this assumption. There are several possible reasons for this result. The principal reason might be that the quality of the data is not good enough to arrive to a precise conclusion on the existence or otherwise of a relationship between topography and avalanche activity. Another possibility might be that other variables can be adopted to describe the avalanche activity (as it is determined in this work) and perform statistical analysis; or even a different definition of avalanche activity can be used, i.e. frequency together with release area of the largest event.

In this work, three statistical techniques were adopted to analyze the possible relation between avalanche activity and topographical features and each of them gave interesting results.

The application of linear regression models to predict avalanche activity on the basis of seven topographical parameters failed. This result implies that, under the assumption that the model was correct, no statistically significant linear relation between the aforementioned variables exists. Other linear models may be used, for example including different topographic parameters or different numbers of them. Methods like stepwise regression or regression applied on PCA-variables (variables transformed by the Principal Component Analysis) might give information about which are the most significant variables and build models to predict avalanche activity only using those variables. But in general, stepwise regression and regression with PCA-variables almost always gives results that are worse, in terms of prediction's accuracy, than the results of the regression model performed with all the independent variables [Harrell, 2001; MathSoft, 2000].

Alternatively, linear regression models can be used to predict avalanche activity described by *numava* and *skew* instead of by a vector as in equation 5.1. The variables *numava* and *skew* were found to be suitable to describe avalanche activity in the agglomerative clustering method, therefore it may be interesting to see if linear models may work in predicting these variables.

Another statistical method that could be applied is multivariate regression, which does not imply the assumption of independence between the components y_i of the vector representing avalanche activity; it predicts the whole vector

simultaneously.

An important achievement of this chapter is the results of the CART method, which gave information about which topographical variables most influence avalanche activity. These were found to be: standard deviation of slope, distance to ridge, plan and profile curvature for every size class of the potential release area. Recalling the citation of Gleason [1995] given on p. 56-57, the present study adds a contribution to the investigation of the influence of topographic features on avalanche activity, but it is still true that further work is needed to quantify it more precisely. Future studies should focus also on standard deviation of slope, distance to ridge and curvature, to be more complete in the analysis of the avalanche activity with respect to terrain characteristics. In order to confirm the findings of the present study, it will be important to apply this methodology in other regions where good avalanche databases are available.

The agglomerative hierarchical clustering approach applied to topographical parameters identified clusters which are not perfectly homogeneous in terms of avalanche activity, but special features of the avalanche activity were found within these clusters. The reexamination of the clusters that are similar in terms of avalanche activity, in order to find potential similarity in topography, did not provide a positive result. On the other hand, the agglomerative hierarchical clustering approach applied to avalanche activity identified clusters that are very inhomogeneous in terms of topographic attributes. In conclusion, although good examples of PRAs similar both in terms of topographical parameters and of avalanche activity could be found, no general and precise statistical rules could be derived to relate different avalanche activities to different kinds of terrain characteristics. A reason for this might be that in reality a specific avalanche activity can be related to different combinations of topographical attributes. In this case, it is possible that homogeneous clusters in terms of avalanche activity contain PRAs characterized by different topographical parameters. This would mean that our initial assumption was wrong.

The statistical analysis provided a further important result: it underlined the fact that there are large uncertainties in determining avalanche activity, here related to release area. In the procedure of avalanche hazard mapping, the determination of the release area is an important step which contains uncertainties that have to be taken into account. The aim of this work is to use the distributions of the avalanche activity as input for the release area in avalanche simulations. The Monte Carlo approach to avalanche hazard mapping will use these distributions to create, as outputs, distributions for the runout distance and for the impact pressure, which are analyzed in order to account for those uncertainties. Chapter 6 explains the procedure in details and with a real case study.

Chapter 6

Monte Carlo simulation

6.1 Introduction

This chapter addresses the problem of uncertainties in avalanche simulation, especially regarding the avalanche hazard mapping procedure. The basic idea is to consider the uncertainties of each avalanche model input parameter, i.e. release area, fracture depth and friction coefficients, in terms of probability distributions and, in a second step, use these probability distributions as input for Monte Carlo simulations. In this chapter, a first section gives an insight into the methodology of Monte Carlo simulation: the general theory as well as the theoretical basis of its application in case of avalanche simulations is presented. In a second section, a case study is shown to illustrate the methodology. Finally, the results are discussed and the quality and usefulness of the Monte Carlo procedure in avalanche hazard mapping is evaluated.

6.2 Monte Carlo simulation

6.2.1 Theory

Monte Carlo methods are probabilistic analysis techniques that involve using random numbers and probability to quantify uncertainty [Robert & Casella, 1999].

Computer simulations mean using computers to model real life or make predictions. In general, a numerical model involves a certain number of input parameters and equations that use those inputs to produce a set of outputs (or response variables). This type of model is usually deterministic. A deterministic model needs precise values for the input parameters, but in reality, and especially in models of complex processes such as avalanches, it is sometimes very difficult, if not impossible, to provide accurate input parameters. Therefore, it is important to take the related uncertainties into account and to check the sensitivity of the model to the input parameters.

Monte Carlo (MC) simulation can be understood as a method for iteratively evaluating a deterministic model using sets of random numbers as inputs. This technique is often used when the model is complex, nonlinear, or involves many

uncertain input parameters. A simulation can involve thousands of evaluations of the model, a task which in the past could be handled only by using supercomputers [Wittwer, 2004]. The Monte Carlo (MC) method is one of many methods for analyzing uncertainty propagation that aim to determine how random variations, lack of knowledge, or errors affect the sensitivity, or reliability of the system that is being modelled. MC simulation is classified as a sampling method because the inputs are randomly generated from probability distributions to simulate the process of sampling from an actual population. Therefore, an important task is to choose a distribution for the inputs that matches as closely as possible the real data. The outputs generated from the MC simulations are usually represented as probability distributions (or histograms), but summary statistics can also be generated.

6.2.2 Monte Carlo approach to avalanche simulation

The application of the Monte Carlo methodology to avalanche simulation implies several steps:

1. definition of the distributions for the model input parameters,
2. random sampling process,
3. iterative runs of the dynamical avalanche model,
4. analysis of the outputs.

Figure 6.1 shows graphically the steps of the Monte Carlo approach to avalanche simulation.

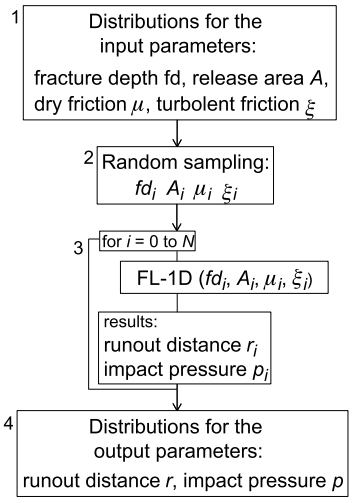

Figure 6.1: Monte Carlo approach to avalanche simulation: N runs of the model FL-1D are performed with different values of fd_i, A_i, μ_i, ξ_i to calculate different values of r_i and p_i. N is the number of sampling for the input parameters generated from their distributions. The resulting runout distance and impact pressure are also represented as distributions.

The deterministic dynamic model used to simulate avalanches is the model FL-1D described in Section 2.3. The inputs of FL-1D are: avalanche profile, release area A, fracture depth fd and friction coefficients μ and ξ. The model outputs relevant for the avalanche hazard assessment are runout distance and impact pressure. Barbolini et al. [2000] performed a sensitivity analysis of different models of avalanche dynamics, FL-1D included. The results showed that the runout distance calculated by FL-1D is sensitive to all of the input parameters. A variation of 30% in the value of the friction parameter μ can produce a variation of up to 20% in the runout distance; variations of 30% in the values of the friction parameter ξ, the fracture depth fd and the release area A produce variations for the runout distance of the order of 5%. Therefore, it is important to take into account the uncertainties present in the determination of the input parameters, given that the outputs of the model are sensitive to their variation. A variation in the definition of the profile might also have influence on the model outputs, but in this study the profile was always defined only once and kept constant for all the simulations.

The first step was to determine the distributions for the fracture depth, the release area and the friction coefficients. This study focuses on the uncertainty of the release area; for this input parameter a precise definition of the distribution is provided. For the other parameters simple approaches were applied. MC simulations were used in this study for two applications with different purposes, therefore the distributions for the input parameters were derived in two different ways according to the considered aim.

Reproduction of Historical Avalanche Events (RHAE). In this case, the aim was to inverse model the known historical avalanche events, therefore real data were used directly to derive the distributions both for the release area and for the fracture depth. For friction parameters μ and ξ, normal distributions were chosen with a mean value linearly interpolated from the values suggested by the Swiss Guidelines (see Table 2.2 in Section 2.3). The standard deviation was chosen to be equal to 10%, 20% and 30% of the mean value in order to test the sensitivity of the model to the standard deviation. These standard deviations cover a range of friction values which are realistic and within the range proposed by SLF [1999b]. The results of the three simulations should tell which is the best value for the standard deviation to inverse model historical avalanche events; this value will then be used in future applications.

Avalanche Hazard Mapping (AHM). In this case, the Monte Carlo procedure was applied in order to estimate the uncertainties present in an avalanche hazard map. Recall that in avalanche hazard mapping, avalanches with a return period (T) of 30 and 300 years, respectively, have to be simulated (see Section 2.4). The input for the fracture depth were normal distributions centered on mean values suggested by the Swiss Guidelines, for avalanches with a return period of 30 and 300 years, and a standard deviation equal to the 15% of these values. For the release area, the total extent of the potential release area was used as an input for avalanches with a return period of 300 years. For avalanches with a return period of 30 years, the Gumbel statistic [Reiss & Thomas, 1997] was applied to the data representing release areas of past avalanche events, to determine a value that was taken as the mean value of the

normal distribution used as input for the release area. The distributions for the friction coefficients μ and ξ were chosen to be a normal distribution with a mean value given by the Swiss Guidelines (see Table 2.2 in Section 2.3) and a standard deviation equal to 15% of this value.

The example of Brämabüel given in the next section describes these two cases in more detail (reproduction of historical avalanche events and avalanche hazard mapping).

The second step of the procedure was to perform random sampling of the distributions of the input parameters, in order to create N different scenarios and, in **the third step**, run the dynamical model FL-1D as many times as the sampling number N. In this study, N was chosen equal to 500.

The fourth step was the analysis of the outputs given in the form of distributions. Runout distance and impact pressure are described by the mean value and standard deviation of their distributions which take into account the uncertainties in their determination.

A bespoke program that integrates AML (ArcInfo Macro Language), C and S-Plus was written for the implementation of this Monte Carlo procedure.

6.3 Application to a real case study: Brämabüel

In this section, a real case study is considered and the procedure of the MC simulation is applied to the two different cases explained in Section 6.2.2.

The avalanche slope of Brämabüel is situated at the beginning of the Dischma valley in the region of Davos (see Figures 6.2 and 6.3). It is a steep constant slope, always above 30°, from an altitude of 2300 m a.s.l. down to the valley bottom at 1560 m a.s.l., where the inclination becomes gentler. It has a N-NE aspect. On the Northern side of Brämabüel, avalanches are frequent. They can break loose from different release areas and run down the slope taking as path one of the four channels through the forest. The avalanche track considered in this case study is shown in Figure 6.2. As potential release area for this avalanche track, the PRA resulting from the automatic procedure explained in Section 4.2 was used; the total extent of this PRA is 39800 m^2 (Fig. 6.2).

6.3.1 Brämabüel: reproduction of historical avalanche events (RHAE)

In the reproduction of historical avalanche events (RHAE) case, the goal is to reproduce the past avalanche events by the MC simulation. From the analysis carried out in Section 4.2, the avalanche activity of the considered PRA consists of a total of 20 avalanches occurring within the 49 years of the database (1949-1997).

The first step is to determine the distributions for the input parameters, namely fracture depth (fd), release area (A) and friction coefficients (μ and ξ).

The friction coefficients μ and ξ are represented by a distribution centered on a mean value linearly interpolated from the values given by the Swiss Guidelines [SLF, 1999b]. For the Brämabüel avalanche track and assuming a return period of 30 years, the mean value $\overline{\mu}$ was taken equal to 0.25 and the mean value $\overline{\xi}$

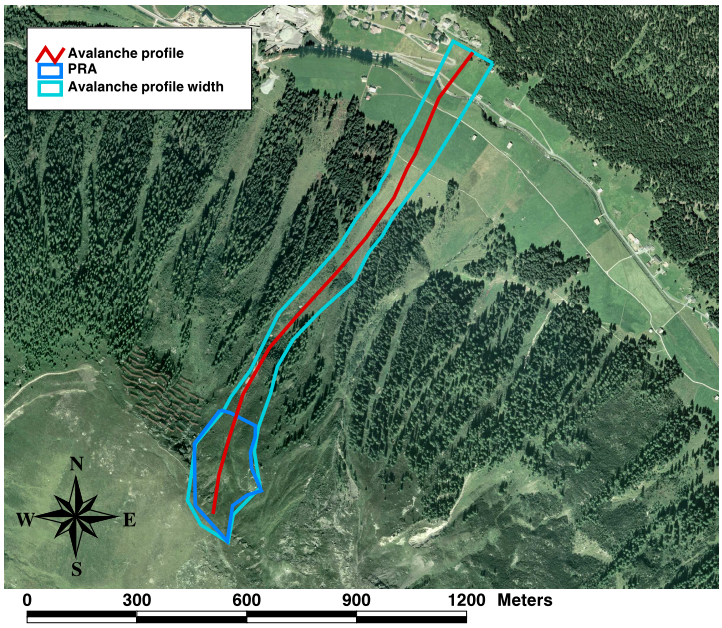

Figure 6.2: Orthophoto of the Brämabüel slope. The considered avalanche track and potential release area are shown. Topographic base map reproduced by permission of swisstopo (BA046644). Orthophoto: SWISSIMAGE ©2000 swisstopo (DV023193).

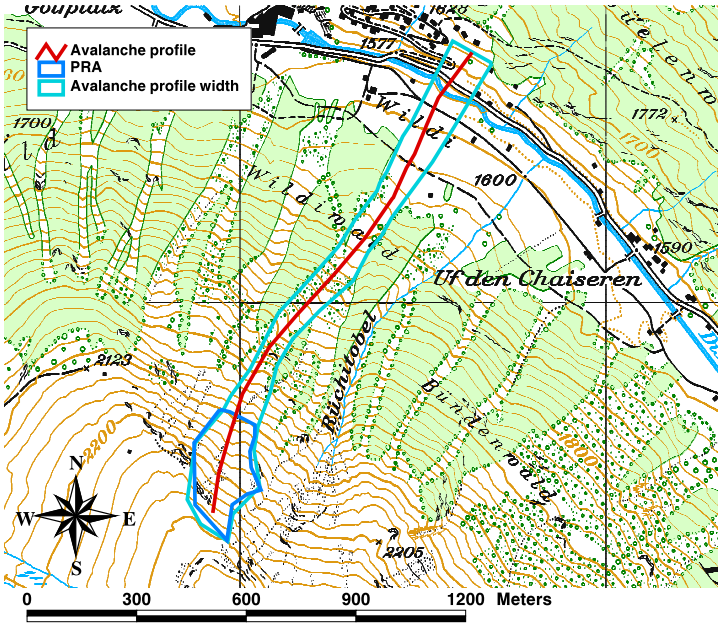

Figure 6.3: Map of the Brämabüel slope. The considered avalanche track and potential release area are shown. Topographic base map reproduced by permission of swisstopo (BA046644).

equal to 1555 m/s^2 (the reference avalanche volume to determine the friction coefficients was 23880 m^3). Three different values for the standard deviation were used, equal to 10%, 20% and 30% of the mean values.

For the release area, the distribution generated from the analysis of the past avalanches that released from the considered PRA was used. This distribution was extracted from the database of PRAs with the related avalanche activity resulting from the analysis described in Section 4.4. Figure 6.4a shows the distribution for the release area of the considered PRA at Brämabüel, not as a percentage of the total potential release area but with absolute values.

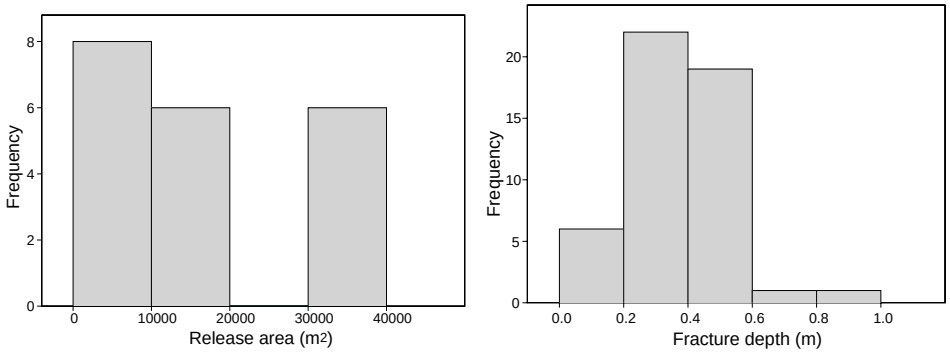

(a) (b)

Figure 6.4: Release area and fracture depth distributions used as input for the MC simulation in the RHAE case study.

The fracture depth distribution was derived using the results of the procedure that is used in Switzerland for avalanche hazard mapping [Salm et al., 1990]. This procedure assumes that the maximum yearly increase of snow cover within three days (HS_DIF3D) is representative for the fracture depth of avalanches. For avalanche hazard mapping purposes, the yearly maxima of HS_DIF3D are extrapolated using the extreme-values statistics technique of Gumbel analysis. This technique is able to relate the maximum values of a variable (in this case HS_DIF3D) with its return period [Reiss & Thomas, 1997]. In Figure 6.5 an example of such an analysis is shown for the snow measurement site Weissfluhjoch. This plot can be used to extrapolate the values of the fracture depth for the desired return period. According to the Swiss Guidelines, the extracted value has to be corrected by factors related to the slope angle and the altitude of the release area and to the snow drift process (refer to Salm et al. [1990] for the description of these correction factors).

However, in this case study, the goal is not to extrapolate the fracture depth for 30 and 300 years avalanche events, but to reproduce historical avalanche events that occurred between 1949 and 1997. Therefore, the values of HS_DIF3D, recorded at the snow measurement site Weissfluhjoch during the same time period have been directly used, after applying the slope, altitude and snow-drift corrections, to create the corresponding fracture depth distribution (see Figure 6.4b).

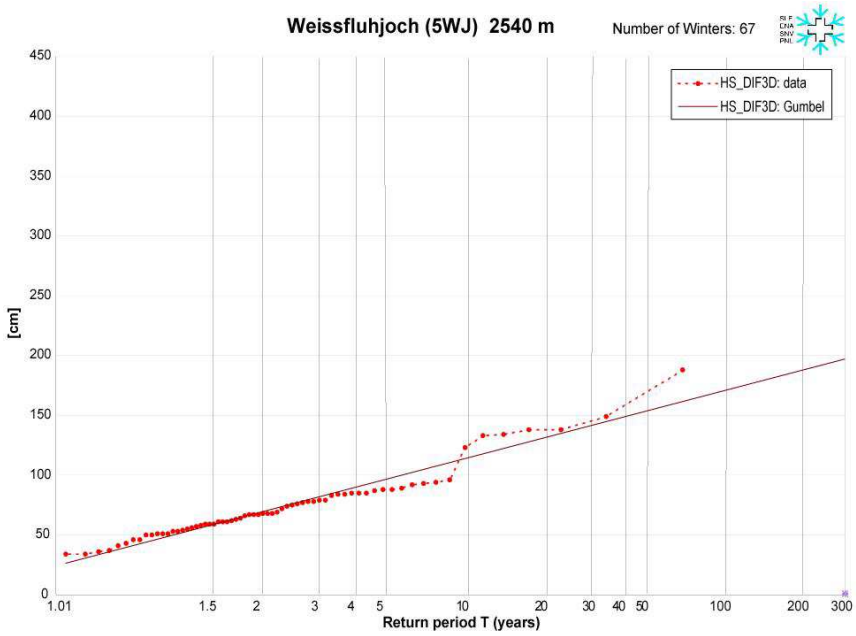

Figure 6.5: Gumbel statistic for the data of the snow measurement site Weissfluhjoch: maximum difference of the snow height over three days (HS_DIF3D) versus the return period (T). Source: SLF Database.

After all the necessary inputs for the MC simulation were determined, random sampling was performed and $N = 500$ runs (N = number of sampling) of the FL-1D model were made. The outputs of the MC simulation procedure are represented by distributions. In the RHAE case study, the interesting outputs are the runout distances, which were compared to the runout distances of the real historical data. In Figure 6.6 the results of the MC simulations are shown, together with the outline of the historical events. Figure 6.7 shows the distributions of the runout distances of the simulated avalanches for the three different standard deviations for the friction parameters. As expected, the runout distances of the simulation with 30% covered a wider range than the ones of the simulation with 10% and 20%, respectively. However, the mean values are all placed at an altitude of about 1620 m a.s.l., corresponding to an avalanche length of 1140 $\pm$ 15 m.

A comparison with the runout distances of the historical avalanches was made visually on the map and along the avalanche profile as displayed in Figure 6.7. The MC simulation results with standard deviation for the friction coefficients μ and ξ equal to 30% show a good fit to the real medium and large size avalanche events. The MC simulations with standard deviations equal to 10% and 20% underestimated the range of the real medium and large size avalanche events.

Most historical avalanches stopped at an altitude of 1610-20 m a.s.l. where the simulated avalanches also mostly stopped. But the five smallest avalanche events were not reproduced by the MC simulation, because they stopped at

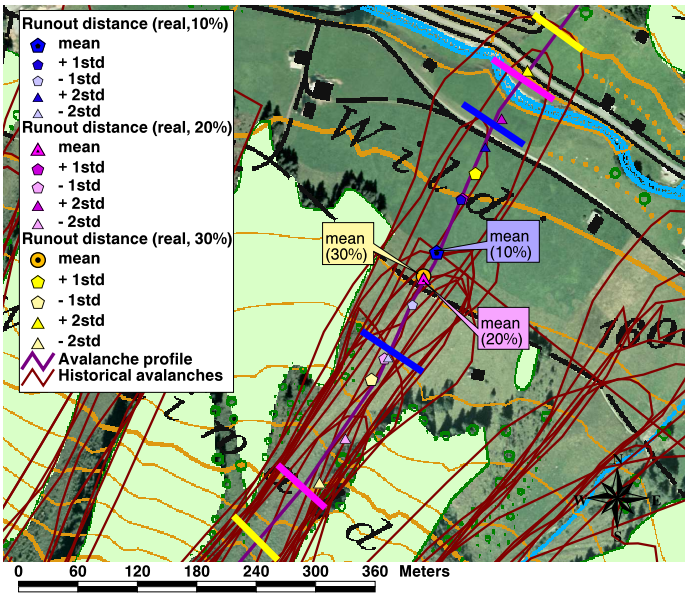

Figure 6.6: Runout distances resulting from the three MC simulations in the RHAE case study, in comparison with the runout distances of the historical avalanches. The yellow, pink and blue lines show the range of the runout distances for the three different MC simulations. Topographic base map reproduced by permission of swisstopo (BA046644). Orthophoto: SWISSIMAGE ©2000 swisstopo (DV023193).

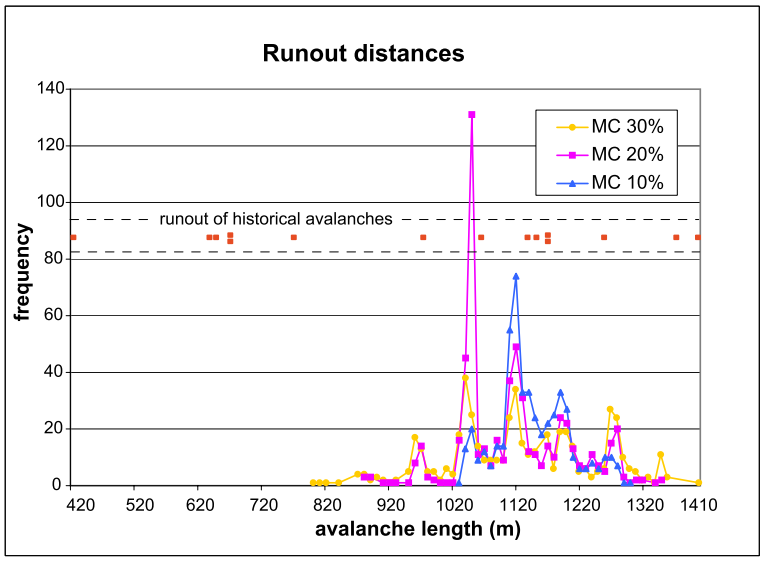

Figure 6.7: Distribution of the runout distances resulting from the three MC simulations in the RHAE case study. The red dots represent the runout distances of the historical avalanches. The avalanche length is calculated from the beginning of the avalanche profile.

an altitude between 1800 and 2000 m a.s.l. and on terrain steeper than 29°. This slope angle is considered, within the FL-1D model, too steep for a runout zone. Therefore, these avalanches were directly checked in the winter reports [SLF, 2002], where it was found that they were effectively avalanches of small dimension. Most likely, they were small avalanches with high friction and insufficient mass to carry on further down the slope. This is a clear indication that the model FL-1D is not calibrated for such small avalanches and therefore has difficulties reproducing them. However, although the aim of this section is to reproduce, as closely as possible, historical avalanche events, the fact that these small avalanches were not well reproduced is not necessarily a problem when considering the global usefulness of this procedure. The possible usefulness of the proposed procedure is in estimating the avalanche activity in the lower part of avalanche paths where avalanches have a significant influence on land use by humans. For example, in the case of the avalanche path of Brämabüel, it is useful to know the frequency of avalanches crossing the main road or the cross-country skiing path situated by the river, but it is only of marginal interest whether a small avalanche occurred in the upper part of the slope.

6.3.2 Brämabüel: Avalanche Hazard Mapping (AHM)

In the avalanche hazard mapping (AHM) case, the goal is to generate an avalanche hazard map that includes uncertainties, using the MC simulation procedure.

In Switzerland, the Swiss Guidelines recommend simulating avalanches with return periods of 30 and 300 years (also referred to as 30yr and 300yr avalanches, respectively) to calculate impact pressures and runout distances of frequent and extreme avalanches. Therefore, the MC simulation was used in both cases, with appropriate input parameters.

For avalanches with a return period of 300 years, normal distributions for μ, ξ and fracture depth were built with mean values equal to the values suggested by the Swiss Guidelines [SLF, 1999b; Salm et al., 1990] and standard deviations equal to 15% of these values: $\overline{\mu} = 0.2$, $\overline{\xi} = 2000$ m/s^2 and fracture depth $\overline{fd} = 1.27$ m (the reference avalanche volume to determine the friction coefficients was 50546 m^3). In this case, the standard deviation was chosen to be 15% because the aim is to reproduce a particular return period (e.g. 30 or 300 years), whereas the goal of the RHAE case was to reproduce a larger spectrum of return periods (i.e. return periods from about 2 to 50 years). Another reason for the choice of the standard deviation equal to 15% was that larger values of the standard deviation would produce unrealistic values for the input parameters (given a return period, the values suggested by the Swiss Guidelines lie within a specific range which would be not conformed with when using distributions with larger standard deviations). The release area is assumed to be equal to the total extent of the potential release area (39800 m^2), which is normally the case with extreme avalanches. The MC simulation consisted of 500 runs, resulting in the runout distance distribution shown in Figures 6.8 and 6.9. In Figure 6.8, the limit between the red and the blue zones for avalanches with return period of 300 years is also shown. These results have to be combined with the outputs

of the MC simulation for avalanches with return period of 30 years to produce the final avalanche hazard map.

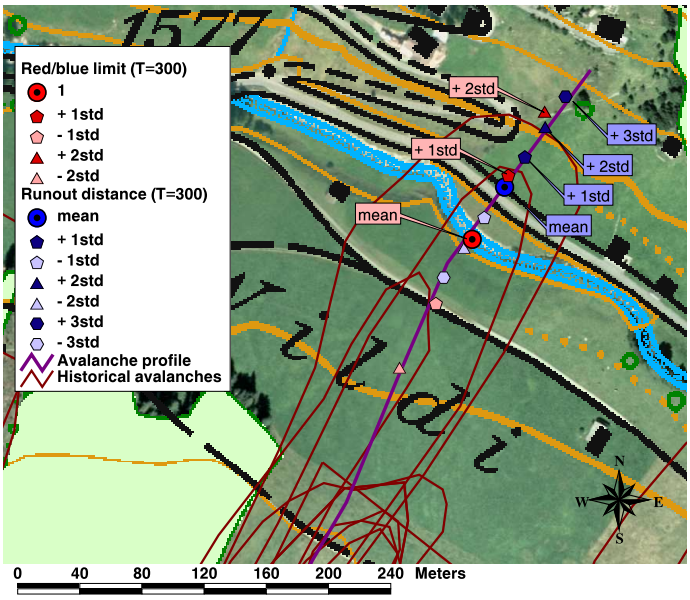

Figure 6.8: Runout distances and red/blue limit resulting from the MC simulation for 300yr avalanches in the AHM case study. The runout distances of the historical avalanches are also shown. Topographic base map reproduced by permission of swisstopo (BA046644). Orthophoto: SWISSIMAGE ©2000 swisstopo (DV023193).

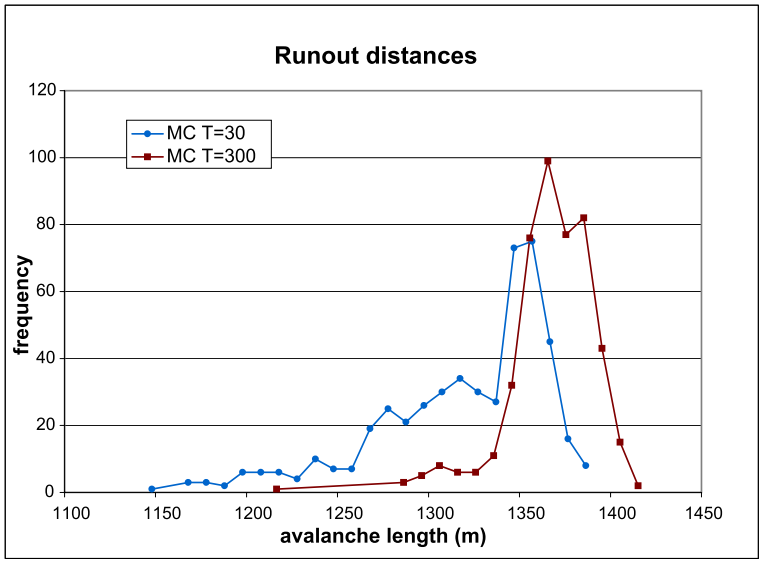

Figure 6.9: Distributions of the runout distance resulting from the MC simulations for 300 and 30 years avalanches in the AHM case study. The avalanche length is calculated from the beginning of the avalanche profile.

For avalanches with a return period of 30 years, normal distributions for μ, ξ and fracture depth were built with mean values equal to the values suggested by the Swiss Guidelines [SLF, 1999b; Salm et al., 1990] and standard deviations equal to 15% of these values: $\overline{\mu} = 0.25$, $\overline{\xi} = 1555$ m/s^2 and fracture depth $\overline{fd}$ = 0.94 m (the reference avalanche volume to determine the friction coefficients was 37412 m^3).

The input for the release area is, in this case, also a normal distribution, but centered on a value determined by the following procedure; the standard deviation was again chosen as 15% of the mean value. A Gumbel statistic, similar to that usually carried out with snow data, was calculated with the data of the release area of the past avalanches that released from the considered PRA at Brämabüel. Of the 20 avalanches that occurred there in the 49 years of the avalanche database, the extent of the maximum release area per year is stored. The Gumbel statistic applied on these maximum values results in the fit shown in Figure 6.10, which relates the extent of the release area, in percentage of the total PRA, to the return period T.

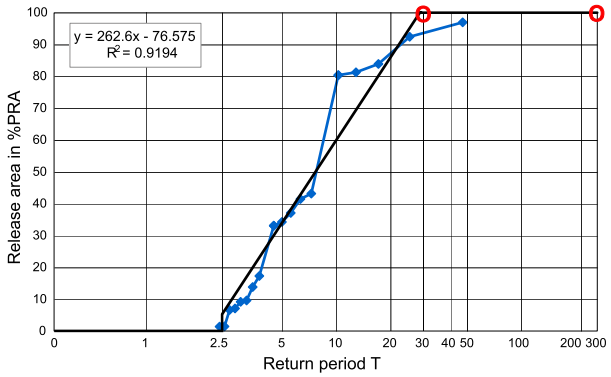

Figure 6.10: AHM case study: Gumbel statistic for the release area plotted against the return period. See text for explanations.

Since the release area cannot assume negative values, a minimum value for the release area had to be found. A total of 20 avalanches in 49 years means that on average there was an avalanche every 2.5 years and that avalanches with a smaller return period had a release area equal to zero, i.e. there were no avalanches with a return period T lower than 2.5 years. From the fitted curve, the release area becomes equal to 100% of the total PRA for avalanches with a return period of 28 years. This finding supports our assumption that for a 300yr avalanche the total extent of the PRA has to be taken as input for the avalanche simulations. Also a 30yr avalanche has the release area already equal to 100% of the PRA, therefore, in this case, the input to the MC simulations is the constant value 39800 m^2 (total extent of the PRA).

As with the friction coefficients μ and ξ, the standard deviation for the release area was taken to be equal to 15 % of the mean release area value.

Figures 6.9 and 6.11 show the distribution of the runout distance resulting from the MC simulation for avalanches with return period of 30 years. These re-

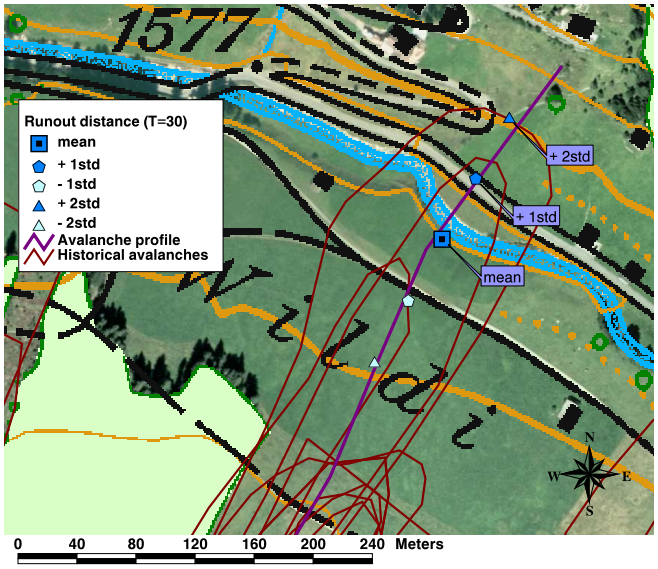

Figure 6.11: Runout distances resulting from the MC simulation for 30yr avalanches in the AHM case study. The runout distances of the historical avalanches are also shown. Topographic base map reproduced by permission of swisstopo (BA046644). Orthophoto: SWISSIMAGE ©2000 swisstopo (DV023193).

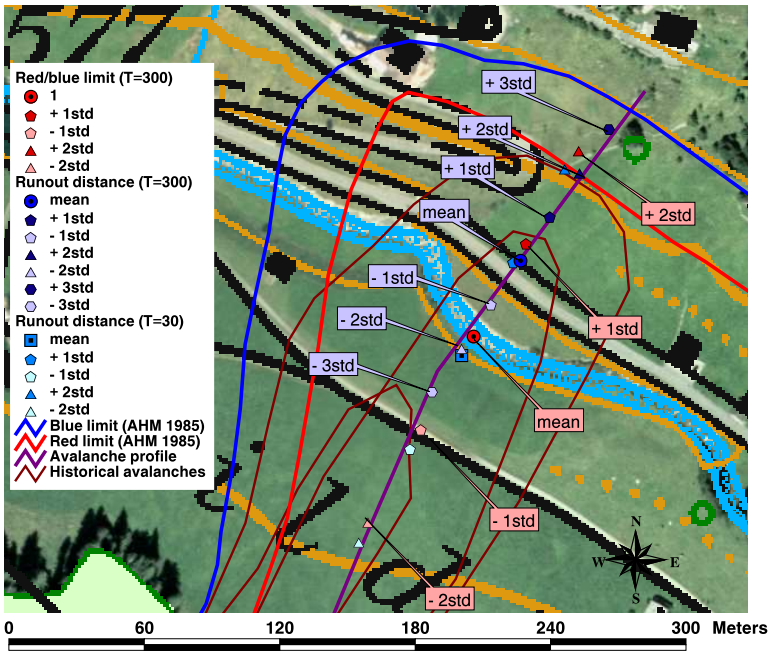

Figure 6.12: Output of the MC simulation to be used to define the hazard zones for the avalanche track at Brämabüel. Also the official avalanche hazard map is shown (continuous red and blue lines). Topographic base map reproduced by permission of swisstopo (BA046644). Orthophoto: SWISSIMAGE ©2000 swisstopo (DV023193).

sults, together with the results of the MC simulation for avalanches with a return period of 300 years, are able to represent the two big avalanches which crossed the road and climbed the opposite slope and which were not caught by the MC simulation in the RHAE case study (see Section 6.3.1). Figure 6.9 shows how most of the 30yr avalanches stopped, as expected, before the 300yr avalanches. Combining the two MC simulations, the possible avalanche hazard map which includes uncertainties for the considered avalanche path at Brämabüel could be drawn (Fig. 6.12 and 6.13). Recall that the red/blue limit is defined either by the position where the 300yr avalanches have a pressure of 30 kPa or by the runout distance of the 30yr avalanches. For the modelled path, the worst case for the definition of the red/blue limit is given by the simulation of avalanches with a return period of 300 years, which is therefore used to define the hazard zones (see Section 2.4). The mean values for the red/blue limit and for the blue limit (runout distance) are placed at a distance of 40 m. The standard deviations for the distributions of the red/blue limit and of the blue limit are equal to 47 and 24 m, respectively.

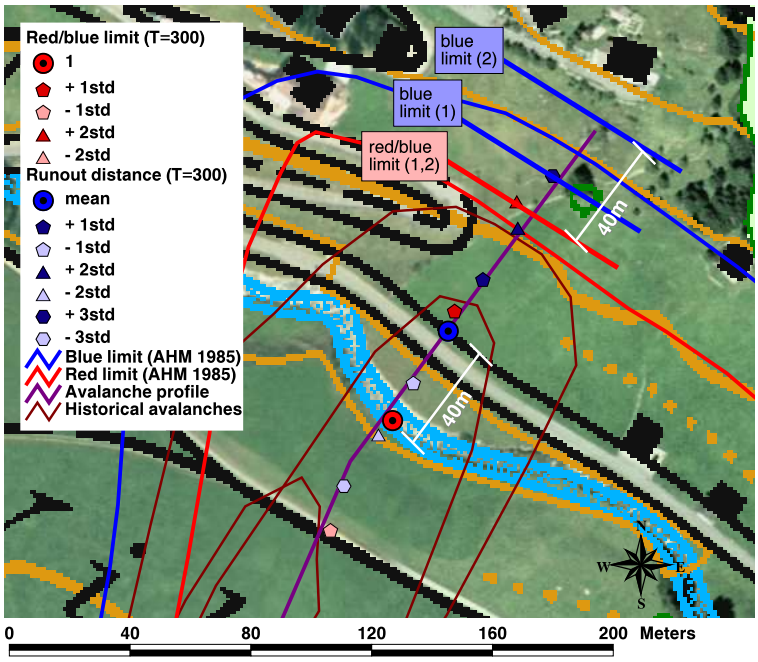

Figure 6.13: Proposed delineations (1 and 2) of the avalanche hazard map for the considered avalanche track at Brämabüel. The straight red and blue lines represent the limits of the red and blue zones, respectively. The official avalanche hazard map is also shown. Topographic base map reproduced by permission of swisstopo (BA046644). Orthophoto: SWISSIMAGE ©2000 swisstopo (DV023193).

The initial idea was to use the *mean value + 2std* to define the limits of the hazard zones. In this case, there would be no blue zone because the position of the *mean value + 2std* for the blue limit lies before the position of the *mean value + 2std* for the red/blue limit (Fig. 6.12). This happened

because of the presence of the opposite slope at the end of the runout zone of the avalanche path of Brämabüel. Due to the opposite slope, the avalanches can not develop further along the avalanche path, therefore the distribution of the runout distance (blue limit) is less spread than the distribution for the red/blue limit. Recall that, in this case, the red/blue limit is defined as the position where the pressure of the 300yr avalanches is equal to 30 kPa (see Section 2.4). The avalanches reached this pressure while still travelling downslope and therefore this distribution is not affected by the presence of the opposite slope. In general, models of avalanche dynamics encounter difficulties in simulating avalanches with such runout zones. Therefore, two solutions are proposed for this, and similar cases.

The first solution (1) suggests defining the red/blue limit by the *mean value + 2std* and the blue limit by the *mean value + 3std* (Fig. 6.12 and 6.13).

The second solution (2) takes into consideration only the mean value for the position of the blue limit and determines the corresponding standard deviation using the assumption underlying the analytical model of Voellmy-Salm [Salm et al., 1990]. Salm et al. [1990] considered that the pressure decreases linearly in the runout zone. Under this assumption, the standard deviation for the distribution of the blue limit can be taken as equal to the standard deviation of the distribution of the red/blue limit, therefore, the distance between the mean value for the red/blue limit and the mean value for the blue limit (40 m) is equal to the distance between the corresponding *mean values + 2std*. Therefore, the position of the *mean value + 2std* for the blue limit is placed 40 m after the one of the red/blue limit. With this solution, the limits of the hazard zones are defined by the *mean value + 2std* (Fig. 6.12 and 6.13).

Both proposed solutions to analyze the output of the MC simulations for the definition of the avalanche hazard zones defined the red/blue and the blue limits at positions near to the limits of the official avalanche hazard map [Summaprada, 1985]. The variability of the red/blue limit defined by the MC procedure is high and the *mean value + 2std* can represent the red/blue limit proposed by the official hazard map. The official blue limit is located between the two possible blue limits delineated by the two aforementioned proposals.

6.4 Discussion

MC simulation was shown to be a valuable method to estimate possible avalanche hazard in an avalanche path. For the Brämabüel avalanche path, in the reproduction of historical avalanche events case study, the comparison of the runout distances of the historical avalanche events with the runout distances resulting from the MC simulation are in good agreement with the historical avalanches of medium and large dimension.

The MC simulations in the AHM case study produced avalanche runout distances shorter than the blue limit delineated by the official hazard map [Summaprada, 1985]. As explained in Section 6.3.2, in this case study, this is related to the presence of an opposite slope. The two proposed solutions are able to overcome this problem and produce realistic avalanche hazard maps

similar to the official one.

The example of Brämabüel highlighted the fact that the Monte Carlo approach to avalanche hazard mapping cannot give precise and faultless rules about how to define hazard maps, but can provide useful information about the uncertainties in determining the red and blue limits. An expert might find support in this tool which provides results that, however, have to be critically analyzed in each special case. For example, in the considered avalanche path, the presence of the opposite slope was taken into consideration in drawing the final hazard limits. In another case, the presence of an abrupt increase of the steepness within the runout zone might produce the opposite effect, namely a more extended distribution for the blue limit than for the red/blue limit. All possible different cases have to be critically judged by the expert who has to draw avalanche hazard maps. Moreover, it has to be recalled that the procedure to generate avalanche hazard maps includes different aspects (see Section 2.4), and that here only avalanche simulation has been considered.

The most relevant result of this chapter is the proposal of a procedure to create avalanche hazard maps which include uncertainties. Barbolini [1999] combined avalanche dynamics calculations with statistical analysis to create a methodology to quantify these uncertainties; he also used the Monte Carlo technique. The main improvement over that work is that here the distribution for the release area was generated by studying past avalanche events and not simply with a triangular distribution function centered on an assumed most probable value for the release area and ranging between estimated minimum and maximum values. As said in Section 6.2.1, it is important to use as input distributions that are as close as possible to real data, because, in this way, the random sampling is able to reproduce scenarios representative of the reality.

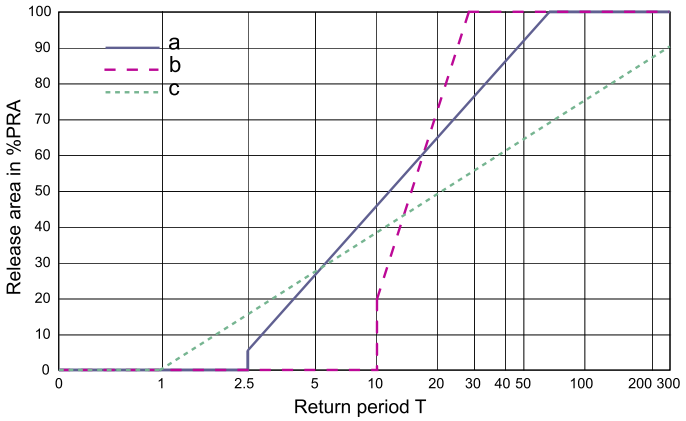

Figure 6.14: Fictitious examples of possible results of the Gumbel statistics applied on the data of release areas of past avalanche events within three different potential release areas.

The Gumbel statistic provides information about the extent of the release area (as a percentage of the total PRA) of an avalanche with a specific return period. Figure 6.14 provides fictitious examples of the possible results of the

Gumbel statistic applied to different PRAs. For PRAb, as for the PRA at Brämabüel (see Fig. 6.10), the release area of an avalanche with a return period of 30 years already covers the total extent of the PRA. In case of PRAa, 100% of the PRA is reached by an avalanche with a return period T of 90 years and the extent of the release area for an avalanche with a return period T of 30 years is equal to 77% of the PRA. PRAb is an example of a potential release area with only 5 avalanches within the 49 years of the recording period. In such a case it is not possible to have information about avalanches with a return period of less than 10 years. For both PRAa and PRAb, as well as for Bramabüel, the release area of avalanches with a return period of 300 years covers the total extent of the PRA, while for PRAc these avalanches have a release area equal to 90% of the PRA.

Analyzing the Gumbel statistic produced for all the PRAs in the database would be an interesting exercise to see whether the assumption that avalanches with a return period of 300 years have a release area equal to the total extent of the PRA is correct. Moreover, it would be possible to give recommendations about the extent of the release area of avalanches with a return period of 30 years for the avalanche hazard mapping procedure. In cases where an expert has to create an avalanche hazard map for an avalanche site with good records of past avalanche events, they could apply the Gumbel statistic to the values of the historical release areas, in order to derive the information about the extent of the release area for avalanches with return periods of 30 and 300 years, respectively. In cases where an avalanche path with no historical data exists, the expert could use the procedure that will be explained and illustrated with three examples, in the next chapter.

Chapter 7

Applications for avalanche hazard assessment

7.1 Introduction

In this chapter, the main goal is to develop a useful methodology to assess the hazard level (as defined in Section 2.4) in the zone of influence of avalanches for areas where there are insufficient and/or poor quality records of past avalanche events. This methodology combines the procedures described in chapters 4 and 6.

The underlying idea is to use information about avalanche activity from other avalanche paths, with similar PRAs in terms of topographical characteristics, where avalanche information are available, and apply it to the undocumented avalanche paths. Here, the Monte Carlo simulation can be applied to determine the avalanche hazard level and its related uncertainties.

The chapter is structured into two main sections: first, the method is explained in detail and secondly, three case studies are presented. The final discussion describes the strengths and weakenesses of the proposed procedure and possible future developments.

7.2 Method

The proposed procedure to estimate possible avalanche activity for an undocumented avalanche path and to produce an avalanche hazard map that includes uncertainties consists of five steps:

1. Definition of the potential release area.
2. Topographical characterization of the defined PRA.
3. Comparison of the topographical characteristics of the PRA with other PRAs for which avalanche activity is known.
4. Derivation of avalanche activity (or release area distribution) for the PRA from the avalanche activities of the most similar PRAs of the database.

5. Monte Carlo (MC) simulation to estimate possible avalanche runout distances and to produce an avalanche hazard map including uncertainties.

The first and **the second steps** have already been explained in detail in Chapter 4. Therefore, they are only briefly described here. For a new avalanche path, a potential release area has first to be defined. In order to do this, the PRA definition procedure is applied; the necessary input is the Digital Elevation Model. After the PRA has been defined, the PRA characterization procedure is used to determine its characterizing topographical features.

During **the third step** the topographical characteristics of the PRA are compared to those of other PRAs (which have associated data on avalanche activity). Since in Section 5.2.3, no clear relationship in terms of topography and avalanche activity was found within the clusters, the comparison procedure does not use the clusters, but searches for similar PRAs directly in the database. Note that the size of the new PRA is determined first, in order to make comparisons only with PRAs of the same size class.

In Section 5.2.3, the PRAs were represented by pies with sectors defined on the basis of the classification given in Table 5.7. Each of the nine topographic parameters belongs to either class 1, 2 or 3, and is represented in a pie by a sector of a different level of grey (see Figure 5.17). Also here, the PRAs are characterized by the same topographic classification.

The comparison procedure, referred to as a *similarity matching* procedure, calculates the similarities of PRAs in terms of distance between their characterizing topographic parameters. The difference function between two PRAs, represented by the vectors v and p, is given by:

$$d(v,p) = \sum_{i=1}^{9} d(v_i, p_i) \tag{7.1}$$

where $d(v_i, p_i) = 1 - \delta_{v_i,p_i}$, i being the index for the i^{th} topographic parameter. The function *Kronecker delta* δ_{v_i,p_i} implies that the difference $d(v_i, p_i) = 0$ if $v_i = p_i$ and $= 1$ if $v_i \neq p_i$ [Arfken & Weber, 1985]. The difference between two PRAs is equal to the sum of the differences of the topographical features. A PRA in the database is considered similar to the new one, and therefore included in the analysis, if the distance given in equation 7.1 is less than 4 ($d \leq 3$).

The fourth step consists of the determination of the release area distribution of the new PRA from those of the most similar PRAs. This distribution is determined in two different ways depending on the purpose of the analysis, namely, if the goal is the determination of runout distances of frequent avalanches (frequent avalanches (FA) case, as in the reproduction of historical avalanche events (RHAE) case for Brämabüel) or it is the determination of the avalanche hazard zones (as in the avalanche hazard mapping (AHM) case for Brämabüel).

If the purpose is to estimate the runout distances for frequent avalanches (FA case), the release area distribution for the new PRA is represented by a vector determined directly by the avalanche activities of the most similar PRAs of the database. However, PRAs that differ from the new PRA in one, two or three topographic parameters have different weights in determining the avalanche activity (or release area distribution) for the new PRA. The weights were chosen in order that more similar PRAs are more relevant than less similar PRAs (see Table 7.1).

Table 7.1: Weights for the determination of the avalanche activity of a new PRA by the similarity matching procedure.

Number of differences	Weights
0	7
1	3
2	2
3	1

The final avalanche activity for the new PRA is therefore determined as:

$$v_{ava} = \sum_{i=1}^{10}(w_a \cdot a_i + w_b \cdot b_i + w_c \cdot c_i + ...) \tag{7.2}$$

where $a, b, c, ...$ are the vectors of avalanche activity for the similar PRAs and $w_a, w_b, w_c, ...$ are the corresponding weights.

As an example, consider three PRAs found in the database to be similar to the new one. PRAa differs from the new PRA only for 1 topographic feature, therefore is weighted with a factor 3, PRAb has a difference of 3 and is weighted with a factor 1, PRAc has all the nine topographic parameters identical to the new PRA and is weighted with a factor 7. These PRAs have the following associated avalanche activity:

$$a_{ava} = (5, 2, 0, 0, 1, 0, 0, 0, 0, 0)$$

$$b_{ava} = (0, 0, 3, 0, 0, 0, 0, 0, 1, 1)$$

$$c_{ava} = (2, 1, 0, 0, 0, 0, 0, 0, 0, 0)$$

The resulting avalanche activity for the new PRA is represented by:

$$v_{ava} = 3 \cdot a_{ava} + b_{ava} + 7 \cdot c_{ava} = (29, 13, 9, 0, 3, 0, 0, 0, 3, 3)$$

The vector v_{ava}, combined with the extent of the new PRA, gives the necessary information to generate the input for the release area in the MC simulation.

In order to estimate the quality of the similarity matching procedure, it was used for six different potential release areas within the region of Davos, where

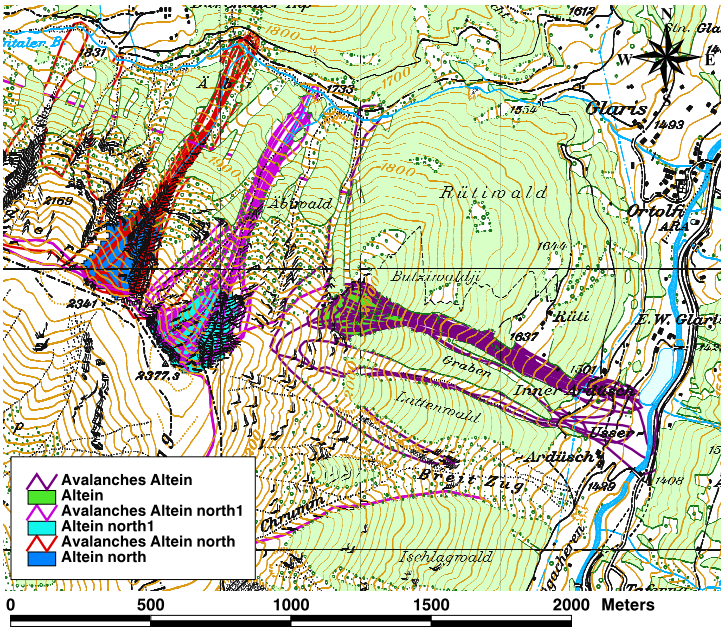

Figure 7.1: Area of Glaris: PRAs for the evaluation of the similarity matching procedure. Furthermore, the historical avalanches that released from those PRAs are shown. Topographic base map reproduced by permission of swisstopo (BA046644).

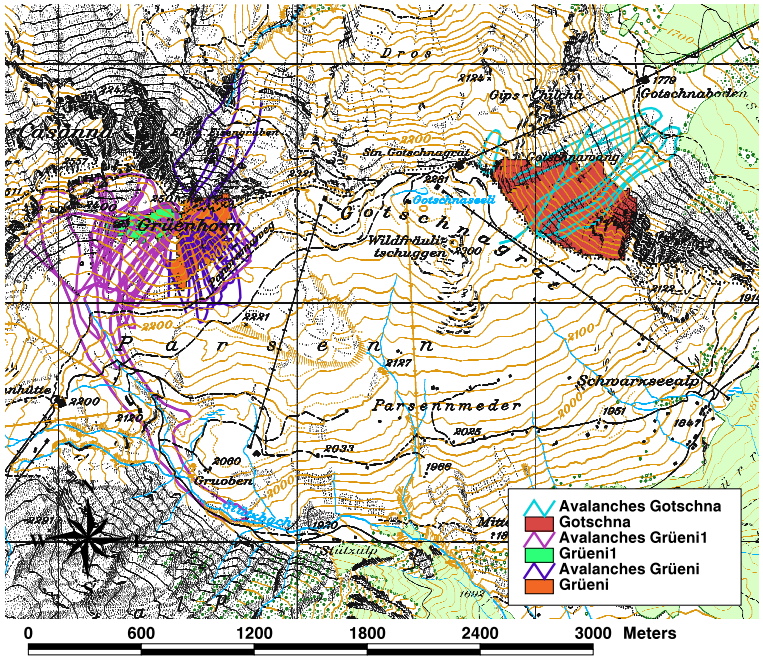

Figure 7.2: Area of Gotschna: PRAs for the evaluation of the similarity matching procedure. Furthermore, the historical avalanches that released from those PRAs are shown. Topographic base map reproduced by permission of swisstopo (BA046644).

past avalanche events have been recorded. In this way, the distribution for the release area resulting from the similarity matching procedure and the one generated from historical avalanche events could be compared. The considered PRAs in the area of Glaris and Gotschna are shown in Figures 7.1 and 7.2. Figure 7.3 shows both the distributions for the considered six PRAs. In the next section, the two distributions are used as input to the MC simulation (see Section 7.3.1) and the results do not show a great difference in the runout distances computed using the two different distributions.

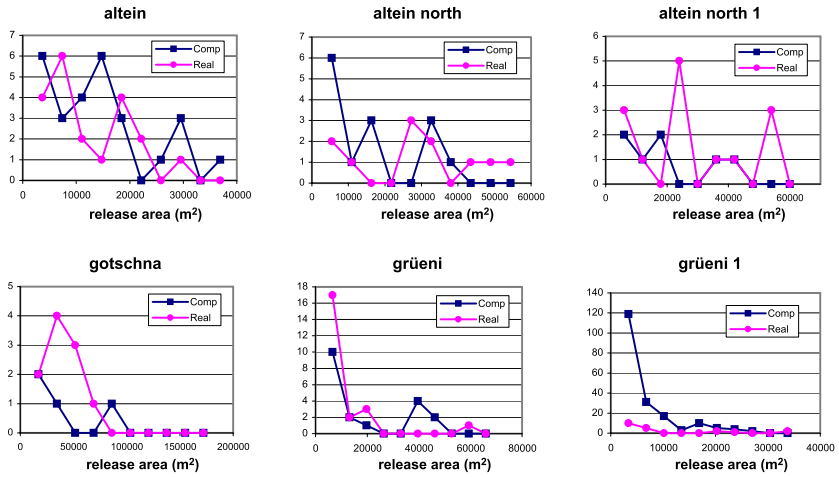

Figure 7.3: Comparison of the release area distribution generated from historical avalanche events and the one resulting from the similarity matching procedure.

A question that therefore arose was whether the choice of the release area distribution has a significant influence on the resulting runout distances – sensitivity tests were therefore performed. Three different MC simulations were carried out for a simple avalanche profile composed of three parts with constant slope inclination (35°, 25° and 9°, from the release zone to the runout zone). The friction coefficients and the fracture depth were represented by normal distributions centered on the values recommended by the Swiss Guidelines; the release area were represented by three distributions, centered on different percentages of the total extent of the PRA (10%, 50% and 90%). The result showed that the mean values for the runout distance of the 50% and 90% MC simulations are placed at a distance of 133 and 200 meters from the mean value of the 10% MC simulation. These results imply that the Monte Carlo procedure is sensitive to the shape of the release area distribution and therefore it is important to find the most realistic representation of the release area distribution as input to the MC simulations.

The fourth step is carried out in a different way if the purpose of the analysis is to determine the release area distribution for MC simulations that aim to assess the avalanche hazard levels for avalanche hazard maps (AHM case).

Within the previously described procedure, the avalanche activity of a new PRA was directly derived from the avalanche activities of other PRAs in the database. These avalanche activities have been generated from real avalanche events that happened over the last 50 years and therefore are characterized by frequent avalanches with an estimated return period T of not more than 50 years (i.e. the recording period). For avalanche hazard mapping purposes, avalanches with return periods of 30 and 300 years have to be simulated and the output analyzed (see Section 2.4). Therefore the release area for these avalanches must be estimated. Again, the comparison between the new PRA and the PRAs of the database in terms of topographical characteristics is performed, in order to find the most similar PRAs. For these similar PRAs, Gumbel statistics are performed using the method described in Section 6.3.2 for the Brämabüel avalanche path. The Gumbel statistics of these PRAs are analyzed to extrapolate the mean value for the release area of the new PRA (in percentage of the total PRA), for return periods of 30 and 300 years.

In Chapter 6, an initial assumption was formulated that avalanches with a return period of 300 years always have a release area equivalent to the total extent of the PRA. Here, based on other examples, this assumption will be further tested. Using the Gumbel statistics approach for the determination of the extent of the release area allows a more precise assessment as to whether the whole PRA has to be taken into account for a 300yr avalanche event.

Finally, normal distributions centered on the calculated mean values of the PRAs and with standard deviations equal to 15% of the mean values are used as input for the release area in the MC simulation for avalanches with return periods of 30 and 300 years, respectively.

The fifth step is to perform MC simulations which give as output a distribution of runout distances for frequent avalanches (FA case) and a distribution of runout distances (blue limit) and of the position of the red/blue limit for 30yr and 300yr avalanches (AHM case). The resulting hazard maps include uncertainties in the form of standard deviations and are created, case by case, on the basis of specific considerations based on the output distributions and on the specific avalanche path. Recall that the blue limit is defined by the runout distance of 300yr avalanches and the red/blue limit is defined either by the position where the 300yr avalanches have a pressure of 30kPa or by the runout distance of the 30yr avalances (see Section 2.4).

7.3 Case studies

7.3.1 Case study 1: Alteingrat

The avalanche slope Alteingrat is situated about 10 km south of Davos in the Southern validation area, as defined in Section 3.3 (see Figures 7.4 and 7.5). It is a slope of constant inclination (mean slope angle 32°) from an altitude of 2200 m a.s.l. down to the valley bottom at 1420 m a.s.l., with an E-SE aspect. On the Eastern side of Alteingrat, avalanches are frequent. They can break loose from different release areas and run down the slope taking as paths one of the three channels through the forest. The avalanche track considered in this study

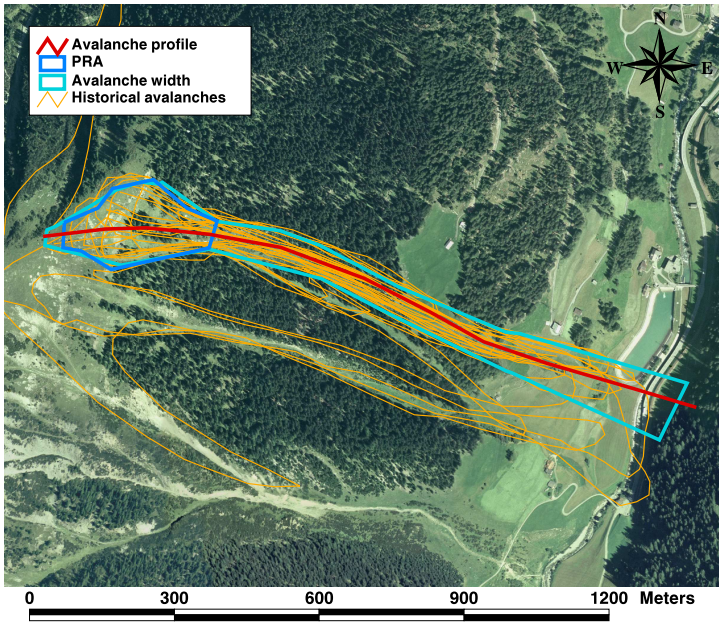

Figure 7.4: Orthophoto of the Alteingrat slope. The considered avalanche track and potential release area are shown, together with the extent of past avalanche events. Topographic base map reproduced by permission of swisstopo (BA046644). Orthophoto: SWISSIMAGE ©2000 swisstopo (DV023193).

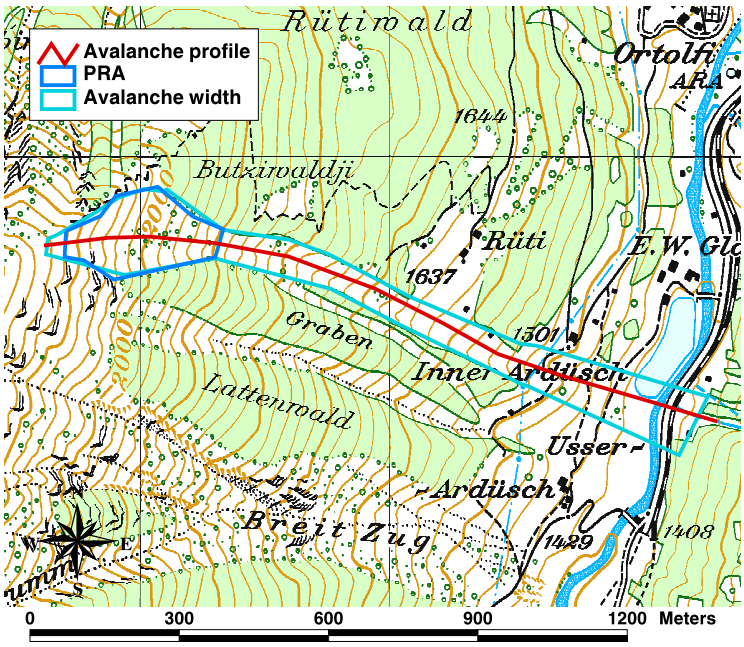

Figure 7.5: Map of the Alteingrat slope. The considered avalanche track and potential release area are shown. Topographic base map reproduced by permission of swisstopo (BA046644).

is the most northern channel shown in Figures 7.4 and 7.5. As potential release area for this avalanche track, the PRA resulting from the automatic procedure explained in Section 4.2 was taken; the total extent of this PRA is 36932 m^2 (Fig. 7.4 and 7.5).

In this case study, the procedure was applied to find the distribution of the runout distance for frequent avalanches (FA case) and to find the distributions of the relevant outputs for avalanche hazard maps (AHM case).

Alteingrat: frequent avalanches (FA) case

In the frequent avalanches (FA) case, the aim was to estimate the distribution of the runout distance of frequent avalanche events, with return periods of less than 50 years (i.e. time range of the avalanche database). The distributions of the model input parameters for the MC simulation had to be determined.

For the friction coefficients, normal distributions were defined as for the reproduction of historical avalanche events (RHAE) case study of Brämabüel (Section 6.3.1). The mean values of the friction coefficients were chosen following the recommendations given by the Swiss Guidelines [SLF, 1999b] and the standard deviation was taken as equal to 30%. The value of 30% was chosen because in Chapter 6 this value was found to be best suited to reproducing the historical avalanche events using the MC simulation in the RHAE case study. In the case of the considered avalanche track and assuming a return period of 30 years, the mean values and the standard deviation of μ and ξ are shown in Table 7.2.

Table 7.2: $\overline{\mu}$ and $\overline{\xi}$ values for frequent avalanches along the avalanche track of Alteingrat. The reference avalanche volume to determine the friction coefficients was 18466 m^3.

altitude (m a.s.l.)	$\overline{\mu}$	std μ	$\overline{\xi}$	std ξ
above 1500:	0.26	0.078	1470	441
below 1500:	0.29	0.087	1340	402

The distribution for the fracture depth was determined, as in the case of Brämabüel, by analyzing data from Weissfluhjoch and applying the corrections related to the slope angle and the altitude of the release area as well as to the snow drift process according to Salm et al. [1990] (Fig. 7.6).

For the release area, two different distributions were used as input to the MC simulations. Because for the considered avalanche track past avalanche events have been recorded, firstly, a distribution generated from analysis of these past avalanches was used (Fig. 7.7a). Secondly, the distribution determined by the similarity matching procedure described in Section 7.2 was used (Fig. 7.7b). The comparison of the results allowed the evaluation of the quality of the procedure to determine the distribution of the runout distance by the similarity matching procedure in areas where no comparison with real past avalanches is possible.

Here, all the steps to determine the release area distribution by the similarity matching procedure are described. The PRA characterization procedure

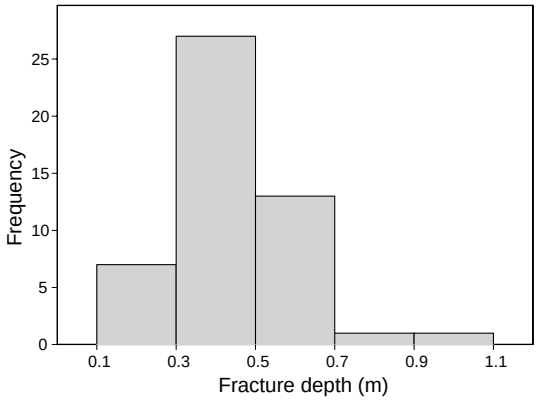

Figure 7.6: Alteingrat: fracture depth distribution used as input for the MC simulation.

was applied to the considered PRA to produce in the characterizing topographical parameters shown in Table 7.3. The resulting PRA belongs to size class

Table 7.3: Characterizing topographical parameters for the PRA of the Alteingrat avalanche path. The first row gives the real values, the second row shows the classification classes according to Table 5.7 in parentheses. The total extent of the PRA is 36932 m^2.

mean aspect	mean slope	std slope	max slope	dist ridge	plan curv	prf curv	max prf curv	shape
105°	35°	2°	41°	130 m	-0.27	-0.06	1.42	1
(1)	(3)	(1)	(2)	(2)	(1)	(2)	(3)	(1)

3. Therefore it was compared with the other 55 PRAs of size class 3 in the database. The similarity matching procedure found three similar PRAs in the database, with a maximum difference of 3 topographic parameters from the PRA under consideration. The avalanche activity of these three PRAs was combined to create the vector representing the distribution of the release area (or avalanche activity) for the PRA at hand (Fig. 7.7b).

Two MC simulations were performed using the two different distributions for the release area and the same distributions for the other input parameters. Figures 7.8 and 7.9 show the results of the two MC simulations. The results of both runs are similar. Most of the simulated avalanches stopped at the valley bottom: the mean values of the runout distance are both at an altitude of 1420 m a.s.l. at a reciprocal distance of 25 m, corresponding to an avalanche length of 1270 and 1245 meters respectively, and the standard deviations are 42 and 65 meters (Fig. 7.8). Comparison with the runout distances of historical avalanche events was carried out visually on the map and along the avalanche profile displayed in Figure 7.9. Most of the historical events also stopped between an altitude of 1500 m a.s.l. and the valley bottom. Six small past avalanches were not reproduced by the MC simulation. This is again, as in the Brämabüel case study, a clear demonstration that the model FL-1D is not calibrated for such

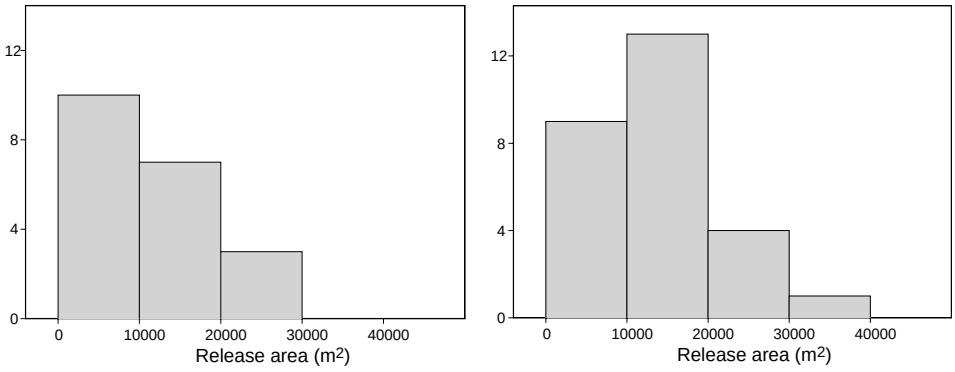

Figure 7.7: Alteingrat: release area distributions used as input for the MC simulations: (a) derived from the past avalanche events, (b) derived from the similarity matching procedure.

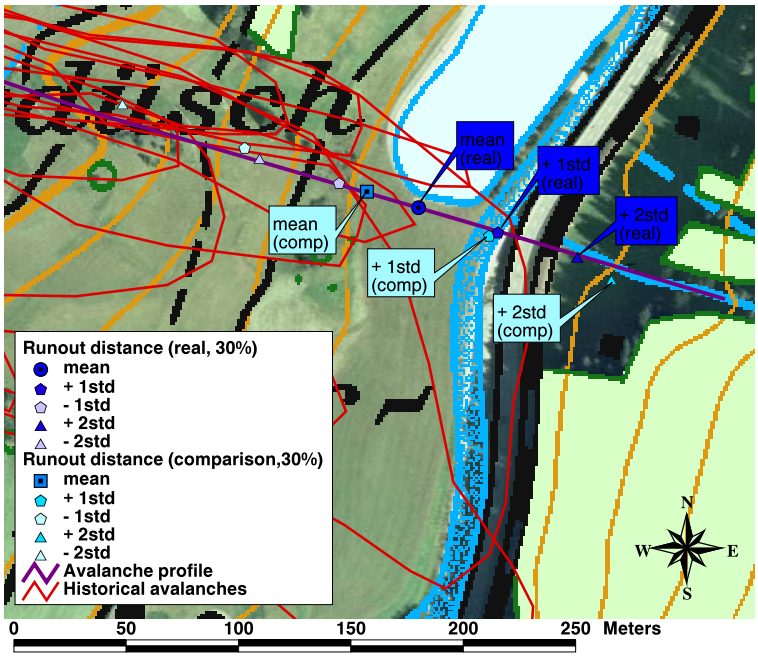

Figure 7.8: Alteingrat: mean value, ±1std and ±2std for avalanche runout distances resulting from the MC simulations, where (a) release area distribution is derived from the past avalanche events on this path (real) and (b) release area distribution is derived by comparison with topographically similar PRAs at other locations (comparison). For comparison, the runout distances of historical avalanches are shown. Topographic base map reproduced by permission of swisstopo (BA046644). Orthophoto: SWISSIMAGE ©2000 swisstopo (DV023193).

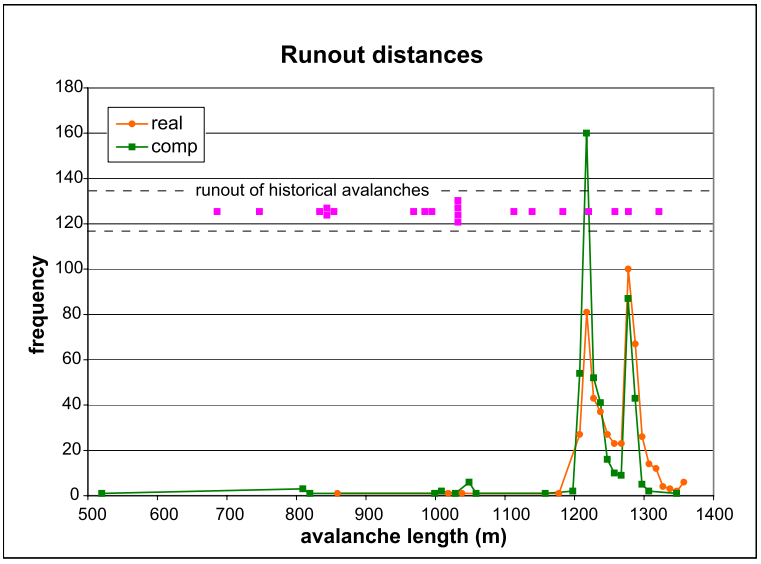

Figure 7.9: Alteingrat: distribution of avalanche runout distances resulting from the MC simulations, in both the "real" and "comparison" cases ("real" and "comparison" cases defined as in Figure 7.8).

small avalanches and therefore has difficulties reproducing them.

In conclusion, the two MC simulations produced similar results for the runout distance, that are in good agreement with the medium and large size past avalanche events. This supports the assumption of using the avalanche activity derived from the similarity matching procedure to simulate frequent avalanches in avalanche tracks where no data are available.

Alteingrat: Avalanche Hazard Map (AHM) case study

In the avalanche hazard map (AHM) case, the aim was to predict the distribution of the output parameters relevant for avalanche hazard mapping, namely runout distance and pressure for avalanches with a return period of 30 and 300 years. To this end, the distributions of the model input parameters for the MC simulation had to be determined first.

For the friction coefficients, normal distributions were defined as for the AHM case study of Brämabüel (Section 6.3.2). The mean values of the friction coefficients were chosen following the recommendations given by the Swiss Guidelines [SLF, 1999b] and the standard deviation was taken as equal to 15% of the mean values. In the case of the considered avalanche track and for return periods of 30 and 300 years, the mean values and the standard deviation of μ and ξ are shown in Table 7.4 and 7.5, respectively.

For the fracture depth, normal distributions centered on mean values suggested by the Swiss Guidelines [SLF, 1999b; Salm et al., 1990] and standard deviations equal to 15% of these values were used. For 30yr avalanches the mean fracture depth $\overline{fd}$ was 0.81 m and for 300yr avalanches it was 1.14 m.

For the release area, as in the previous case (FA case), two different dis-

Table 7.4: $\overline{\mu}$ and $\overline{\xi}$ values for 30yr avalanches along the avalanche track of Alteingrat. The reference avalanche volume to determine the friction coefficients was 29915 m^3.

altitude (m a.s.l.)	$\overline{\mu}$	std μ	$\overline{\xi}$	std ξ
above 1500:	0.21	0.031	1750	262
below 1500:	0.25	0.037	1500	225

Table 7.5: $\overline{\mu}$ and $\overline{\xi}$ values for 300yr avalanches along the avalanche track of Alteingrat. The reference avalanche volume to determine the friction coefficients was 42102 m^3.

altitude (m a.s.l.)	$\overline{\mu}$	std μ	$\overline{\xi}$	std ξ
above 1500:	0.20	0.030	2000	300
below 1500:	0.24	0.036	1500	225

tributions were used as input to the MC simulations, each of them for both T = 30 and 300 years, resulting in four MC simulations. Because, for the considered avalanche track, past avalanche events have been recorded, first, the distribution generated from the Gumbel analysis of these past avalanches was used. Second, the distribution determined by the similarity matching procedure combined with the Gumbel analysis was used.

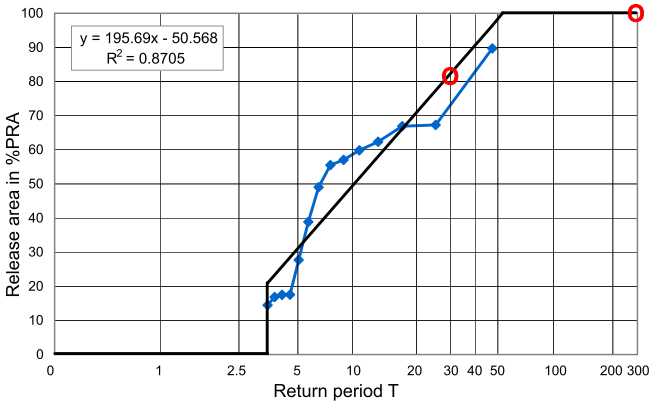

Figure 7.10: Alteingrat: Gumbel statistic for the release areas of historical avalanche events occurred within the considered PRA. The red circles highlight the values of the release area for T = 30 and 300 years, respectively.

Figure 7.10 shows the Gumbel analysis performed on the data of the real past avalanches' release areas. From this analysis, a normal distribution with a mean value $\overline{A}$ equal to the 83% of the total PRA, i.e. $\overline{A}$ = 30653 m^2, and a standard deviation equal to the 15% of this value was chosen as input to the MC simulation for 30yr avalanches. For 300yr avalanches, the total extent of the PRA was used, therefore the constant vector of 36932 m^2 was the input to this first MC simulation.

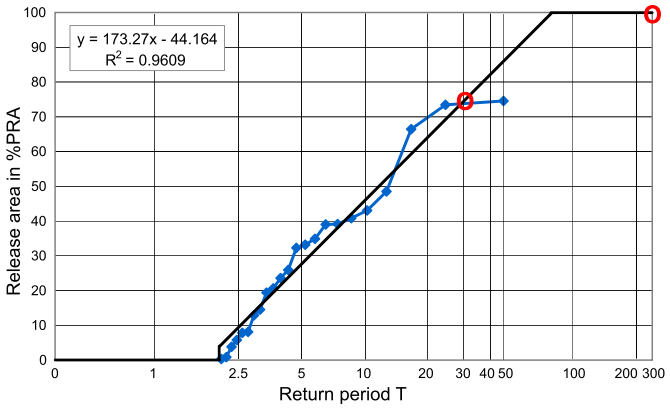

Figure 7.11: Alteingrat: Gumbel statistic for the release areas of historical events within one of the three similar PRAs. The red circles highlight the values of the release area for $T = 30$ and 300 years, respectively.

The second MC simulation was performed with the same input distribution for the fracture depth and the friction coefficients, but with release area distributions derived from the Gumbel analysis performed on the data of the past avalanches' release areas that had the most similar PRAs. Within two of the three similar PRAs found in the database, there occurred only one and three avalanches in the past 50 years, respectively. Therefore it was not possible to perform a significant Gumbel statistic. The Gumbel analysis for the third PRA is shown in Figure 7.11. This PRA was taken to be significant to determine the input for the release area in the MC simulations. From this analysis, a normal distribution with a mean value $\overline{A}$ equal to 75% of the total PRA, i.e. $\overline{A} = 27699$ m^2, and a standard deviation equal to 15% of this value was chosen as input to the MC simulation for 30yr avalanches. For 300yr avalanches, the total extent of the PRA was used, hence once again taking the constant vector of 36932 m^2 as input to this MC simulation.

Note that the release area inputs for 300yr avalanches turned out to be the same whether calculated on the basis of Gumbel analysis of actual past avalanches, or avalanches defined from similar PRAs. Therefore, only one MC simulation for 300yr avalanches was actually performed. For 30yr avalanches there was a difference of 8% in the mean value of the normal distributions for the release area and consequently two different simulations were performed.

Figures 7.12, 7.13 and 7.14 show the results of the three MC simulations. The resulting runout distances using the two different release area distributions for 30yr avalanches are very similar. Most of the simulated 30yr avalanches stopped at the valley bottom: the mean values of the runout distance are at the position of the road (avalanche length equal to 1305 m) at an altitude of 1415 m a.s.l. and the standard deviations are of about 20 m (Fig. 7.12). The simulated 300yr avalanches stopped slightly further along the profile at an altitude of 1419 m a.s.l. on the opposite slope, corresponding to an avalanche length of 1345 m (Fig. 7.13).

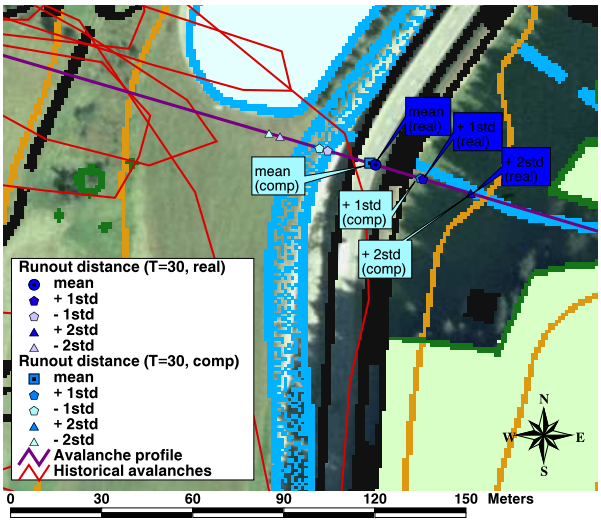

Figure 7.12: Alteingrat: mean value, ±1std, ±2std and ±3std for avalanche runout distances resulting from the MC simulations for 30yr avalanches, in case both of release area distribution derived from the past avalanche events from the considered PRA (real) and of release area distribution derived from the past avalanche events of the similar PRAs (comparison). Furthermore, the runout distances of the historical avalanches are shown. Topographic base map reproduced by permission of swisstopo (BA046644). Orthophoto: SWISSIMAGE ©2000 swisstopo (DV023193).

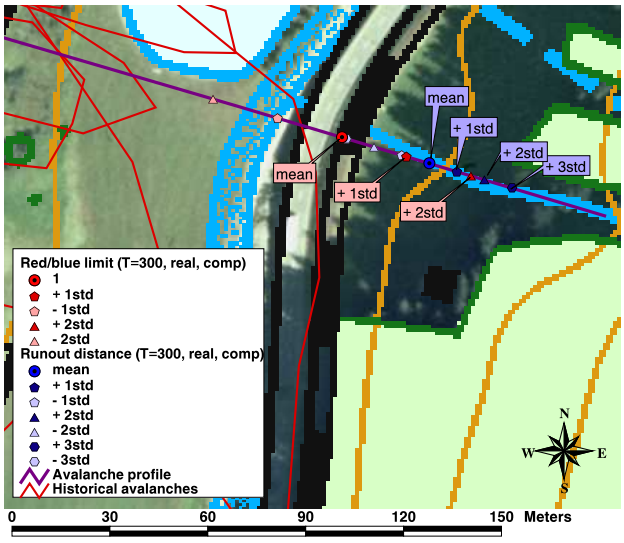

Figure 7.13: Alteingrat: mean value, ±1std and ±2std for avalanche runout distances resulting from the MC simulation for 300yr avalanches. The "real" and "comparison" cases coincide ("real" and "comparison" cases defined as in Figure 7.12). Furthermore, the runout distances of the historical avalanches are shown. Topographic base map reproduced by permission of swisstopo (BA046644). Orthophoto: SWISSIMAGE ©2000 swisstopo (DV023193).

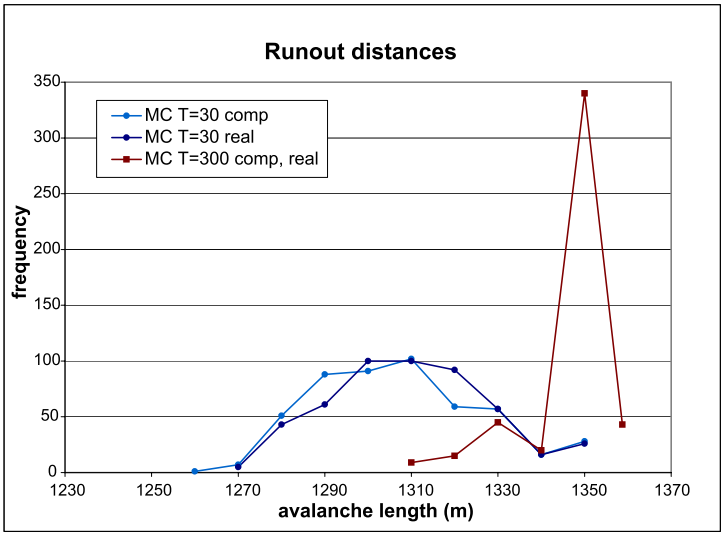

Figure 7.14: Alteingrat: distribution of avalanche runout distances resulting from the MC simulations for avalanches with $T = 30$ and 300 years, in both the "real" and "comparison" cases ("real" and "comparison" cases defined as in Figure 7.12). The avalanche length is calculated from the beginning of the avalanche profile.

For the definition of the hazard zones, the results of the MC simulation for the 300yr avalanches had to be taken both for the red/blue and the blue limits. Because of the presence of the opposite slope, this study case is similar to the one of Brämabüel. The proposed avalanche hazard map would then consider the red/blue limit determined by the *mean value + 2std* and the blue limit by the *mean value + 3std*. For this avalanche path, no avalanche hazard map exists, hence a comparison was not possible. The described example has shown how the results obtained with an analysis made on historical events along the considered path were similar to the results obtained by the application of the proposed similarity matching procedure. This was the main goal of this example.

The next two examples were chosen in the Bernese Oberland region, where avalanche hazard maps exist but only sparse information exists about historical avalanches. In those cases a comparison of the official AHM with the one resulting from the proposed procedure was made.

7.3.2 Case study 2: Guttannen

Guttannen is a village in the Bernese Oberland region (Canton Bern) at an altitude of 1050 m a.s.l. endangered by avalanches from different paths. The chosen avalanche path for this example is one North-East of the village, starting at an altitude of about 2700 m a.s.l. with a SW aspect (see Figure 7.15). Is is mostly unchannelled, with a channelled part between 1440 and 1160 m a.s.l.. The PRA definition procedure was applied to the considered area and resulted in the PRA shown in Figure 7.15; the total extent of the PRA is 91800 m^2 (PRA size class 4).

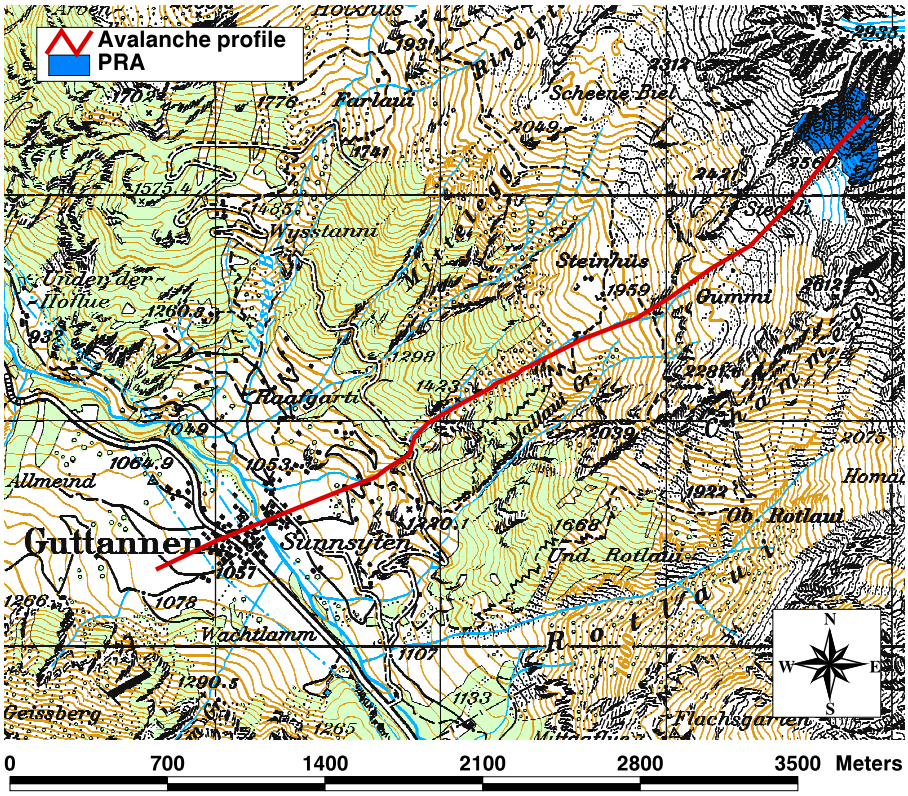

Figure 7.15: Map of the Guttannen avalanche path. The considered potential release area is also shown. Topographic base map reproduced by permission of swisstopo (BA046644).

In this example, the aim was to predict the distribution of the output parameters relevant for avalanche hazard mapping, namely runout distance and pressure for avalanches with a return period of 30 and 300 years, respectively. The distributions of the model input parameters for the MC simulation had to be determined.

For the friction coefficients, normal distributions were again, as in the previous examples, defined with mean values chosen following the recommendations given by the Swiss Guidelines [SLF, 1999b] and standard deviations equal to 15% of the mean values. In this case for a return periods of 30 and 300 years,

the mean values and the standard deviation of μ and ξ are shown in Table 7.6 and 7.7.

Table 7.6: $\overline{\mu}$ and $\overline{\xi}$ values for 30yr avalanches along the avalanche track of Guttannen. The reference avalanche volume to determine the friction coefficients was 73440 m^3.

altitude (m a.s.l.)	$\overline{\mu}$	std μ	$\overline{\xi}$	std ξ
above 1500 (unchannelled):	0.17	0.026	1980	297
below 1500 (channelled):	0.26	0.039	1490	223
below 1500 (unchannelled):	0.19	0.029	1740	261

Table 7.7: $\overline{\mu}$ and $\overline{\xi}$ values for 300yr avalanches along the avalanche track of Guttannen. The reference avalanche volume to determine the friction coefficients was 104652 m^3.

altitude (m a.s.l.)	$\overline{\mu}$	std μ	$\overline{\xi}$	std ξ
above 1500 (unchannelled):	0.16	0.024	2490	373
below 1500 (channelled):	0.25	0.037	1490	223
below 1500 (unchannelled):	0.18	0.027	1990	298

For the fracture depth, normal distributions centered on mean values suggested by the Swiss Guidelines [SLF, 1999b; Salm et al., 1990] and standard deviations equal to 15% of these values were used. The mean fracture depth $\overline{fd}$ was 0.8 m for 30yr avalanches and 1.14 m for 300yr avalanches.

For the release area, the similarity matching procedure combined with Gumbel analysis was applied. First, the characterization procedure was applied to the PRA resulting in the topographic features shown in Table 7.8.

Table 7.8: Characterizing topographical parameters for the PRA of the Guttannen avalanche path. The first row gives the real values, the second row shows the classification classes according to Table 5.7 in parentheses. The total extent of the PRA is 91800 m^2.

mean aspect	mean slope	std slope	max slope	dist ridge	plan curv	prf curv	max prf curv	shape
218°	44°	8°	60°	0 m	-0.35	0.21	2.26	2
(3)	(1)	(3)	(1)	(1)	(1)	(1)	(2)	(2)

The similarity matching procedure found four similar PRAs in the database of Davos for size class 4, one of them only with one historical avalanche. Therefore, the Gumbel analysis of the data of the past avalanches' release areas was performed only for the other three PRAs (see Figures 7.16, 7.17 and 7.18). From the critical analysis of these plots, it was decided to take the worst case for the definition of the mean value $\overline{A}$ of the release area distributions for the MC simulations of 30 and 300yr avalanches. The plot in Figure 7.16 again suggests to taking the total extent of the PRA as release area for a 300yr avalanche.

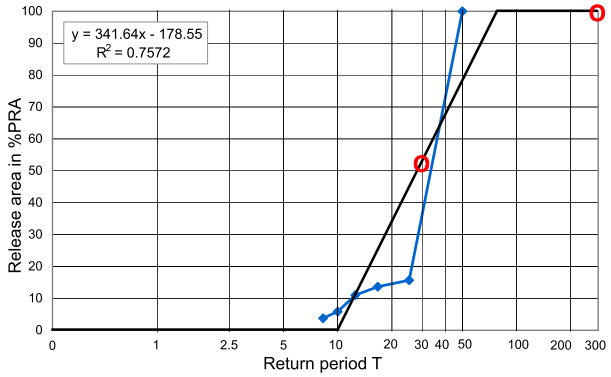

Figure 7.16: Guttannen: Gumbel statistic for the release areas of historical avalanche events within the first of the four similar PRAs. The red circles highlight the values of the release area for $T = 30$ and 300 years, respectively.

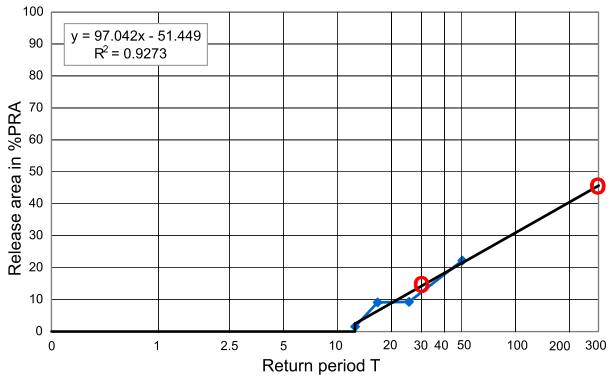

Figure 7.17: Guttannen: Gumbel statistic for the release areas of historical avalanche events within the second of the four similar PRAs. The red circles highlight the values of the release area for $T = 30$ and 300 years, respectively.

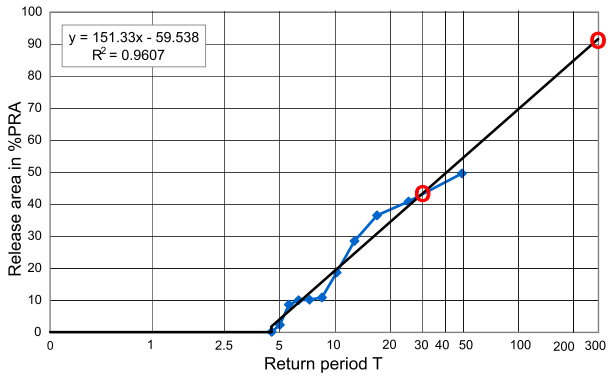

Figure 7.18: Guttannen: Gumbel statistic for the release areas of historical avalanche events within the third of the four similar PRAs. The red circles highlight the values of the release area for $T = 30$ and 300 years, respectively.

The value for $T = 50$ years looks like an outlier, but it indeed exists and in this case it was not possible to ignore it. Instead, for a 30yr avalanche, Figure 7.18 suggested to use a release area equal to 45% of the total PRA.

Figures 7.19, 7.20 and 7.21 present the results of the MC simulations. As expected the 30yr avalanches stopped along the path before the 300yr avalanches (Fig. 7.21). The mean value for the runout distances of the 30yr avalanches is placed at an altitude of 1077 m a.s.l, corresponding to an avalanche length of 3005 m, while for the 300yr avalanches is at an altitude of 1055 m a.s.l., 185 m further down along the profile. In Figure 7.20 the position where the 300yr avalanches have a pressure of 30 kPa (red/blue limit) is shown. The combination of the results of the two MC simulations indicated that the results of the simulation of the 300yr avalanches had to be used to define the hazard zones.

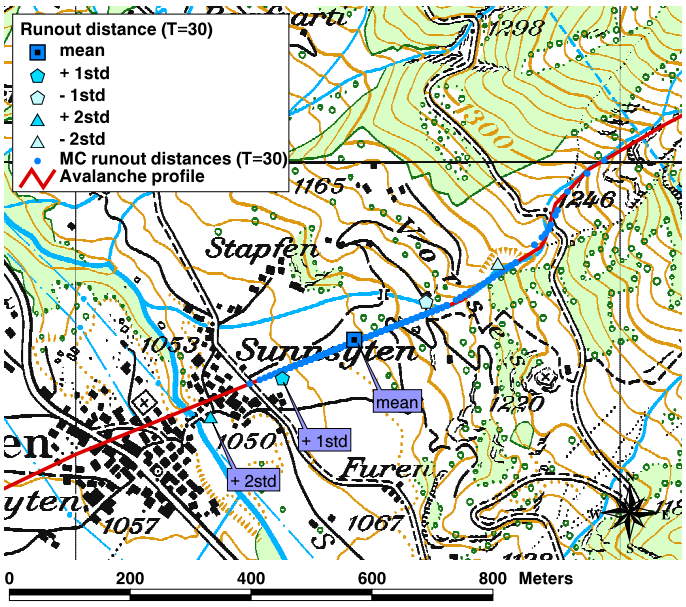

Figure 7.19: Guttannen: runout distances resulting from the MC simulation for avalanches with $T = 30$ years. Topographic base map reproduced by permission of swisstopo (BA046644).

Figure 7.22 shows the avalanche hazard situation for the considered path together with the official avalanche hazard map. Applying the same considerations as for the Brämabüel case, the red/blue limit would be placed exactly at the same position as the official one, but the blue limit extended about 65 m from the official one. The runout zone below 1060 m is a very flat area (inclination of 4-5°) where the small-scale topography has a strong influence on the avalanche motion. The profile for the simulation was not defined in such a detailed way, therefore the topography was little smoothed.

Figure 7.23 shows the deposition of the avalanche that occurred along the considered avalanche path at Guttannen in February 1999. This picture illustrates well how in such a flat zone the small-scale topography can influence the avalanche motion.

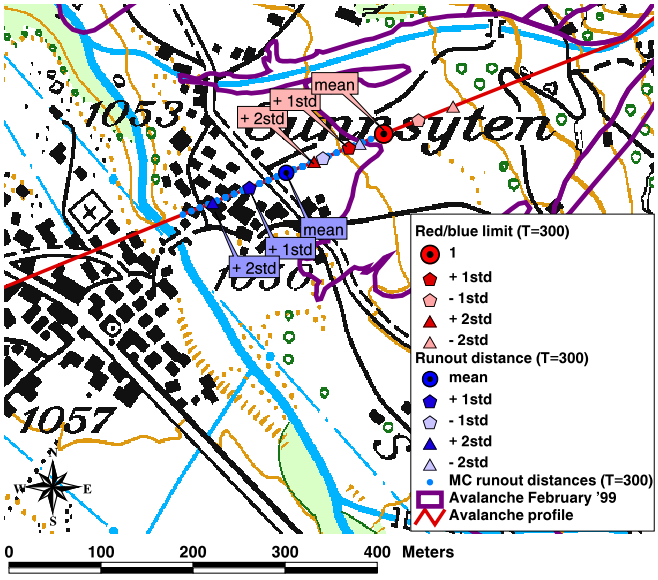

Figure 7.20: Guttannen: runout distances and red/blue limit resulting from the MC simulation for avalanches with $T = 300$ years. Furthermore, the outline of the avalanche that occurred in February '99 is shown. Topographic base map reproduced by permission of swisstopo (BA046644).

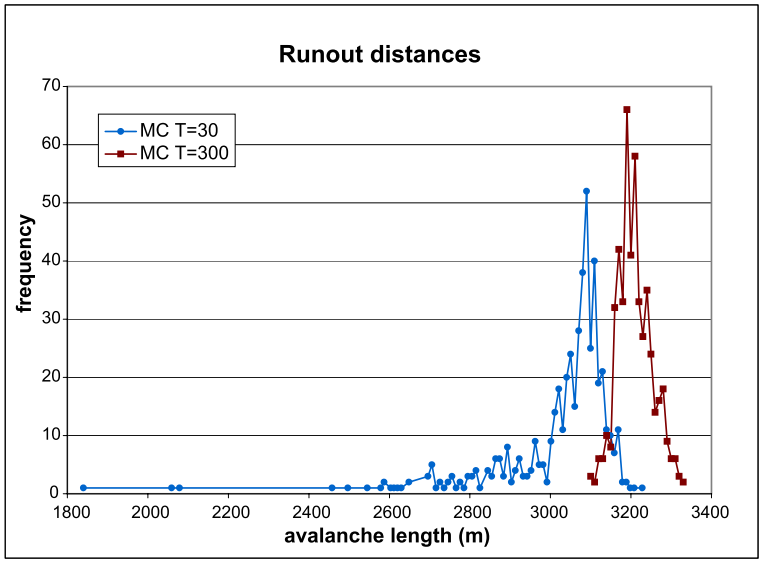

Figure 7.21: Guttannen: distribution of the runout distances resulting from the MC simulations for avalanches with $T = 30$ and 300 years. The avalanche length is calculated from the beginning of the avalanche profile.

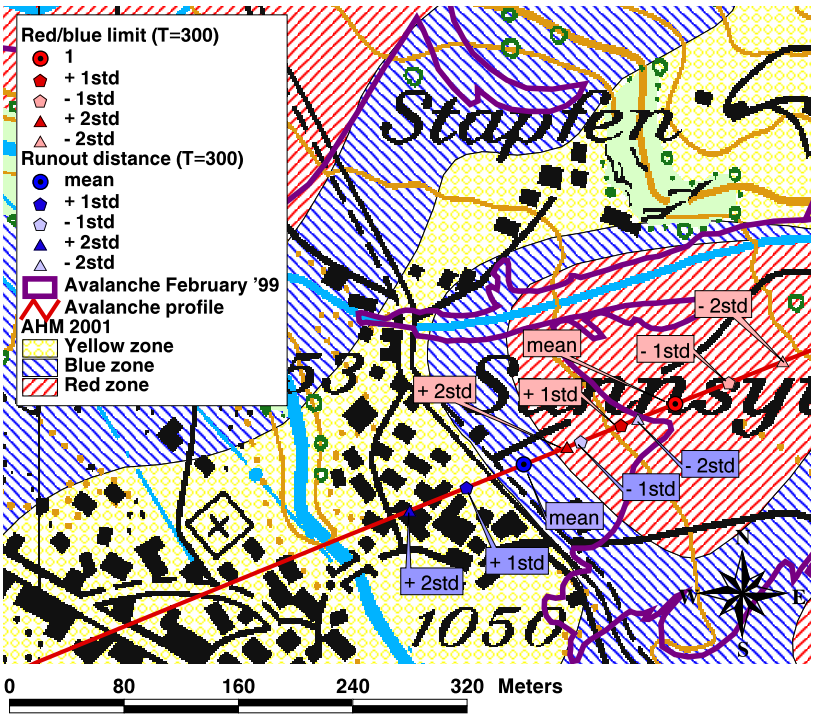

Figure 7.22: Guttannen: official AHM (2001) and proposed definition of the hazard zones followingr the MC simulations. Furthermore, the outline of the avalanche of February 1999 is shown. Topographic base map reproduced by permission of swisstopo (BA046644).

Figure 7.23: Guttannen: deposition of an avalanche in February 1999. It is interesting to observe how the avalanche followed different directions in the runout zone, probably due to the interaction of the avalanche flow with the small-scale topography. Source: SLF archive.

Another important factor that has to be taken into account in drawing the final detailed hazard map is the presence of houses in the runout zone. In fact, a house might be protected by the presence of another house placed before it along the main avalanche track.

Another point that has to be considered for the path under study is that avalanches that release from the corresponding PRA might split at an altitude of about 2000 m a.s.l. between the modelled path and the one with a more southern direction. In this case, the mass along the modelled path would decrease and the resulting runout distance be shorter.

The results of the MC simulation, together with all the aforementioned considerations, might be used by the commune of Guttannen to estimate the uncertainties related to the definition of the hazard limits. The knowledge of the uncertainties is helpful for example in extreme situations when an evacuation plan has to be applied. In this case, the commune of Guttannen might decide to extend the evacuation plan in place for the blue zone to the houses in the yellow zone (usually the area endangered by powder avalanches) below the road, because the MC simulation showed that in practice the blue zone might extended that far. The MC simulation results might also be taken as an indication that the blue zone should be extended to include the first row of houses below the road. Furthermore, Figure 7.23 shows that avalanches can go further down the road; if the avalanche of February 1999 had taken a direction a bit more to the North-West it could have reached the village. But, of course, more detailed investigations would be necessary since this example can only be used to explain the application of the MC method.

Finally, considering the presence of the road and of the possible splitting point along the path, the proposed blue limit was defined by the *mean value + 1std* and the red/blue limit was defined by the *mean value + 2std*. However, the goal of this procedure was not to propose a final hazard map for a village where it already exists, but to suggest a method to quantify the uncertainties in defining hazard limits. With this technical instrument available, the commune should take into consideration all the different aspects related to the hazard mapping problem, including social and political ones, to draw the consequent land use plan.

7.3.3 Case study 3: Niesen

Niesen is a mountain close to the Lake Thun (Canton Bern) that has the general shape of a pyramid with many steep slopes facing in different directions. The chosen avalanche path for this example is the one along the North-Western slope from an altitude of around 2700 m a.s.l. down to the upper part of the village of Oberdorf at an altitude of 680 m a.s.l.; it has a channelled section between 1400 and 1000 m a.s.l.. A peculiarity of this avalanche path is the presence of the forest within the runout zone (see Figure 7.24). The PRA definition procedure was applied to the considered area resulting in the PRA shown in Figure 7.24; the total extent of the PRA is 99600 m^2 (PRA size class 4).

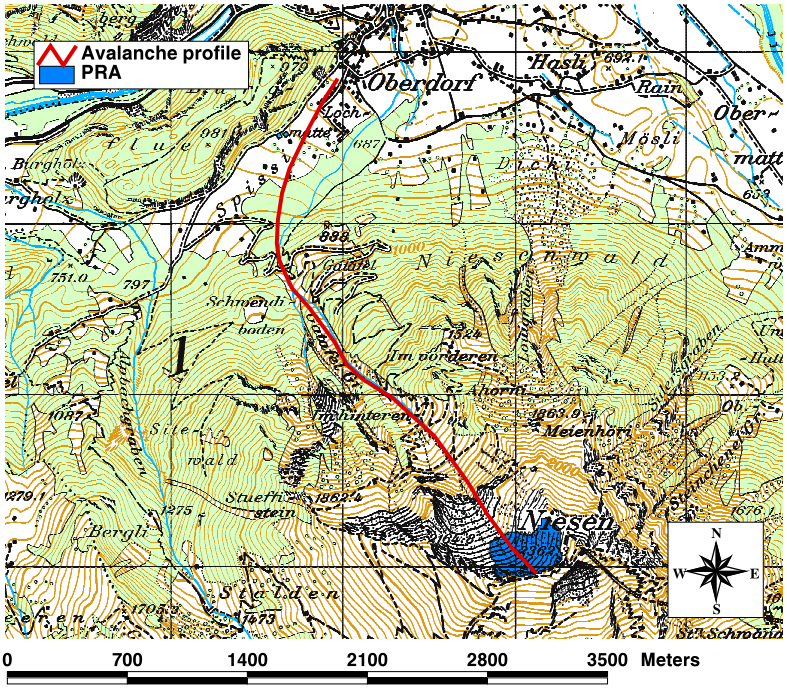

Figure 7.24: Map of the Niesen avalanche path. The corresponding potential release area is also shown. Topographic base map reproduced by permission of swisstopo (BA046644).

In this example, as for Guttannen, the aim was to predict the distribution of the output parameters relevant for avalanche hazard mapping, namely runout distance and pressure for avalanches with a return period of 30 and 300 years, respectively. The distributions of the model input parameters for the MC simulation were determined using the same procedure as for the previous case.

For the friction coefficients, normal distributions were defined with mean values chosen following the recommendations given by the Swiss Guidelines [SLF, 1999b] and standard deviations equal to 15% of the mean values. The presence of the forest between 960 and 760 m a.s.l. has to be taken into account in the choice of the friction parameters. They were chosen following the sug-

gestions given by Lorenzato [2001], who analyzed the interaction of avalanches with forest, using the FL-1D model. In the case of the considered avalanche track and for a return period of 30 and 300 years, the mean values and the standard deviations of μ and ξ are shown in Table 7.9 and 7.10.

Table 7.9: $\overline{\mu}$ and $\overline{\xi}$ values for 30yr avalanches along the avalanche track of Niesen. The reference avalanche volume to determine the friction coefficients was 72708 m^3.

altitude (m a.s.l.)	$\overline{\mu}$	std μ	$\overline{\xi}$	std ξ
above 1500 (unchannelled):	0.17	0.025	1990	298
1500 - 1000 (unchannelled):	0.19	0.028	1740	261
1500 - 1000 (channelled):	0.26	0.039	1490	223
below 1000 (forest, unchannelled):	0.22	0.033	600	90
below 1000 (unchannelled):	0.21	0.031	1500	225

Table 7.10: $\overline{\mu}$ and $\overline{\xi}$ values for 300yr avalanches along the avalanche track of Niesen. The reference avalanche volume to determine the friction coefficients was 101592 m^3.

altitude (m a.s.l.)	$\overline{\mu}$	std μ	$\overline{\xi}$	std ξ
above 1500 (unchannelled):	0.16	0.024	2490	373
1500 - 1000 (unchannelled):	0.18	0.027	1990	298
1500 - 1000 (channelled):	0.25	0.037	1490	223
below 1000 (forest, unchannelled):	0.22	0.033	600	90
below 1000 (unchannelled):	0.20	0.030	1740	261

For the fracture depth, normal distributions centered on mean values suggested by the Swiss Guidelines [SLF, 1999b; Salm et al., 1990] and standard deviations equal to 15% of these values were used. For 30yr avalanches the mean fracture depth $\overline{fd}$ was 0.73 m and for 300yr avalanches it was 1.02 m.

For the release area, the similarity matching procedure combined with Gumbel analysis was applied. First, the characterization procedure was applied to the considered PRA resulting in the characterizing topographic features shown in Table 7.11.

Table 7.11: Characterizing topographical parameters for the PRA of the Niesen avalanche path. The first row gives the real values, the second row shows the classification classes according to Table 5.7 in parentheses. The total extent of the PRA is 99600 m^2.

mean aspect	mean slope	std slope	max slope	dist ridge	plan curv	prf curv	max prf curv	shape
306°	37°	4°	50°	50 m	-0.40	0.03	1.23	3
(2)	(2)	(2)	(2)	(1)	(1)	(2)	(3)	(3)

The similarity matching procedure found five similar PRAs in the database

of Davos, but in one of them only two historical avalanches released and in another one no avalanches were recorded. Therefore, the Gumbel analysis of the data of the past avalanches' release areas was carried out only for the other three PRAs (see Figures 7.25, 7.26 and 7.27).

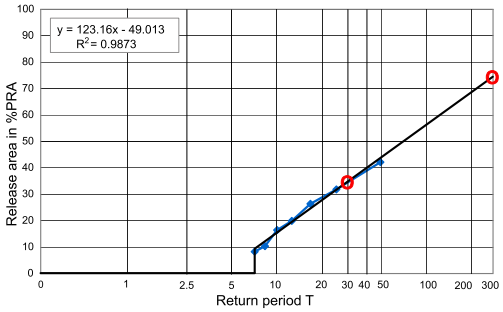

Figure 7.25: Niesen: Gumbel statistic for the release areas of historical avalanche events within the first of the five similar PRAs. The red circles highlight the values of the release area for $T = 30$ and 300 years, respectively.

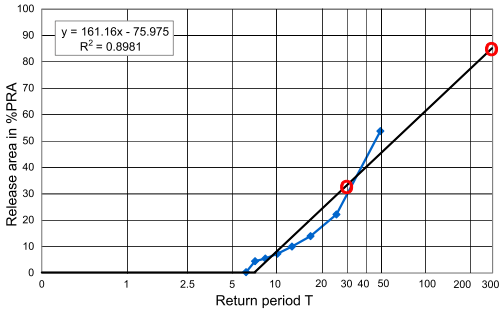

Figure 7.26: Niesen: Gumbel statistic for the release areas of historical avalanche events within the second of the five similar PRAs. The red circles highlight the values of the release area for $T = 30$ and 300 years, respectively.

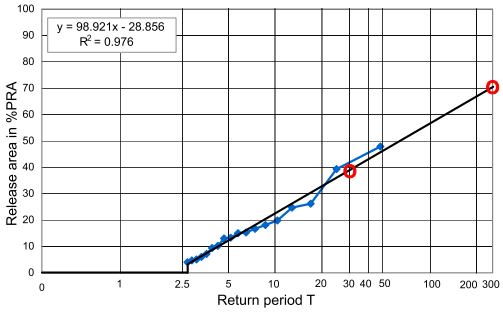

Figure 7.27: Niesen: Gumbel statistic for the release areas of historical avalanche events within the third of the five similar PRAs. The red circles highlight the values of the release area for $T = 30$ and 300 years, respectively.

From the critical analysis of these plots, it was decided to take the worst case for the definition of the mean value $\overline{A}$ of the release area distributions for the MC simulations of 30 and 300yr avalanches. In this example, all the plots suggested a mean value $\overline{A}$ for the release area of a 300yr avalanche which was less than the total extent of the PRA. The worst case is given by Figure 7.26 with a value $\overline{A}$ of 85% of the total PRA. For a 30yr avalanche, Figure 7.27 suggested using a mean release area $\overline{A}$ equal to the 40% of the total PRA.

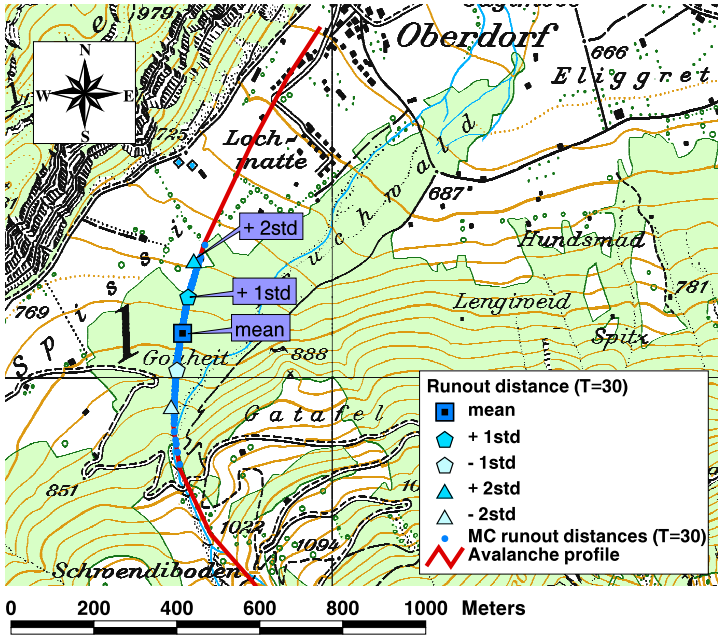

Figure 7.28: Niesen: runout distances resulting from the MC simulation for avalanches with $T = 30$ years. Topographic base map reproduced by permission of swisstopo (BA046644).

Figures 7.28, 7.29 and 7.30 present the results of the MC simulations. As expected, the 30yr avalanches stopped along the path before the 300yr avalanches (Fig. 7.30). The mean value for the runout distances of 30yr avalanches is placed at an altitude of 791 m a.s.l, corresponding to an avalanche length of 2700 m, while for 300yr avalanches is at an altitude of 765 m a.s.l., 135 m further down the slope. Figure 7.29 also depicts the position where the 300yr avalanches have a pressure of 30 kPa (red/blue limit). The combination of the results of the two MC simulations revealed that the blue limit has to be defined by the MC simulation for the 300yr avalanches and the red/blue limit has to be defined by the MC simulation for the 30yr avalanches. Recall that the red/blue limit is defined either by the position where the 300yr avalanche have a pressure of 30 kPa or by the runout distance of the 30yr avalanches (see Section 2.4). In this case, the mean position where the 300yr avalanches have a pressure of 30 kPa is before the mean runout distance of the 30yr avalanches.

Figure 7.31 shows the derived avalanche hazard for the path together with the official avalanche hazard map. The initial idea of defining the hazard limit

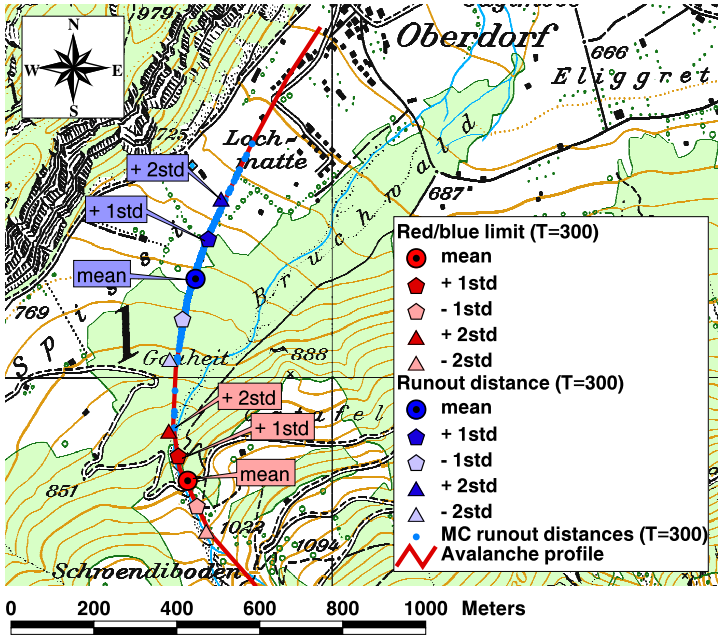

Figure 7.29: Niesen: runout distances and red/blue limit resulting from the MC simulation for avalanches with $T = 30$ years. Topographic base map reproduced by permission of swisstopo (BA046644).

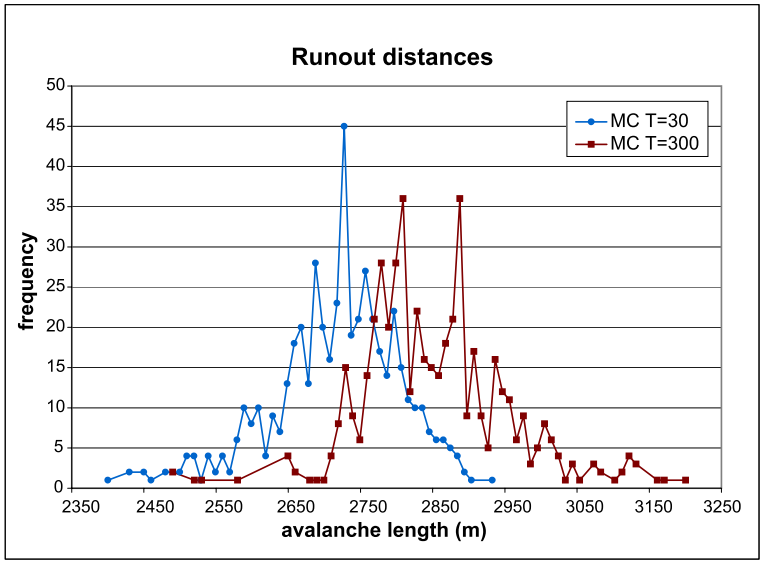

Figure 7.30: Niesen: distribution of the runout distances resulting from the MC simulations for avalanches with $T = 30$ and 300 years, respectively. The avalanche length is calculated from the beginning of the avalanche profile.

by the *mean value + 2std* would place the red/blue limit 100 m further downslope from the official one, at an altitude of 757 m a.s.l., and the blue limit 50 m further downslope the official one, at an altitude of 731 m a.s.l. In terms of altitude, the blue limit of the MC simulation is placed at the same altitude as the official blue limit. In fact, the official blue zone extends in a diagonal way with respect to the slope, being longer on the eastern part of the runout zone. Considering a profile a bit more to the East of the modelled one, the results would probably match the official blue limit quite well. The downslope shift for both the limits might be due to the presence of the forest in the runout zone, that has a retarding effect. Though this was included in the model, uncertainties are still present in the choice of the correct friction coefficients for avalanches interacting with forest. In conclusion, the results of the MC simulations are useful, for example, to state that the area above Lochmatte at altitudes around 730-40 m a.s.l. is a critical area not completely safe of avalanches and that the red/blue limit incorporates large uncertainties. As for Guttannen, the community of the village of Oberdorf might use these results to elaborate a better land use plan and avalanche security program.

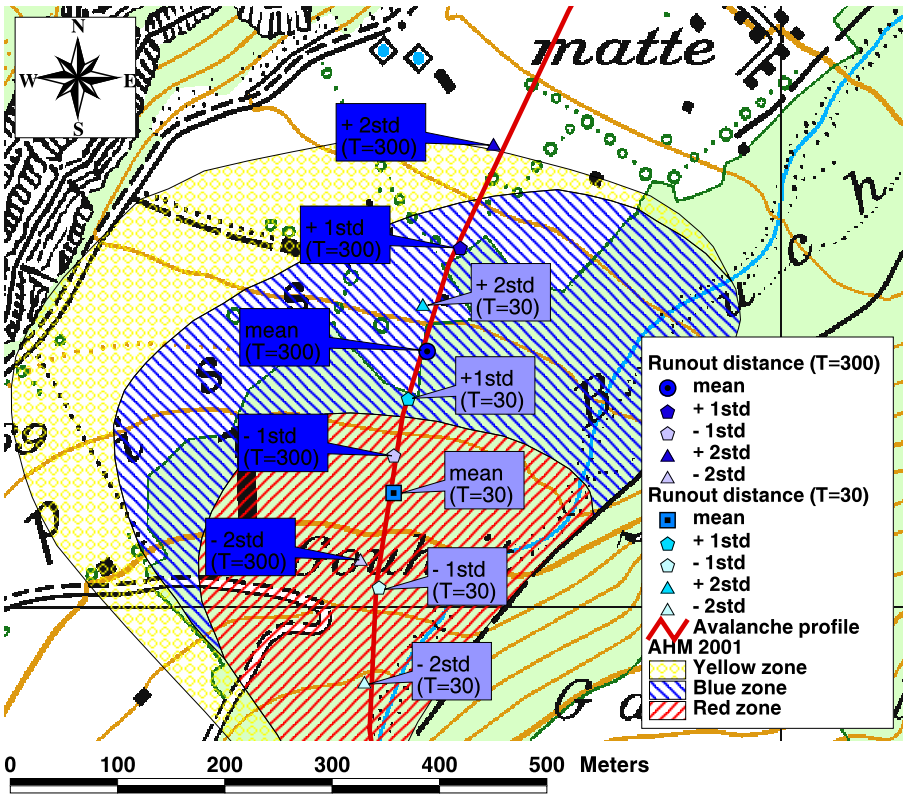

Figure 7.31: Niesen: official AHM (2001) and proposed definition of the hazard zones following the MC simulations. Topographic base map reproduced by permission of swisstopo (BA046644).

7.4 Discussion

The goal of the proposed procedure was to create a useful method to assess the avalanche hazard in areas where no data about past avalanche events are available.

The combination of the PRA definition and characterization procedures with the similarity matching procedure turned out to be useful to determine the possible avalanche activity for an undocumented avalanche path. An expert who has to assess the avalanche danger in an undocumented path can combine this well-defined approach (that relies on a database of similar well-documented release areas) and their personal experience in order to produce a comprehensive overview of the avalanche hazard level.

In order to yield more accurate results, the similarity matching procedure will have to be tested with more PRAs. The release area distributions generated by the proposed similarity matching procedure and the release area distributions derived from the historical avalanche events will have to be compared and a clear measure of their similarity has to be given. In case of the six PRAs considered here to compare the two release area distributions, no perfect similarity was found and on many occasions only a few PRAs were available for comparison. One of the reasons might be that, as stated at the beginning of this thesis, avalanche activity is a combination of many factors, terrain characteristics being only one of them. Here, the snowpack characteristics and the meteorological conditions are not considered, but they might have a relevant influence on the determination of avalanche activity. However, even if no perfect similarity exists in the case of the six considered PRAs, the results of the MC simulations performed with the two different distributions showed a great deal of agreement in the runout distances. If, with a higher number of avalanche paths, the simulated avalanches matched the historical avalanches, the procedure might be used to simulate possible avalanches along undocumented avalanche paths with a good degree of accuracy.

In the examples described in this chapter, the similarity matching procedure found PRAs similar to the PRA at hand that do not in fact have, between them, similar avalanche activities. In this case, the expert has to evaluate which of the PRAs is taken as reference for the determination of the release area distribution for the PRA at hand. In the cases of Alteingrat and Niesen, the similar PRAs where no or only few avalanches released in the past are found in the middle part of a slope. Therefore, it is likely that they are often crossed by avalanches from above, which disturb the snowpack at the position of these PRAs. Because of this, there is seldom the possibility of releasing avalanches. This fact suggests including, in the future, also the elevation of the PRAs or a measure of the PRAs' position with respect to the beginning of the slope as a characterizing parameter.

The proposal of using the similarity matching procedure combined with Gumbel analysis of the release area data in avalanche hazard mapping is a new idea, which might be very useful to evaluate the extent of the release area for avalanches with a specific return period. In the case of undocumented paths, this input for avalanche models can be estimated on the basis of the Gumbel

statistic of the similar PRAs in the database. Therefore, it is necessary to generate the Gumbel statistic for all PRAs and create a corresponding database. In this case, after the similarity matching procedure, the Gumbel statistic of the most similar PRAs in the database can be directly used to estimate the release area distribution for the newly considered PRA.

In the case studies described, the strategy of using the worst case from the Gumbel analysis was adopted. This is the main suggestion for using this procedure, but the exploration of a larger number of Gumbel analyses might find and provide a more specific rule. The problem of the estimation of the extent of the release area for 300yr avalanches is considered to be less important, because the experts tend, being correctly on the safe side, to use the total area of the PRA to simulate extreme avalanches. But for 30yr avalanches, the analysis of all the Gumbel statistic for the PRAs in the database might provide more information about which proportion of the total PRA should be used as input for the release area of these avalanches.

The application of the MC simulation for avalanches with return periods of 30 and 300 years, respectively, will allow the elaboration of hazard maps which include uncertainties, as well as for avalanche paths where records of past avalanche events do not exist. In general, the quantification of these uncertainties is useful in cases where, for example, houses belong to the blue zone, but are only 5 meters away from the limit to the red zone. If the uncertainties in the definition of this limit are high, for example if the standard deviation is equal to 30 meters, it is important to evaluate the zoning and probably include these houses in a specific security plan.

The result of the MC simulation for frequent avalanches might be used to improve risk assessment for areas endangered by avalanches. Risk analysis includes the probability of property being exposed to a particular phenomenon, in this case avalanches. The output of the MC simulations can be converted into probabilities that indicate how often a house might be reached by avalanches, and used to create avalanche risk maps, together with all the other necessary information involved in risk analysis.

In conclusion, the proposed procedure provides an alternative method to perform avalanche simulations for the assessment of avalanche hazard in areas where no historical avalanche data are available. With respect to the commonly used procedure of making avalanche simulations, the expert might count on a well-defined procedure to determine the extent of the release area for avalanches with specific return periods, i.e. 30 and 300 years in the case of Switzerland, and run MC simulations to generate several different hazard scenarios. All these resulting scenarios should then be critically analyzed to define the final avalanche hazard map.

Chapter 8

Conclusions and Outlook

8.1 Conclusions

The four main goals of this research were:

1. to define potential avalanche release areas on the basis of topographical characteristics;
2. to find a possible relationship between topography and avalanche activity, defined as release area extent and frequency;
3. to determine the extent of the release area for avalanches with specific return periods;
4. to quantify the uncertainties present in the avalanche hazard mapping procedure by a Monte Carlo technique.

Concerning the **first goal**, a GIS-based procedure was developed to define potential avalanche release areas on the basis of several parameters, namely slope angle, curvature, aspect and forest cover. This was the first attempt to create a systematic procedure to improve the common definition of avalanche release areas that is based generally only on the slope angle of the terrain.

The results have shown that the proposed procedure worked well in the study area of Davos, where it was able to identify 79% of the release areas of past avalanche events. It will be important to apply the proposed procedure to other regions where historical avalanches have been recorded, in order to evaluate the quality of the procedure for its general applicability. Further research could be carried out to find whether inclusion of other terrain characteristics, e.g. surface roughness, might improve the results. Previous to this approach, the delineation of potential avalanche release areas was based only on the personal experience of avalanche experts. Therefore, the GIS tool developed here provides a more objective and repeatable tool for the definition of potential avalanche release areas.

To achieve the **second goal**, different statistical analyses have been performed. However, they gave results that do not support the initial hypothesis

of the existence of a significant statistical relationship between avalanche activity and topography.

In particular, linear regression models have not been found appropriate to predict the avalanche activity of a potential release area from its topographical characteristics. Within the cluster analysis, good examples of PRAs similar both in terms of topographical attributes and of avalanche activity were found, but no general and precise statistical rules could be derived to relate different avalanche activities to different types of terrain characteristics.

An important achievement of the statistical analysis are the results of the CART method, which gave information about which topographical variables most influence avalanche activity. These were found to be: standard deviation of slope, distance to ridge, plan and profile curvature. Future research should focus on these topographical parameters to be more complete in the analysis of the avalanche activity with respect to terrain characteristics. In order to confirm the findings of the present study, it will be important to apply this methodology in other regions where good avalanche databases are available.

In summary, the results of the statistical analysis do not fully support the hypothesis of a relationship between avalanche activity and topographical characteristics. The principal reason might be that the quality of the data is not good enough to arrive at a robust conclusion, which states that there exists, or not, a relationship between topography and avalanche activity. Another possibility might be that other variables can be adopted to describe the avalanche activity, now described by *numava* and *skew*, and perform statistical analysis; or even a different definition of avalanche activity can be used, for example frequency together with release area of the largest event.

The **third goal** was to create a method to determine the extent of the release area for avalanches with specific return periods. For avalanche paths where historical data exist, the Gumbel statistic on the release area of these past avalanche events can be used to find a relationship between the extent of the release area and the return period. This relationship helps avalanche experts to choose the value of the release area for the simulations of avalanches with return periods of 30 and 300 years, which are the relevant return periods for the avalanche hazard mapping procedure in Switzerland.

But more important is the proposed procedure to derive the extent of the release area of avalanches of specific return periods for avalanche sites, where no or only few historical data are available. The combination of the similarity matching procedure with the Gumbel statistic provides a good tool to achieve this task. Where the lack of data does not give the experts information about the release area, the proposed procedure does, relying on release area information from similar well-documented PRAs. This is a relevant achievement because it provides a scientific procedure for a task that until now has been achieved only by the personal and subjective evaluations of avalanche experts.

The **fourth goal** of this thesis, the determination of uncertainties in avalanche hazard maps by the Monte Carlo approach, is an improvement to a similar procedure described in Barbolini [1999], because here distributions de-

rived from real historical data have been used as inputs for the release area. The usefulness of the Monte Carlo procedure lies in the fact that it gives an overview of the avalanche hazard situation in terms of probability. Therefore, it gives the expert the possibility to decide which degree of security to take for the delineation of the avalanche hazard zones.

The result of the MC simulation for frequent avalanches might be used to improve the risk assessment for areas endangered by avalanches. Risk analysis includes the probability of property being exposed to a potentially hazardous process, in this case avalanches. The output of the MC simulations can be converted into probabilities, that indicate how often a house or a road may be reached by avalanches, and used to create avalanche risk maps, together with all the other necessary information involved in risk analysis.

In summary, an important feature of the proposed procedure is that it is composed of well defined modules which might also be applied individually. The procedure for the definition of potential release areas might be used alone without being combined with the Monte Carlo simulations or the MC simulations might be applied for avalanche paths where the release area was defined on the basis of historical data, terrain surveys and expert knowledge and not with the automatic PRA definition procedure.

Moreover, this work made a step forward in research concerning avalanche release area, above all, proposing a method to determine the release area of avalanches of specific return periods which poses a real and practical problem in avalanche hazard mapping.

The two case studies in the Bernese Oberland region described in Chapter 7 showed the usefulness of the complete procedure in other regions of Switzerland for practical applications. They show that this methodology is able to determine the extent of the release area to be used in MC simulations for the generation of realistic avalanche hazard maps. The advantage of this methodology is that the release area is more objectively defined and that additional information about the uncertainties is available. Avalanche experts can decide the degree of security to be adopted in defining the hazard zones. Taking the *mean value + 3std* for the definition of the hazard limits means having a degree of confidence of 99%. In critical situations, such as when public buildings such as schools are present in the avalanche runout zone, this might be advisable, while at other times a lower degree of confidence might be sufficient.

8.2 Outlook

In the following section, possible future research developments are briefly suggested:

- Concerning the definition of potential avalanche release areas, it will be interesting to apply the methodology by Ghinoi [2003] to compare the results of his procedure applied in the region of Davos with the PRAs defined in the present study.

- An important topic that will have to be addressed is the simultaneous release of several PRAs resulting in a large release area, which can produce avalanches of very large dimensions. It is important to identify slopes where multiple releases can happen and to estimate under what conditions (topographical characteristics and nivo-meteorological conditions) this phenomenon occurs.

- The topic of the influence of topographical characteristics on avalanche activity is not closed. This study adds some more contributions and suggests further research with statistical analysis performed on a very well documented high quality database.

- A possible improvement to all the performed statistical analyses is thought to be the inclusion of the position of the PRAs within a slope. This parameter would take into account the fact that PRAs placed in the middle of a slope, below other PRAs, might have a lower frequency because their snow cover is often disturbed by the passage of avalanches starting from above. If this parameter is weighted properly, it is thought that the results of the cluster analysis might change significantly.

- Together with the research about the influence of topographical characteristics on avalanche activity, it is important to continue to study the relationship between avalanche activity and nivo-meteorological conditions. In the literature, many studies exist on this topic, for example Föhn et al. [1977], Davis & Elder [1995], Hendrikx et al. [2004]. What is of interest is the combination between topographical and nivo-meteorological characteristics with respect to avalanche activity.

- This work proposed an approach to define the release area distribution on the basis of real historical data which is used as input to the Monte Carlo procedure. A further step will be to derive distributions based on real data for the other model input parameters, namely the friction coefficients and the fracture depth.

From a practical point of view, the proposed procedure can reproduce historical avalanches and define hazard limits. However, possible future developments in terms of applications are suggested as follows:

- The Monte Carlo procedure might be applied to more avalanche paths, where avalanche hazard maps already exist, to evaluate the uncertainty with which they have been defined.

- The same procedure might be carried out but using the two-dimensional version of FL-1D [Gruber, 1998]. Due to the modular structure of the complete procedure, it would also be possible to use other models of avalanche dynamics for the Monte Carlo simulations.

- The complete procedure, from the PRA definition to the Monte Carlo simulations, is already implemented in ArcInfo, but it is still a research

model. To be able to distribute it among practitioners, it is necessary to create a user-friendly program which includes all the different steps as separate modules. Each single step might be performed sequentially to reproduce the complete procedure or individually according to the current need. The goal is to provide to avalanche experts an easy-to-use program that produces well interpretable results.

Bibliography

Arfken, G. B. & Weber, H. J. (1985). *Mathematical Methods for Physicist*. Academic Press.

Armstrong, B. & Williams, K. (1986). *The avalanche book*. Golden, Colorado, Fulcrum Inc.

Aschwanden, A. (1996). Bereinigte Zeitreihen: Die Ergebnisse des Projektes KLIMA90. Klimatologie 1961-1990. Technical report, Hrsg. MeteoSchweiz, Zürich.

Bakkehoi, S. & Norem, H. (1994). Sammenlikning av metoder for beregning av maksimal utlopsdistanse for snoskred (Comparison of methods for calculation of maximum avalanche runout distance). Technical Report 581200-30, Norwegian Technical Institute. in norwegian.

Barbolini, M. (1999). *Dense Snow Avalanches: Computational Models, Hazard Mapping and Related Uncertainties*. Ph. D. thesis, Dipartimento di Ingegneria Idraulica e Ambientale. Università di Pavia, Italia.

Barbolini, M., Gruber, U., Keylock, C., Naaim, M., & Savi, F. (2000). Application of statistical and hydraulic-continuum dense-snow avalanche models to five real European sites. *Cold Regions Science and Technology 31*, 133–149.

Bartelt, P., Salm, B., & Gruber, U. (1999). Calculating dense-snow avalanche runout using a Voellmy-fluid model with active/passive longitudinal straining. *Journal of Glaciology 45*(150), 242–254.

Bartelt, P. A., Kern, M. A., & Christen, M. (2000). A mixed flowing/powder snow avalanche model. In *Proceedings of the International Snow Science Workshop, Big Sky, Montana, U.S.A., October 1st - 6th, 2000*, pp. 280–289. Int. Snow Sci. Workshop by Montana State University.

BBF & SLF (1984). Richtlinien zur Berücksichtigung der Lawinengefahr bei raumwirksamen Tätigkeiten. Technical report, Eidgenössisches Drucksachen- und Materialzentrale: Bundesamt für Forstwesen; Eidgenössisches Institut für Schnee- und Lawinenforschung.

Bertogg, R. (2001). Analyse der Topographie von Lawinenanrissgebieten im Lawinenwinter 1999. Master's thesis, Universität Salzburg, Österreich.

Bovis, M. J. & Mears, A. (1976). Statistical prediction of snow avalanche runout from terrain variables in Colorado. *Arctic and Alpine Research 8*, 145–147.

Breiman, L., Friedman, J. H., Olshen, R., & Stone, C. J. (1984). *Classification and Regression Tree*. Monterey: Wadsworth and Brooks/Cole.

Brown, C. B., Evans, R. J., & LaChapelle, E. R. (1972). Slab avalanching and the state of stress in fallen snow. *Journal of Geophysical Research 77*(24), 4570–4580.

Buisson, L. & Charlier, C. (1989). Avalanche starting-zone analysis by use of a knowledge-based system. *Annals of Glaciology 13*, 27–30.

Butler, D. & Walsh, S. (1990). Lithologic, structural and topographic influences on snow avalanche path location, Eastern Glacier National park, Montana. *Annals of the Association of American Geographers 80*(3), 362–378.

Carter, J. R. (1988). Digital representations of topographic surfaces. *Photogrammetric Engineering and Remote Sensing 54*, 1577–80.

Christen, M., Bartelt, P., & Gruber, U. (2002). AVAL-1D: an avalanche dynamics program for the practice. In T. E. B. of the Organizing Committee for INTRAPREVENT 2002 (Ed.), *Congress publication*, Volume 2, pp. 715–725. International Research Society INTERPRAEVENT for the Pacific Rim.

Coppock, J. T. & Rhind, D. W. (1991). The history of GIS. In D. J. Maguire, M. F. Goodchild, & D. W. Rhind (Eds.), *Geographic Information Systems: principles and applications*, Volume 1, Chapter 2, pp. 21–43. London: Longman.

Davis, R. E. & Elder, K. (1995). Application of classification and regression trees: selection of avalanche activity indices at Mammoth Mountain. In *Proceedings of the International Snow Science Workshop, Snowbird, Utah, U.S.A.,30 October - 3 November 1994*, pp. 285–294. Int. Snow Sci. Workshop 1994 Organ Comm., Snowbird, Utah.

D'Souza, V. P. C. & Morgan, R. P. C. (1976). A laboratory study of the effect of slope steepness and curvature on soil erosion. *J. Agric. Engineering Res. 21*, 21–31.

EAWS (2003). Glossar Schnee und Lawinen, Glossair neige et avalanches, Glossario neve e valanghe. Technical report, European Avalanche Warning Services, Munich, Germany.

ESRI (2001). ArcInfo Online Help. ArcDoc Version 8.1 Service Pack 1. Manual, Enviromental Systems Research Institute.

Evans, I. S. (1980). An integrated system of terrain analysis and slope mapping. *Zeitschrift für Geomorphologie Supplement Band 36*, 274–95.

Föhn, P., Good, W., Bois, P., & Obled, C. (1977). Evaluation and comparison of statistical and conventional methods of forecasting avalanche hazard. *Journal of Glaciology 19*(81).

Föhn, P., Stoffel, M., & Bartelt, P. (2002). Formation and forecasting of large (catastrophic) new snow avalanches. In *Proceedings of the International Snow and Science Workshop, Penticton, B. C.*, pp. 141–148. The Canadian Avalanche Association.

Fisher, P., Wood, J., & Cheng, T. (2003). Where is Helvellyn? Fuzziness of multi-scale landscape morphometric. *Transactions of the Institute of British Geographers 29*(1), 106–128.

Florinsky, I. V. (1998). Accuracy of local topographic variables derived from digital elevation models. *International Journal of Geographical Information Science 12*(1), 47–61.

Frey, W., Frutiger, H., & Good, W. (1987). Human impacts and management of mountain forest. In T. Fujimori & M. Kimura (Eds.), *Openings in the forest caused by forest deperishment and their influence on avalanche danger*, pp. 223–238. For. and Forest Prod. Res. Inst., Ibaraki, Japan.

Fukushima, Y. & Parker, G. (1990). Numerical simulation of powder snow avalanches. *Journal of GLaciology 36*(123), 229–237.

Gallant, J. C. & Wilson, J. P. (2000). Primary Topographic Attributes. In J. P. Wilson & J. C. Gallant (Eds.), *Terrain Analysis: Principles and Applications*, Chapter 3, pp. 51–85. John Wiley & Sons, Inc.

Gauer, P. (1999). Blowing and drifting snow in alpine terrain: a physically-based numerical model and related field measurements. Mitteilungen Eidg. Institut für Schnee- und Lawinenforsch., Swiss. Fed. Inst. for Snow and Avalanche Res. SLF, Davos, Switzerland.

Ghinoi, A. (2003). *A new contribution to the assessment of snow avalanche susceptibility: Applications in Tyrol (Austria) and in Alta Val Badia (Dolomites, Italy)*. Ph. D. thesis, Dipartimento di Scienze della Terra. Università degli Studi di Modena e Reggio Emilia.

Glazovskaya, T. G. (1998). Global distribution of snow avalanches and changing activity in the Northern hemisphere due to climate change. *Annals of Glaciology 26*, 337–342.

Gleason, J. A. (1995). Terrain parameters of avalanche starting zones and their effect on avalanche frequency. In *Proceedings of the International Snow Science Workshop, Snowbird, Utah, U.S.A.,30 October - 3 November 1994*, pp. 393–404. Int. Snow Sci. Workshop 1994 Organ Comm., Snowbird, Utah.

Gordon, A. D. (1981). *Classification: Methods for the Exploratory Analysis of Multivariate Data*. London: Chapman and Hall.

Gruber, U. (1998). *Der Einsatz numerischer Simulationsmethoden in der Lawinengefahrenkartierung*. Ph. D. thesis, Geography Department. University of Zürich.

Gruber, U. & Bartelt, P. (2000). Study of the 1999 avalanche winter in the Obergoms valley, Switzerland, with respect to avalanche hazard mapping. In *Proceedings of the International Snow Science Workshop, Big Sky, Montana, U.S.A., October 1st - 6th, 2000*, pp. 495–500. Int. Snow Sci. Workshop by Montana State University.

Gruber, U. & Margreth, S. (2001). Winter 1999: a valuable test of the avalanche hazard mapping procedure in Switzerland. *Annals of Glaciology 32*, 328–332.

Gubler, H. & Rychetnik, J. (1991). Effects of forests near the timberline on avalanche formation. In H. Bergmann, H. Lang, W. Frey, D. Issler, & B. Salm (Eds.), *Symposium at Vienna 1991 - Snow, Hydrology and Forests in High Alpine Areas*, pp. 138–143. International Association of Hydrological Science.

Harbitz, C. (1998). A survey of computational models for snow avalanche motion. Technical Report NGI Report 581220-1, Norwegian Geotechnical Institute, Oslo.

Harrell, F. E. (2001). *Regression Modeling Strategies: With Applications to Linear Models, Logistic Regression, and Survival Analysis*. New York: NY: Springer-Verlag.

Hartigan, J. A. (1975). *Clustering Algorithms*. New York: John Wiley and Sons.

Hastie, T., Tibshirani, R., & Friedman, J. (2001). *The Elements of Statistical Learning*. New York: Springer.

Hendrikx, J., Owens, I., Carran, W., & Carran, A. (2004). Avalanche activity in an extreme maritime climate: the application of classification and regression trees. In A. K. Richter (Ed.), *Geophysical Research Abstracts*, Volume 6. European Geosciences Union: Copernicus GmbH.

Horn, B. K. P. (1981). Hill shading and the reflectance map. In *Proceeding IEEE*, Volume 69, pp. 14–47.

Jamieson, J. B. & Geldsetzer, T. (1996). Avalanche accidents in Canada–Vol.4: 1984-1996. Technical report, Can. Avalanche Assoc., Revelstoke, B. C., Canada.

Jamieson, J. B. & Johnston, C. D. (1992). A fracture-arrest model for unconfined dry slab avalanches. *Canadian Geotechnical Journal 29*, 61–66.

Johnson, B. C., Jamieson, J. B., & Stewart, R. R. (2003). Seismic measurement of fracture speed in a weak snowpack layer. *Cold Regions Science and Technology*. in press.

Judson, A. & King, R. M. (1984). Effect of simple terrain parameters on avalanche frequency. In *Proceedings of the International Snow Science Workshop, Aspen, Colorado, U.S.A.*, pp. 12–20.

LaChapelle, E. R. (1985). *The ABC of avalanche safety*. Seattle, Washington.

Lied, K. & Bakkehoi, S. (1980). Empirical calculations of snow avalanche runout distance based on topographic parameters. *Journal of Glaciology 26*(94), 165–177.

Lorenzato, L. (2001). Analyse von Waldschadenlawinen hinsichtlich der Bremswirkung von Wald auf Lawinen. Master's thesis, Institut für Gographie Ludwigs-Maximilians-Universität München.

Luckman, B. H. (1978). Geomorphic work of snow avalanches in the Canadian Rocky Mountains. *Arctic anc Alpine Research 10*, 261.

Maggioni, M. & Gruber, U. (2003). The influence of topographic parameters on avalanche release dimension and frequency. *Cold Regions Science and Technology 37*, 407–419.

Maguire, D. J. & Dangermond, J. (1991). The functionality of GIS. In D. J. Maguire, M. F. Goodchild, & D. W. Rhind (Eds.), *Geographic Information Systems: principles and applications*, Volume 1, Chapter 21, pp. 319–335. London: Longman.

Maguire, D. J. & Raper, J. F. (1990). An overview of GIS functionality. In *Proceedings of the Design Models and Functionality Conference*, Leicester, pp. 10pp. Midlands Regional Reseach Laboratory.

Margreth, S., Stoffel, L., & Wilhelm, C. (2003). Winter opening of high alpine pass roads – analysis and casa studies from the Swiss Alps. *Cold Regions Science and Technology 37*, 467–482.

MathSoft (2000). *S-PLUS 2000 User's Guide*. Seattle, WA: Data Analysis Products Division, MathSoft.

McClung, D. M. (2001). Characteristics of terrain, snow supply and forest cover for avalanche initiation by logging. *Annals of Glaciology 32*, 223–229.

McClung, D. M. & Lied, K. (1987). Statistical and geometrical definition of snow avalanche runout. *Cold Regions Science and Technology 13*(2), 107–119.

McClung, D. M. & Schaerer, P. A. (1993). *The Avalanche Handbook*. The Mountaineers, Seattle, WA.

Moore, I. D. (1996). Hydrologic modelling and GIS. In M. F. Goodchild, L. T. Steyaert, B. O. Parks, M. P. Crane, C. A. Johnston, D. R. Maidment, & S. Glendinning (Eds.), *GIS and Enviromental Modeling: Progress and Research Issues*, GIS World Books, pp. 143–8. Fort Collins, CO.

Moore, I. D., Grayson, R. B., & Ladson, A. R. (1991). Digital terrain modelling: a review of hydrological, geomorphological an ecological applications. *Hydrological Processes 5*, 3–30.

Moore, I. D., Turner, A. K., Wilson, J. P., Jenson, S. K., & Band, L. E. (1993). Gis and land surface-subsurface modeling. In M. F. Goodchild, B. O. Parks, & L. T. Steyaert (Eds.), *Enviromental Modeling with GIS*, pp. 196–230. New York: Oxford University Press.

Mosley, M. P. (1974). Experimental study of hill erosion. *Trans. Ameri. Soc. Agric. Engineers, Soil and Water Division 17*(909-913).

Munter, W. (1997). *3x3 Lawinen – Entscheiden in kritischen Situationen*. Agentur Pohl & Schellhamer.

Naaim, M. & Gurer, I. (1998). Two-phase numerical model of powder avalanche. theory and application. *Natural Hazards 17*(2), 129–145.

Norem, H., Irgens, F., & Schieldrop, B. (1986). A continuum model for calculating snow avalanche velocities. In *Proceedings of Avalanche Formation, Movements and Effect, Davos 1986*, pp. 363–378. International Association of Hydrological Science.

Onorati, G., Poscolieri, M., Ventura, R., Chiarini, V., & Crucilla, U. (1992). The digital elevation model of Italy for geomorphology and structural geology. *Catena 19*(2), 147–178.

Panuska, J. C., Moore, I. D., & Kramer, L. A. (1991). Terrain analysis: integration into the agriculture non-point source (AGNPS) pollution model. *Journal of Soil and Water Conservation 46*, 59–64.

Perla, R. & Martinelli, M. (1976). *Avalanche Handbook*, Volume USDA Agricultural Handbook No. 489. Washington: U.S. Government Printing Office.

Perla, R. I. (1977). Slab avalanches measurements. *Canadian Geotechnical Journal 14*(2), 206–213.

Peucker, T. K. & Douglas, D. H. (1975). Detection of surface specific points by local parallel processing of discrete terrain elevation data. *Computer Graphics and Image Processing 4*, 375–87.

Peucker, T. K., Fowler, R. J., Little, J. J., & Mark, D. M. (1978). The triangulated irregular network. In *Proceedings of the ASP Digital Terrain Models (DTM) Symposium*, Falls Church Virginia, pp. 516–40. American Society of Photogrammetry.

Peuquet, D. J. (1984). A conceptual framework and comparison of spatial data models. *Cartographica 21*, 66–113.

Quinn, F. P., Beven, K. J., Chevallier, P., & Planchon, O. (1991). The prediction of hillslope flow paths for distributed hydrological modelling using digital terrain models. *Hydrological Processes 5*(59-79).

Reiss, R.-D. & Thomas, M. (1997). *Statistical Analysis of Extreme Values*. Birkhäuser Verlag.

Robert, C. P. & Casella, G. (1999). *Monte Carlo Statistical Methods*. Springer-Verlag New York, Inc.

Salm, B. (1982). *Lawinenkunde für den Praktiker*. Bern: Verlag Schweizer Alpen-Club.

Salm, B., Burkard, A., & Gubler, H. (1990). Berechnung von Fliesslawinen: eine Anleitung für Praktiker mit Beispielen. Mitteilung 47, Eidg. Institut für Schnee- und Lawinenforschung.

Sartoris, G. & Bartelt, P. (2000). Upwinded finite difference schemes for dense snow avalanche modeling. *International Journal for Numerical Methods in FLuids 32*, 799–821.

Schaerer, P. (1977). Analysis of snow avalanche terrain. *Canadian Geotechnical Journal 14*(3), 281–287.

Schmid, U. G. & Sardemann, S. (2003). High-frequency avalanches: release area characteristics and run-out distances. *Cold Regions Science and Technology 37*, 439–451.

Schmidt, J., Evans, I. S., & Brinkmann, J. (2003). Comparison of polynomial models for land surface curvature calculation. *International Journal of Geographical Information Science 17*(8), 797–814.

Schneebeli, M. & Meyer-Grass, M. (1993). Avalanche starting zone below the timber line - Structure of the forest. In *Proceedings of the International Snow Science Workshop, Breckenridge, Colorado, U.S.A., 4-8 October 1992*, pp. 176–181. Colo. Avalanche Inf Cent., Denver, Colo.

Schweizer, J. & Jamieson, J. B. (2001). Snow cover properties for skier triggering of avalanches. *Cold Regions Science and Technology 33*, 207–221.

Schweizer, J., Jamieson, J. B., & Schneebeli, M. (2003). Snow avalanche formation. *Review of Geophysics 41*(4), 1016.

Schweizer, J., Jamieson, J. B., & Skjonsberg, D. (1998). Avalanche forecasting for transportation corridor and backcountry in Glacier National Park (BC, Canada). In E. Hestnes (Ed.), *25 Years of Snow Avalanche Research, Voss, Norway, 12-16 May 1998*, NGI Publication, pp. 238–24. Norwegian Geotechnical Institute, Oslo, Norway.

Schweizer, J. & Lütschg, M. (2001). Characteristics of human-triggered avalanches. *Cold Regions Science and Technology 33*(2-3), 147–162.

Shary, P., Sharaya, L. S., & Mitusov, A. V. (2002). Fundamental quantitative methods of land surface analysis. *Geoderma 107*, 1–32.

Skidmore, A. K. (1989). Comparison of techniques for calculating gradient and slope from a gridded digital elevation model. *International Journal of Geographical Information Systems 3*(4), 323–334.

SLF (1949-2002). Schnee und Lawinen in den Schweizer Alpen, Winter 1949-2003. Winterbericht, Eidg. Institut für Schnee- und Lawinenforschung.

SLF (1952). Schnee und Lawinen in den Schweizer Alpen, Winter 1950/51. Winterbericht 15, Eidg. Institut für Schnee- und Lawinenforschung.

SLF (1969). Schnee und Lawinen in den Schweizer Alpen, Winter 1967/68. Winterbericht 32, Eidg. Institut für Schnee- und Lawinenforschung.

SLF (1999a). European avalanche test sites - Overview and analysis in view of coordinated experiments. Mitteilungen 59, Eidg. Institut für Schnee- und Lawinenforschung.

SLF (1999b). *Neue Berechnungsmethoden in der Lawinengefahrenkartierung*. Davos, Switzerland: Eidg. Institut für Schnee- und Lawinenforschung.

SLF (2000). Der Lawinenwinter 1999. Technical report, Eidg. Institut für Schnee- und Lawinenforschung.

SLF (2003). Lawinenniedergänge Region Davos vom 6.-7.2.03. map.

Smith, M. J. & McClung, D. M. (1997). Avalanche frequency and terrain characteristics at Rogers' Pass, British Columbia, Canada. *Journal of Glaciology 43*(143), 165–171.

Sovilla, B. (2004). *Field experiments and numerical modelling of mass entrainment and deposition processes in snow avalanches*. Ph. D. thesis, Institute für Hydromechanik und Wasserwirtschaft. Eidgenössische Technische Hochschule Zürich.

Stoffel, A., Meister, R., & Scwheizer, J. (1998). Spatial characteristics of avalanche activity in an Alpine valley – a GIS approach. *Annals of Glaciology 26*.

Summaprada, P. (1985). Gefahrenzonenplan landschaft davos, aussschnitt landwassertal. Technical report, Kanton Graubünden, Gemeinde Davos.

Torgrip, R. (2002). Cluster analysis and classification. Course material for the Chemometrics course, Stockholm University.

UNESCO (1981). *Avalanche Atlas. Illustrated International Avalanche Classification*. Paris.

USDA (1961). *Snow Avalanches*, Volume USDA Handbook No. 194. Washington: U.S. Government Printing Office.

Venables, W. N. & Ripley, B. D. (1997). *Modern Apllied Statistics with S-Plus* (second ed.). New York: NY: Springer-Verlag.

Voellmy, A. (1955). Über die Zerstörungskraft von Lawinen. *Schweiz. Bauzeitung 73*, 159–165,212–217,246–249,280–285.

Weibel, R. & Heller, M. (1991). Digital Terrain Modelling. In D. J. Maguire, M. F. Goodchild, & D. W. Rhind (Eds.), *Geographic Information Systems: principles and applications*, Volume 1, Chapter 19, pp. 269–297. London: Longman.

Weir, P. (1989). Geographic Information Systems for planning ski area developments. In *NZ Mountain Safety Council's "Avalanche 1990" Symposium, Quennstone, June 1989*.

Wilson, J. P. & Gallant, J. C. (2000). Digital Terrain Analysis. In J. P. Wilson & J. C. Gallant (Eds.), *Terrain Analysis: Principles and Applications*, Chapter 1, pp. 1–27. John Wiley & Sons, Inc.

Wilson, J. P., Repetto, P. L., & Snyder, R. D. (2000). Effect of Data Source, Grid Resolution, and Flow-Routing Method on Computed Topographic Attributes. In J. P. Wilson & J. C. Gallant (Eds.), *Terrain Analysis: Principles and Applications*, Chapter 5, pp. 133–161. John Wiley & Sons, Inc.

Wise, S. M. (1998). The effect of GIS interpolation errors on the use of digital elevation models in geomorphology. In S. N. Lane, K. S. Richards, & J. H. Chandler (Eds.), *Landform Monitoring, Modelling and Analysis*, pp. 139–64. New York: Wiley.

Wittwer, J. W. (2004). Monte Carlo Simulation Basics. http://vertex42.com/ExcelArticles/mc/MonteCarloSimulation.html.

Wolock, D. M. & Price, C. V. (1994). Effect of digital elevation model and map scale and data resolution on a topography-based watershed model. *Water Resources Research 30*, 3041–52.

Wonnacott, T. H. & Wonnacott, R. J. (1972). *Introductory Statistics* (second ed.). John Wiley & Sons, Inc.

Wood, J. (1996). *The geomorphological characterisation of digital elevation models*. Ph. D. thesis, Department of Geography - University of Leicester.

Zevenbergen, L. W. & Thorne, C. R. (1987). Quantitative analysis of land surface topography. *Earth Surface Process and Landforms 12*, 47–56.

Zhang, W. H. & Montgomery, D. R. (1994). Digital elevation model grid size, landscape representation, and hydrologic simulations. *Water Resources Research 30*, 1019–28.

Curriculum vitae

Margherita Maggioni
born October 29^{th}, 1973, Milano
citizen of Milano, Italy

Education

1987 - 1992 High school in Milano, Liceo Scientifico A. Einstein.

1992 Matura with final mark 46/60.

1992 - 1999 Studies in physics at the University of Milan.

1999 Diploma in physics, title of the thesis "Variazioni del geopotenziale indotte da instabilità glaciali e da cambiamenti del livello medio del mare" (Variations of the geopotential due to glacial instabilities and to sea-level changes).

1999 - 2000 Research project at the Departement of Earth Science (University of Milan) and at the Institute of Earth Science (SUPSI, Cadenazzo), title of the project "Present-day crustal stress and strain in the Swiss Central Alps".

2001 - 2004 Dissertation at the Swiss Federal Institute for Snow and Avalanche Research (SLF, Davos), title of the thesis "Avalanche release areas and their influence on uncertainty in avalanche hazard mapping" advised by Prof. Robert Weibel (Dep. of Geography, University of Zürich).